

---

# DIODE LASER RAMAN SCATTERING PROTOTYPE GAS-PHASE ENVIRONMENTAL MONITORING

Robert E. Benner, Lee M. Smith, Ming-Wei Pan, Carl W. Johnson,  
Daniel D. Knowlton, and Ralph Price

Process Instruments, Inc.  
825 North 300 West, Suite 225  
Salt Lake City, UT 84103-1414

July 1999

Final Report

APPROVED FOR PUBLIC RELEASE; DISTRIBUTION IS UNLIMITED.

20000710 156



**AIR FORCE RESEARCH LABORATORY**  
**Directed Energy Directorate**  
**3550 Aberdeen Ave SE**  
**AIR FORCE MATERIEL COMMAND**  
**KIRTLAND AIR FORCE BASE, NM 87117-5776**

AFRL-DE-TR-1999-1063

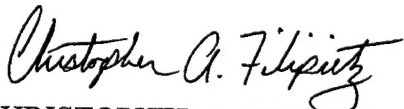
Using Government drawings, specifications, or other data included in this document for any purpose other than Government procurement does not in any way obligate the U.S. Government. The fact that the Government formulated or supplied the drawings, specifications, or other data, does not license the holder or any other person or corporation; or convey any rights or permission to manufacture, use, or sell any patented invention that may relate to them.

This report has been reviewed by the Public Affairs Office and is releasable to the National Technical Information Service (NTIS). At NTIS, it will be available to the general public, including foreign nationals.

If you change your address, wish to be removed from this mailing list, or your organization no longer employs the addressee, please notify AFRL/DELS, 3550 Aberdeen Ave SE, Kirtland AFB, NM 87117-5776.

Do not return copies of this report unless contractual obligations or notice on a specific document requires its return.

This report has been approved for publication.



CHRISTOPHER A. FILIPIETZ, Capt, USAF  
Project Manager

FOR THE COMMANDER



SYLVIA DORATO, DR-III  
Chief, Advanced Tactical DE Systems



R. EARL GOOD, SES  
Director, Directed Energy Directorate

REPORT DOCUMENTATION PAGE				Form Approved OMB No. 0704-0188	
Public reporting burden for this collection of information is estimated to average 1 hour per response, including the time for reviewing instructions, searching existing data sources, gathering and maintaining the data needed, and completing and reviewing this collection of information. Send comments regarding this burden estimate or any other aspect of this collection of information, including suggestions for reducing this burden to Department of Defense, Washington Headquarters Services, Directorate for Information Operations and Reports (0704-0188), 1215 Jefferson Davis Highway, Suite 1204, Arlington, VA 22202-4302. Respondents should be aware that notwithstanding any other provision of law, no person shall be subject to any penalty for failing to comply with a collection of information if it does not display a currently valid OMB control number. PLEASE DO NOT RETURN YOUR FORM TO THE ABOVE ADDRESS.					
1. REPORT DATE (DD-MM-YYYY) 12-07-1999		2. REPORT TYPE Final Report		3. DATES COVERED (From - To) 14 Feb 1997 to 31 May 1999	
4. TITLE AND SUBTITLE  Diode Laser Raman Scattering Prototype Gas-Phase Environmental Monitoring				5a. CONTRACT NUMBER F29601-97-C-0019	
				5b. GRANT NUMBER	
				5c. PROGRAM ELEMENT NUMBER 63605F	
6. AUTHOR(S)  Robert E. Benner, Lee M. Smith, Ming-Wei Pan, Carl W. Johnson, Daniel D. Knowlton, and Ralph Price				5d. PROJECT NUMBER 3005	
				5e. TASK NUMBER C0	
				5f. WORK UNIT NUMBER RY	
7. PERFORMING ORGANIZATION NAME(S) AND ADDRESS(ES)  Process Instruments, Inc. 825 North 300 West Suite 225 Salt Lake City, UT 84103-1414				8. PERFORMING ORGANIZATION REPORT NUMBER	
9. SPONSORING / MONITORING AGENCY NAME(S) AND ADDRESS(ES)  AFRL/DELS 3550 Aberdeen Ave SE Kirtland AFB NM 87117-5776				10. SPONSOR/MONITOR'S ACRONYM(S)	
				11. SPONSOR/MONITOR'S REPORT NUMBER(S) AFRL-DE-TR-1999-1063	
12. DISTRIBUTION / AVAILABILITY STATEMENT  Approved for public release; distribution is unlimited.					
13. SUPPLEMENTARY NOTES					
14. ABSTRACT We proposed developing a diode-laser-based, full spectrum Raman scattering instrument incorporating a multipass, external cavity enhancement cell for full spectrum, gas phase analysis of environmental pollutants. Narrow, well-defined Raman peaks and insensitivity to moisture contamination allow for full-spectrum with detection on the order of 1 percent sensitivity with 1 to 2 minute integrations. Conventional Raman instrumentation is too expensive and not sensitive enough for industrial applications. For excitation of Raman scattering Ar-ion lasers have too short of a life and are too expensive for continuous use. Semiconductor laser diodes offer longer life than conventional lasers and now have sufficient power for rapidly obtaining Raman signals. Traditionally environmental instrumentation requires hot stack gases to be cooled prior to being measured. Cooling stack gas results in condensation and loss of water soluble species. Phase II focused on a laser power build-up of cavity design that would be stable, simple to reproduce, and cost effective. We assembled a bench prototype power build-up cavity with solid-state laser diode pumping that incorporated an efficient spectrograph (patent pending), application specific software, user interface, and calibration procedures. Although the prototype was not stable for on-line testing in industrial environmental monitoring applications, the bench prototype was extensively tested in the laboratory.					
15. SUBJECT TERMS Frequency-Stabilized Diode Laser, Gas-Phase Raman Scattering, Laser-Based Environmental Monitoring					
16. SECURITY CLASSIFICATION OF:			17. LIMITATION OF ABSTRACT  Unlimited	18. NUMBER OF PAGES  134	19a. NAME OF RESPONSIBLE PERSON Capt Christopher A. Filipietz
a. REPORT Unclassified	b. ABSTRACT Unclassified	c. THIS PAGE Unclassified			19b. TELEPHONE NUMBER (include area code) (505) 846-4758





# CONTENTS

<u>Section</u>	<u>Page</u>
1.0 INTRODUCTION .....	1
1.1 Historical .....	1
1.2 Key Advantages of Modern Raman Scattering Technology .....	1
1.3 The Problems .....	3
1.3.1 Environmental Applications .....	4
1.3.1.1 Industrial Stack Gas Monitoring .....	4
1.3.1.2 Vehicle Emissions - Automotive and Alternative Fuels .....	4
1.3.1.3 Fuel Gas - Refining Industry .....	4
1.3.2 Process Applications .....	9
1.3.2.1 Bromine Detection - Purified Terephthalic Acid Production .....	9
1.3.2.2 Iron and Steel Production .....	9
1.3.2.3 Natural Gas Transmission Lines .....	10
1.3.2.4 Ethylene Production .....	10
1.3.2.5 Ammonia Production .....	10
1.4 Phase II Technical Objectives .....	10
2.0 INSTRUMENTATION DEVELOPMENT AND TESTING .....	13
2.1 Introduction .....	13
2.2 Laser Sources Evaluated and Developed .....	21
2.2.1 Diode Array .....	21
2.2.2 External Cavity Power Build-up Cavity .....	22
2.2.2.1 Narrowed Line width .....	31
2.3 Sample Cells .....	38
2.3.1 Diode Laser Testing in Power Build-up Cavity .....	47
2.3.2 Determination of Prototype's Detection Limits .....	54
2.4 Spectrograph Development and Patent Application .....	58
2.5 CCD Detectors .....	61
2.5.1 Santa Barbara Instruments Group Cameras .....	61
2.5.2 Photometric Sensys CCD Camera System .....	66
2.5.3 Andor CCD Camera Evaluation .....	73
2.6 Performance of Current Prototype Instrument .....	78
2.6.1 Filter Comparison .....	83
2.6.2 System Stability .....	90
2.6.3 Narrow Line Width Laser Operation .....	90
2.6.4 12-Hour Stability Measurements .....	98

3.0	BUSINESS DEVELOPMENT AND MARKETING.....	103
3.1	Marketing.....	103
3.1.1	Commercial Applications - Market Opportunity .....	103
3.1.2	Geographic Distribution of Process Instrument Market .....	103
3.1.3	Market Segmentation by End-User Group .....	103
3.1.4	Potential OEM Instrument Company Customers .....	103
3.1.5	Prototype's Cost-of-Goods .....	105
3.2	Economic Benefits .....	109
3.2.1	Health and Safety Considerations .....	109
3.4.1.1	Ethylene Oxide Sterilization Monitoring .....	109
3.2.2	Economic Benefit to the Steel Industry .....	109
3.2.3	Potential Post Applications .....	110
3.3	Patent Application .....	111
3.4	Center for Devices and Radiological Health (CDRH) Certification .....	111
3.5	Trade Shows .....	111
3.5.1	Pittsburgh Conference - March 1999 - Orlando, Florida .....	111
3.5.2	Compact Robust Spectrometer .....	112
3.6	Strategic Alliance - Laser Corporation .....	113
3.7	Possible OEM Relationship - Atmospheric Recovery Incorporated .....	113
4.0	CONCLUSIONS .....	114
4.1	Raman Instrument Definition .....	114
4.1.1	Laser Source .....	114
4.1.2	Sample Cell Design .....	114
4.1.3	Compact, Robust, and Optically Fast Spectrograph .....	114
4.1.4	System Performance .....	115
4.1.5	Calibration Schemes .....	115
4.1.6	Software Control .....	115
4.1.7	Applications - Process Control and Pipe-line Monitoring .....	116
	REFERENCES .....	117

## FIGURES

<u>Figure</u>	<u>Page</u>
1. Raman peak location (frequency shift) and scattering cross section intensity of selected components typically associated with industrial stack gas emissions.	5
2. Raman peak spectra location (frequency shift) and scattering cross section intensity of selected components associated with vehicle emissions.	6
3. Raman peak spectra location (frequency shift) and scattering cross section intensity of selected components associated with alternative fuels used to reduce vehicle emissions.	7
4. Raman peak spectra location (frequency shift) and scattering cross section intensity of selected components associated with industrial fuel gas combustion and control.	8
5. Initial design for our gas-phase Raman prototype. An argon laser operating at 488 nm with a power level of approximately 2 W is used as the excitation source for the Raman measurements. Light from the laser is focused using the lens $L_1$ to a point near the center of the mirror cavity formed by mirrors $M_1$ and $M_2$ .	14
6. Raman data from ambient nitrogen obtained with this prototype system using a single pass of laser light, a double pass of laser light, and a double pass of laser light in conjunction with the rear mirror.	15
7. Raman data from ambient oxygen exhibiting enhancement factors of 1.85 and 3.12	16
8. Measurement of the ability of the multipass cell to enhance Raman data from ambient air by comparing signals obtained with a single pass of laser light to those obtained with the multipass cell optimally aligned.	17
9. One hundred Raman spectra from ambient air. The data exhibit good repeatability, but there are a few spectra with lower peak heights which may have been collected as dust particles passed through the excitation light.	19
10. The nitrogen and oxygen peak heights observed in the 100 spectra. The nitrogen and oxygen signals have standard deviations of 0.93% and 0.82%, respectively.	20
11. Circulating power inside the cavity from a 300 mW visible diode laser at 665 nm.	23

12.	Simulation of Optical Feedback (OFB) from the power buildup cavity to the laser diode.	24
13.	LI curves for diode laser in non-coated, coated, and coated plus microlens configurations.	25
14.	Process Instruments' external cavity diode laser configuration.	27
15.	Power build-up curve for external cavity diode laser.	28
16.	Laser output with and without feedback.	29
17.	Experimental optical setup allowing for tunability of laser wavelength and linewidth narrowing.	30
18.	Results of linewidth narrowing with grating feedback.	32
19.	Circulating power inside cavity with grating feedback versus the pumping current.	33
20.	Experimental setup for collection of Raman data with Power build-up cavity (PBC).	34
21.	Raman spectrum obtained from ambient air with no laser linewidth narrowing.	35
22.	Raman spectra from ambient air with two different laser polarization directions.	36
23.	Nitrogen peak and integrated Raman signal stability over a period of 14 hours.	37
24.	Flat window gas flow cell	39
25.	Glass tube gas flow cell	40
26.	Spectra obtained with a one second integration time for both glass and quartz cell materials. The fluorescence background of the pyrex is eight times that of the quartz.	41
27.	Ambient air control spectrum, obtained without tubing nor windows to contain the air. The spectrum has a nitrogen peak intensity of 1,155,300 counts, an oxygen peak intensity of 380,730 counts, and a mean background intensity of 1955 counts.	43
28.	Ambient air spectrum with quartz tubing in place.	44

29.	Raman spectrum of ambient air with flat glass window. The Raman peak intensities of nitrogen and oxygen were similar at 1,161,100 and 364,800 counts, respectively compared to the signal without any window.	45
30.	Spectrum obtained with 1.8 watts rather than 1.9 watts causing the signal to be slightly lower (nitrogen peak of 1142000 and oxygen peak of 350790).	46
31.	Raman spectrum of 1% nitrogen in argon gas	48
32.	Gas-Phase sample flow cell for environmental monitoring.	49
33.	Power Build-up cavity gas cell.	50
34.	Raman spectrum from ambient air contained within the gas cell.	52
35.	Raman spectrum from argon contained within the gas cell.	53
36.	Improved ambient air spectrum obtained by subtracting the measured background in (Fig. 31) from the air spectrum in (Fig. 30).	55
37.	Raman spectra obtained from a commercial gas mixture containing 95% CO <sub>2</sub> , 4% N <sub>2</sub> , and 1% O <sub>2</sub> .	56
38.	Raman spectra obtained as the gas within the sample cell changed from the carbon dioxide mixture to ambient air with the cell inlet and outlet open.	57
39.	Spectrograph drawing	59
40.	Newly designed spectrograph using s a 600 grooves/mm grating which gives about 3000 cm <sup>-1</sup> coverage and 60 cm <sup>-1</sup> resolution	60
41.	Linearity results for our new 7i camera without anti-blooming based on Raman data from ambient air.	62
42.	Pixel-to-pixel variations observed with the camera in the dark.	63
43.	Summary of the data of Fig. 38 obtained at 0 degrees C.	64
44.	Summary of the data of Fig. 38 obtained at 0 degrees C by plotting the standard deviation of the signals for the light and dark frames.	65
45.	Mean signal data as a function of integration time obtained with the camera at a temperature of - 10 degrees C.	67

46.	Signal standard deviation as a function of integration time obtained with the camera at a temperature of - 10 degrees C.	68
47.	Mean signal data as a function of integration time obtained with the camera at a temperature of - 20 degrees C.	69
48.	Signal standard deviation as a function of integration time obtained with the camera at a temperature of - 20 degrees C.	70
49.	Display of the dark spectra obtained with the camera in the dark and at 10 degrees C with a 10 ms integration time for the three gain factors.	71
50.	The dependence of the mean dark signal on integration time with the camera gain set at its lowest value.	72
51.	Display of some of the spectra associated with the data in Fig. 46.	74
52.	The mean signals recorded as a function of integration time for full vertical binning and with the CCD at -60 degrees C.	75
53.	Signal standard deviation as a function of integration time. For a 5-minute integration time, the measured standard deviation was only 9 counts.	76
54.	Mean signal and standard deviation as a function of integration time for a SBIG camera. SBIG camera signal standard deviations are more than 1000 times greater after a five minute integration time.	77
55.	Effects of filter placement on background noise.	79
56.	Raman spectrum from ambient air with the background subtracted .	80
57.	Peaks from the three gases. There are two Raman peaks for CO <sub>2</sub> near 1350 cm <sup>-1</sup> and one each for O <sub>2</sub> and N <sub>2</sub> at 1555 cm <sup>-1</sup> and 2331 cm <sup>-1</sup> , respectively.	81
58.	Nitrogen peaks obtained using different slit widths.	82
59.	Raman spectra of butane.	84
60.	Raman spectra of gas concentrations over time as CO <sub>2</sub> is replaced by ambient air.	85

61.	Raman spectra from ambient air for an 8-hour period (1000 spectra). The nitrogen peak maximum and integrated nitrogen peak had standard deviations of 6.94 % and 4.75%, respectively.	86
62.	One hundred spectra recorded overnight to get an indication of gas phase Raman prototype stability.	87
63.	Background spectra obtained with argon gas in the sample cell using the color filter and the dielectric filter.	88
64.	Depicts how the background emission appears under the oxygen peak in Raman spectrum collected from ambient air.	89
65.	Display of typical results with the laser operating a full current for the measured variations in the Raman peak intensity and the integrated Raman intensity.	91
66.	Demonstrates that the photodiode output matches the variation in integrated Raman intensity. The photodiode output doesn't track the variation in Raman peak intensity (SDV = 16.3%) nearly as well.	92
67.	Plot of the variation of the nitrogen Raman peak on an expanded scale over the 12-hour period.	93
68.	The nitrogen Raman peak obtained with a laser current of 450 mA continues to exhibit a periodic frequency variation in data collected over a 12-hour period.	94
69.	Twelve hour comparison between the integrated nitrogen peak area and the photodiode output. The variations in the nitrogen peak area and the photodiode output are 8.07 % and 8.06 %, respectively.	95
70.	The measured nitrogen peak areas linearly related to the photodiode output values.	96
71.	Raman spectrum obtained with nitrogen contained within the gas cell.	97
72.	Background on an expanded scale when argon (which doesn't have a detectable Raman signal) rather than nitrogen is contained within the gas cell.	99
73.	Raman data from a gas mixture containing 95% CO <sub>2</sub> , 4% N <sub>2</sub> , and 1% O <sub>2</sub> . Even though O <sub>2</sub> is only present at the 1% level, the oxygen peak is clearly resolved in the tail of the Raman peak from CO <sub>2</sub> .	100

- |     |   |     |
|-----|---|-----|
| 74. | Comparison of the monitor photodiode output and the Raman peak area. The variations are so large that using the photodiode signal to normalize the Raman data would probably not be feasible. | 101 |
| 75. | The frequency profile of the measured nitrogen peaks recorded during the 12-hour period.  | 102 |



## TABLES

<u>Table</u>	<u>Page</u>
1. U.S. Markets for Process Chromatographs and Mass Spectrometers	104
2. U.S. Markets for Selected Process Analyzers - Market Segmentation by End User Group	105
3. Potential Customers - Major Instrument Suppliers	106
4. Worldwide Markets for Selected Instrument Suppliers	107
5. Worldwide Markets for Selected Process Analyzers - 1999 Market Distribution by Geographic Region	108



## 1.0 INTRODUCTION

### 1.1 Historical

The Raman scattering effect was first observed in 1928 and relies on the interaction of monochromatic laser light with the vibrational and rotational modes of molecules to produce scattered light which is shifted in frequency from that of the incident radiation by an amount corresponding to the vibrational and rotational energies of the scattering molecules.<sup>(1)</sup> Since these energies are species-specific, an analysis of the frequency components present in the Raman scattered light provides chemical identification of the components present in the scattering sample. While the Raman process is a very weak effect in terms of conversion efficiency from incident to scattered light, molecular gas phase constituents in the low ppm range have been identified using existing lasers and detectors.<sup>(2,3 & 4)</sup> There is a linear relationship between species concentration and Raman signal intensity. Molecular concentrations are determined from measured Raman band signal intensities and known Raman scattering cross sections.<sup>(5)</sup>

During the past decade, several key instrumentation developments have come together to greatly improve the prospects for Raman scattering becoming a more general purpose analytical technique.<sup>(6)</sup> These developments include: (1) the use of thermoelectric (TE)-cooled charge-coupled-device (CCD) array detectors for parallel detection of Raman spectra with high quantum efficiency and low noise,<sup>(7-9)</sup> (2) the use of excitation sources in the near infrared to reduce fluorescence emission compared to Raman scattering,<sup>(10)</sup> (3) the availability of volume holographic filters and gratings to provide improved overall throughput and elastic light rejection for Raman spectrographs,<sup>(11-13)</sup> and (4) the availability of more economical frequency-doubled, diode-pumped lasers of sufficient power (2 to 4 W).

Unlike mass spectroscopy or GC analysis, Raman has the power to non-destructively identify and quantitate substances in gaseous, liquid, or solid forms. This greatly simplifies any measurement process because little sample preparation is required. Mass spectroscopy can only be used to analyze samples in the gaseous state and quantitates based upon total mass/charge ratio, not molecular structure. Most importantly, solid-state electro-optic Raman technology offers reliable and economic alternatives for military and/or industrial monitoring applications.

### 1.2 Key Advantages of Modern Raman Scattering Technology include:

1. Full Raman spectra can be obtained in parallel with high sensitivity using commercially available silicon CCD arrays.
2. Narrow, well-defined Raman peaks allow for little ambiguity in identification of components of a similar elemental constitution; i.e., chemical isomers can easily be separated, clearly identified and measured *in situ*.<sup>(8)</sup>

3. Sensitivities on the order of a 1 ppm for gas phase constituents such as  $N_2$ ,  $O_2$ ,  $CO_2$ ,  $CO$ ,  $SO_x$  and  $NO_x$  in less than 60 seconds.<sup>(4)</sup>
4. Because the relative sensitivity to various components remains fixed with time, calibration is relatively simple.
5. Designing a Raman instrument with specially designed optical components specifically for on-line, remote monitoring offers potentially lower cost for environmental and process monitoring since one instrument can now replace several individual analyzers and Raman's fast response allows for increased product throughput.
6. Multiplexing offers the capability to monitor many gas streams with one instrument, reducing overall instrument and maintenance costs.
7. The Raman spectrum for water is unique and easily distinguishable from most other components.<sup>(14)</sup> This is not the case with conventional IR absorption technology.

The thrust of this Phase II project was to develop an industrial Raman instrument that would meet the necessary military and/or industrial process monitoring requirements. Phase I demonstrated the feasibility of using low power laser diodes in a power build-up cavity and coupled to a highly sensitive holographic spectrograph and inexpensive CCD array to measure a few gas-phase applications in the process control industry. Phase II continued on with the development of an actual prototype instrument that was sufficiently rugged and "industrially hardened" to be capable of fast, remote, on-line continuous monitoring at a competitive market cost.

One of the key aspects of our design is the use of unique frequency-stabilized, narrow linewidth laser diodes. Because of the weakness of the Raman effect, traditional Raman instrumentation often utilizes high-powered, expensive tunable lasers (costing \$75,000 or more) that have short life spans (2000 to 5000 hours). An argon-ion-laser-pumped Ti:sapphire laser was an integral part of the research grade Raman equipment used in our preliminary research. The replacement cost and lifetime constraints make this light source unacceptable for continuous industrial use. Phase I results have demonstrated that an ideal excitation wavelength for most gas-phase process monitoring applications is in the region of 670 nm.

There are two distinct advantages to exciting at 670 nm:

1. Most gas-phase chemical species of interest can be identified by Raman peaks existing in the frequency shift range from 500 to 4200  $cm^{-1}$ . With excitation at 670 nm, a frequency shift of 4200  $cm^{-1}$  can still be measured using conventional TE-cooled CCD detectors.

2. Fluorescence--normally a significant problem in organic liquid samples--is not really a problem with gas-phase measurements even when measured at these shorter excitation wavelengths. An additional advantage is that the Raman efficiency is inversely proportional to wavelength to the fourth power. Thus, exciting at 670 nm increases the Raman signal by almost a factor of 1.9 compared to more conventional wavelengths, such as 785 nm, which is typically used for measuring liquid and solid samples for elimination of fluorescence.

Commercially available AlGaAs diode lasers with outputs on the order of 50 to 100 mW are now readily available. However, these devices have relatively broad linewidths (2 to 3 nm) which are much too broad for use with conventional Raman. However, our patent pending, volume-holographic, external cavity stabilization allows these laser diodes to be frequency stabilized (no mode hopping) and narrows the linewidth to  $\sim 30$  GHz ( $1 \text{ cm}^{-1}$ ). Diode lasers have long lifetimes ( $> 15,000$  hours @  $25^\circ\text{C}$ ) and lend themselves to being used on a continuous basis, 24 hours per day for up to two years ( $\approx 8800$  hours per year). On a replacement basis, their cost would be approximately \$1000 to \$1500 per year. This is acceptable considering the value of the instrumentation involved. Recent cost reductions in CCD detectors coupled with improvements we made in a compact spectrograph allow both these normally expensive technologies to be combined into affordable Raman instrumentation. Continued advances in optoelectronics are continuing to bring these prices down. This allows the assembly of a full-spectrum Raman analyzer at prices comparable to traditional process instrumentation. An additional cost savings exists with the elimination of the sample handling hardware by remotely coupling the excitation and collection system with fiber optics. Successfully bringing diode-laser-based Raman instrumentation to market will increase the need for laser diodes and subsequently help lower their cost to the military and to industry.

### 1.3 The Problems

Symmetrical diatomic gases such as  $\text{N}_2$ ,  $\text{O}_2$ , and  $\text{Br}_2$  have no dipole moments and cannot be measured by infrared (IR). Raman, however, has easily observable peaks for these simple compounds. Oxygen can be measured electrochemically for ppm levels or paramagnetically for percentile concentrations. Electrochemical sensors such as zirconium oxide only respond at high temperatures, often well above the flash point for many processes, and paramagnetic analyzers are slow to respond. Gas chromatographs (GC) are routinely used to measure multiple components, but their response time is typically slow (15-20 minutes), and they require separate columns for hydrocarbons and inorganics. GC columns can gradually degrade with time, spoiling instrument resolution or altering retention times, either of which require frequent calibration to correct. Mass spectrometers can be used to measure  $\text{N}_2$ , but the technology is very expensive and difficult to maintain and not really suitable for continuous on-line industrial applications. Ammonia can only really be measured via wet chemistry techniques.

### 1.3.1 Environmental Applications

#### 1.3.1.1 Industrial Stack Gas Monitoring

One of the most common industrial environmental applications is the measurement of stack gas effluent. Industrial power plants, steel mills, and any other facilities burning hydrocarbons generate stack gas pollutants and are required by governmental agencies to monitor the stack gas constituents. These compounds typically include the following gases: CO, CO<sub>2</sub>, NO<sub>x</sub>, SO<sub>x</sub>, NH<sub>3</sub>, H<sub>2</sub>S and HCl. The relative Raman scattering cross sections and Raman shifts of these gases are illustrated in Fig. 1. These gases are typically very hot (>200 °C) in the stack. The gases need to be analyzed in their natural state; i.e., hot. If the gases are cooled, the moisture and acids tend to condense taking those compounds and any other compounds that are soluble in the moisture out of the sample. Thus, when these gases are cooled and measured via conventional instrumentation, some of the constituents are missing or appear in much lower concentrations. Raman instrumentation has the ability to measure these gases hot, ensuring that all the individual gas components are measured accurately. Current technology for measuring stack gas emission requires a battery of instruments because not one technology can measure all of the gases present. Infrared can be used to measure CO and CO<sub>2</sub>. NO<sub>x</sub> compounds require chemiluminescent technology. HCl and NH<sub>3</sub> can be measured by mass spectrometry and/or GC instrumentation. Being able to measure all of these components with one instrument would be far superior, saving instrumentation costs, reducing maintenance, and simplifying calibration procedures.

#### 1.3.1.2 Vehicle Emissions - Automotive and Alternative Fuels

Many states have developed specific auto emissions testing procedures to ensure compliance with current state and federal vehicle emissions requirements. This requires specialized testing equipment that needs to have a very fast response time (30 to 60 msec) to allow for real time measurement. The specific testing requirements vary depending upon the type of fuel required; i.e., conventional gasoline or reformulated fuel. Figures 2 and 3 illustrate the typical components of interest.

#### 1.3.1.3 Fuel Gas - Refining Industry

In most petrochemical refining plants byproduct gases are burned to generate heat for distillation and other processes. The fuel stock is made up of a variety of light hydrocarbons such as H<sub>2</sub>, NH<sub>3</sub> and H<sub>2</sub>S (Fig. 4). The combustion gas composition is always changing. This changing fuel mix needs to be burned in such a way that minimizes the air pollutants. Real-time analysis of the fuel mix would allow the carboration to be optimally adjusted for production of minimal emissions. Current GC instrumentation requires 20 to 30 minutes, and after-the-fact analysis is too slow for optimization of the combustion cycle. Better control of the stack emission means considerably less expense to the refinery.

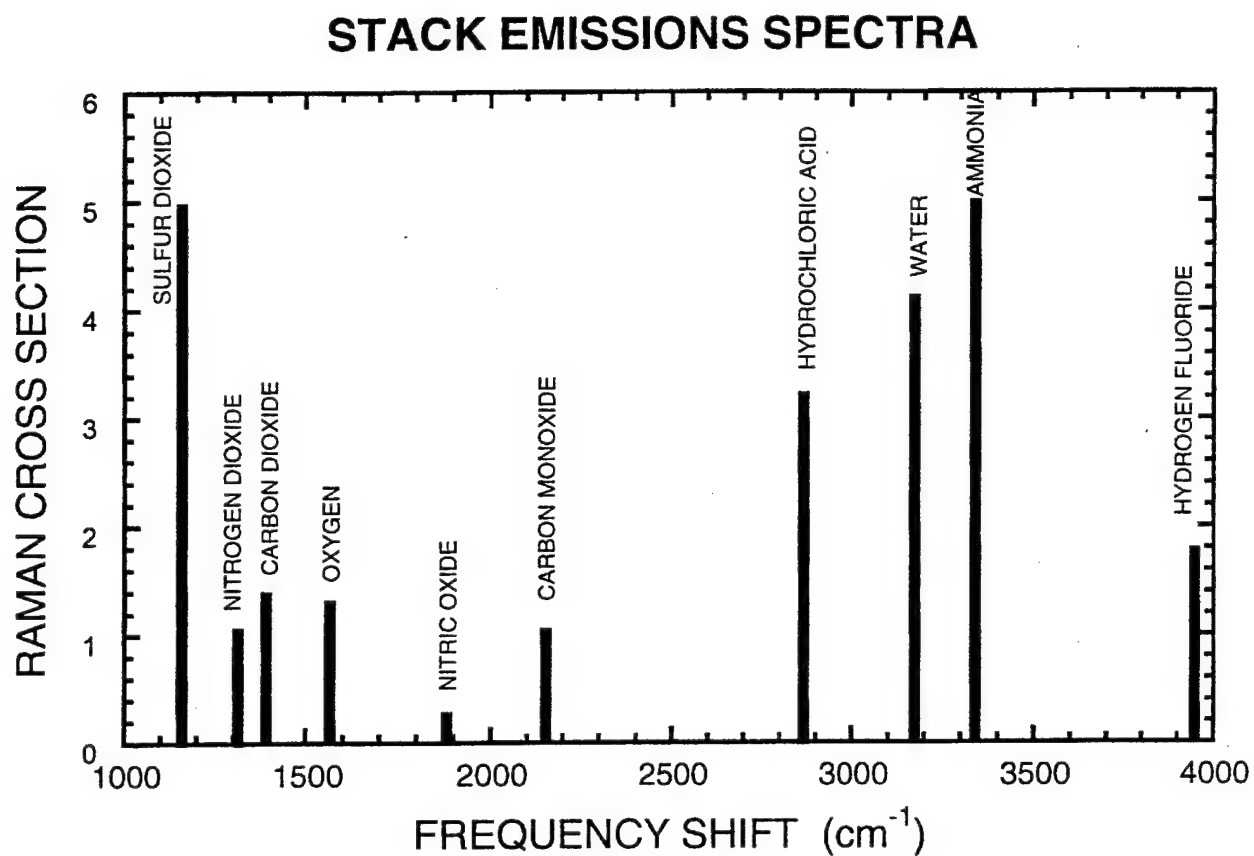


Figure 1. Raman peak location (frequency shift) and scattering cross section intensity of selected components typically associated with industrial stack gas emissions.

## VEHICLE EMISSIONS SPECTRA

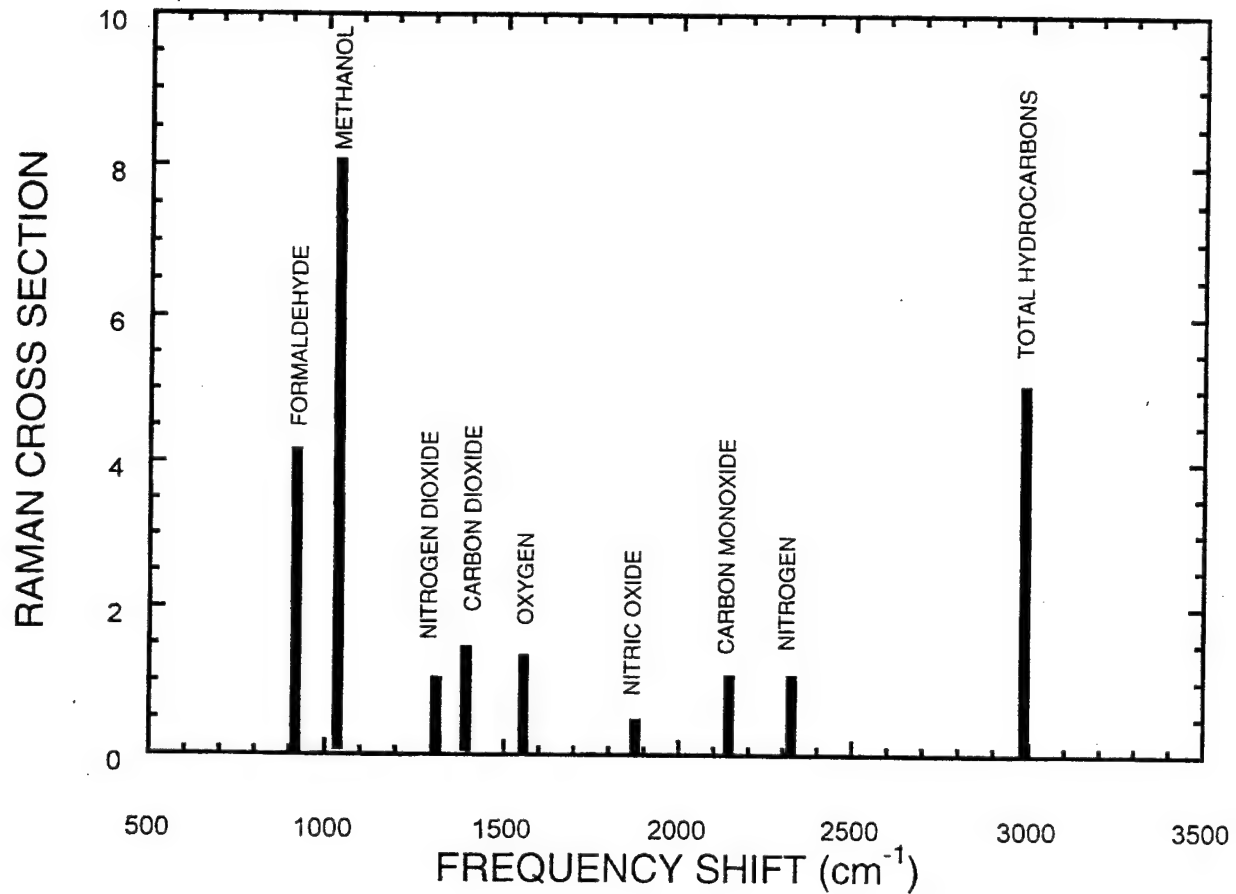


Figure 2. Raman peak spectra location (frequency shift) and scattering cross section intensity of selected components associated with vehicle emissions.



## ALTERNATIVE FUELS (VEHICLE EMISSIONS)

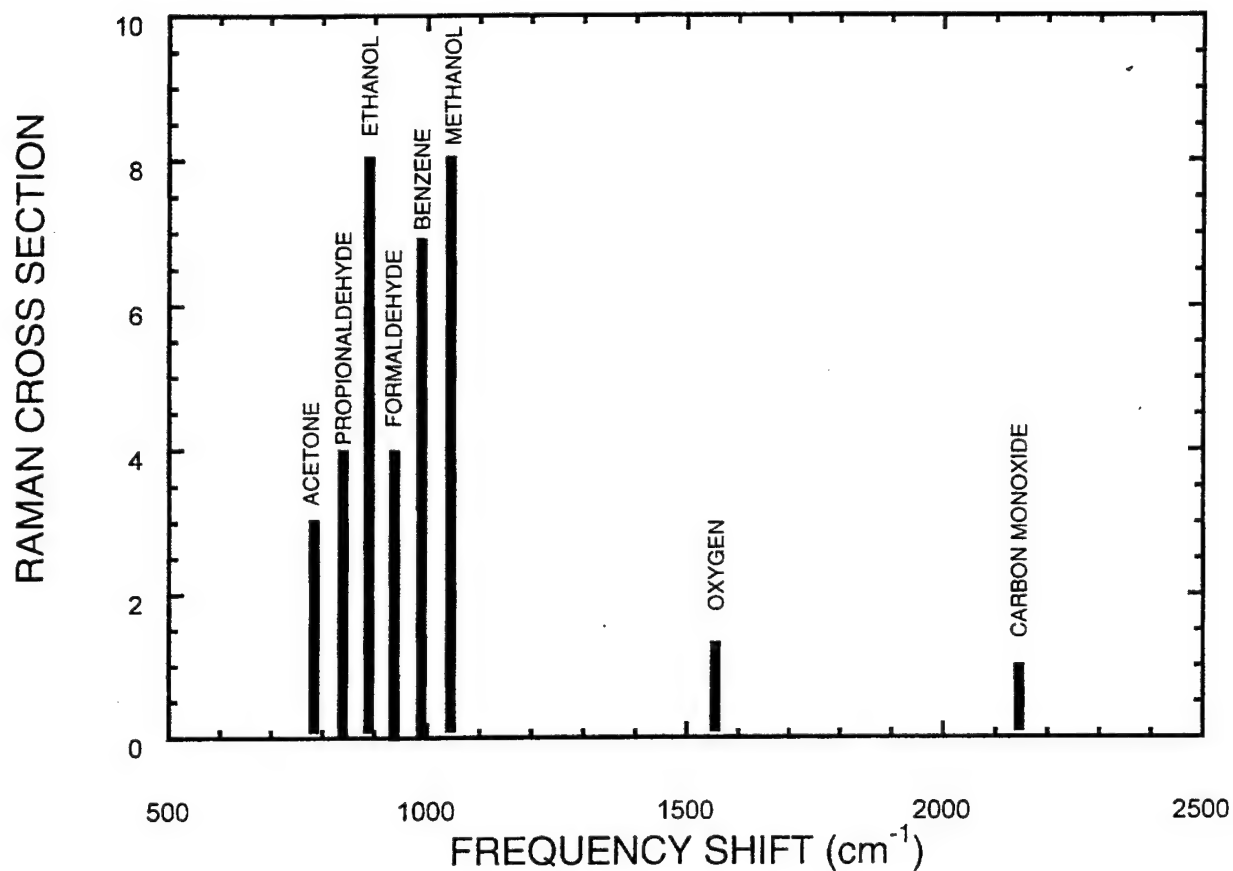


Figure 3. Raman peak spectra location (frequency shift) and scattering cross section intensity of selected components associated with alternative fuels used to reduce vehicle emissions.

## FUEL GAS SPECTRA

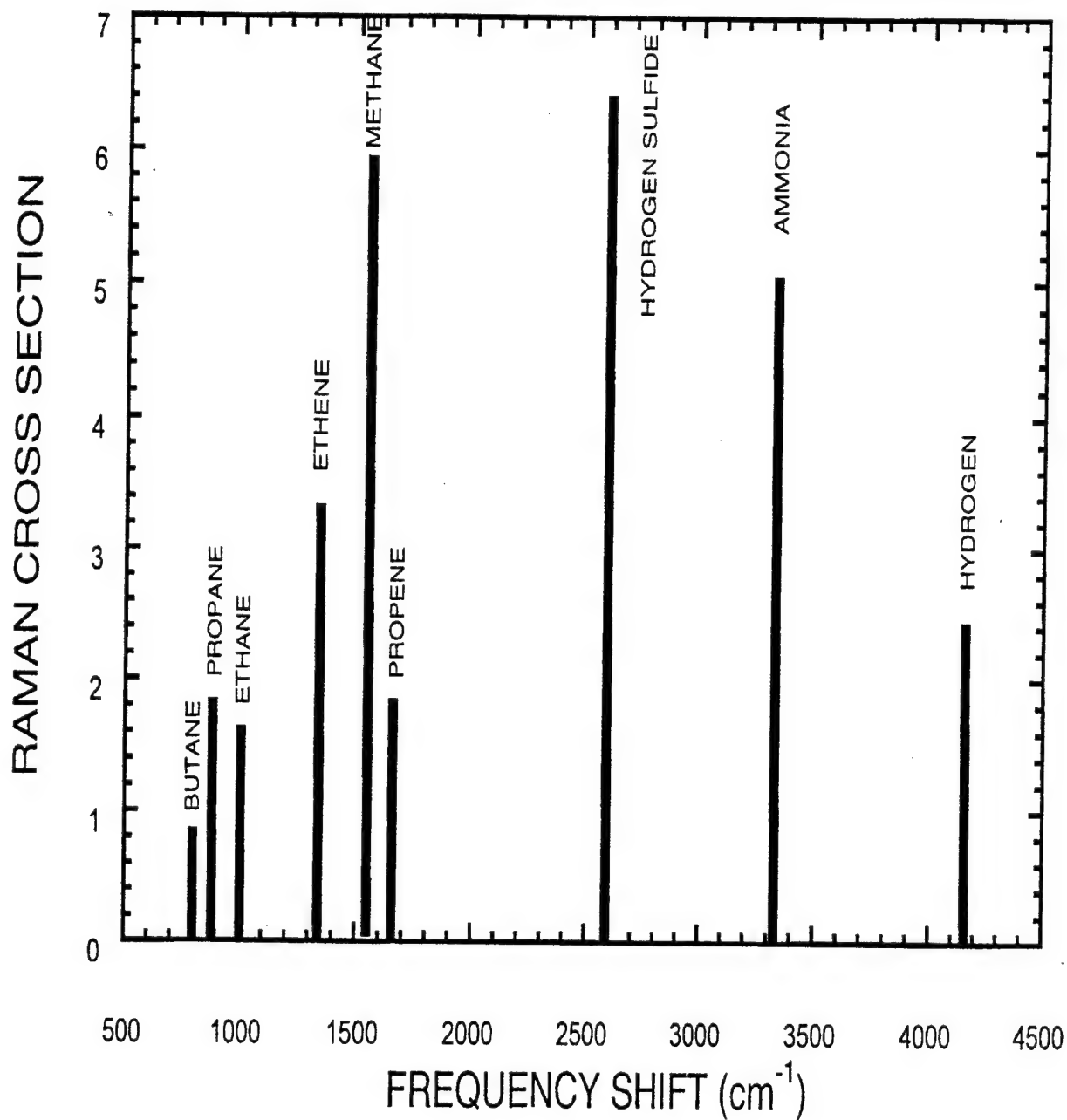


Figure 4. Raman peak spectra location (frequency shift) and scattering cross section intensity of selected components associated with industrial fuel gas combustion and control.

### 1.3.2 Process Applications

#### 1.3.2.1 Bromine Detection - Purified Terephthalic Acid Production

Bromine is used as a catalyst in the oxidation step in the production of purified terephthalic acid (PTA), a major starting component for polyester production. Amoco Chemical is one of the world's largest producers of PTA. Just their chemical plants alone manufacture close to 3 to 4 billions dollars worth of polyester per year. World wide, PTS is the basis of a 10 + billion dollar polyester manufacturing industry. In the course of manufacturing PTA HBr is used as a catalyst. Some of the HBr ends up in the effluent stream even after scrubbing. Water scrubbing converts the HBr to  $\text{Br}_2$ . However, not all of the HBr is removed. The stack gas emission from this type of plant contains both HBr and  $\text{Br}_2$  as contaminants in the 5 to 10 ppm level. Government regulations require the levels of these compounds to be continuously monitored. Currently there is no easy method to measure bromine compounds except by grab samples and wet chemistry. Bromine does, however, have strong Raman peaks at around  $330\text{ cm}^{-1}$  and a strong scattering cross section roughly 6 times that of nitrogen. There are multiple Raman peaks for bromine, since bromine exists as two stable isotopes in roughly a 50/50 mixture. Bromine cannot be easily measured with existing instrumentation. Bromine also has strong absorption at 532 nm, which may allow us to take advantage of resonance Raman enhancement to develop even lower level detection capabilities. This enhancement can improve our detection sensitivity significantly. If the monitoring requirements for bromine increase, we should be able to detect ppb levels using resonance Raman enhancement. Another bromine application exists upstream of the PTA process. Because of the corrosive nature of bromine, it is important to be able to detect it quickly and remove it from the process. Rapid detection with Raman instrumentation could potentially reduce long-term maintenance costs in handling bromine-containing compounds.

#### 1.3.2.2 Iron and Steel Production

When steel is produced in large open hearth blast furnaces or using more modern Q-BOP processes, the molten iron, coke and other products are heated together until the proper concentration of carbon is produced in the molten steel. It is possible to determine the carbon content of the molten steel by analyzing the carbon containing gases that are given off from the molten mix. Measuring the ratios of  $\text{CO}/\text{CO}_2$  in the head space gas, it is possible to more accurately determine when the steel is ready. Currently up to 17% of the steel smelting time is related to obtaining samples for analysis. If the off-gases can be measured quickly, there is a substantial savings in time and money. Other gases of interest in the steel production process include,  $\text{N}_2$ ,  $\text{H}_2$ ,  $\text{O}_2$ ,  $\text{CH}_4$  and  $\text{H}_2\text{O}$ .  $\text{CO}$ ,  $\text{CO}_2$  and  $\text{N}_2$  exist in the range of 10 to 30%. The accuracy required for these gases is on the order of 0.1% (1000 ppm). The other gases are present at less than 10%, and the accuracy required is on the order of 0.01% (100 ppm). The gases start out at 1850 to 2000 °F (1000 to 1100 °C); it is possible to cool the samples down to 450 °F (200 °C) so that they can be monitored without risking condensation.

### 1.3.2.3 Natural Gas Transmission Lines

Natural gas requires continuous monitoring when it is shipped across state or national borders. Natural gas is sold by the heat content in British Thermal Units (BTU). Inert contaminants such as  $N_2$  and  $CO_2$  reduce the potential BTU content of natural gas. It is necessary to know the hydrocarbon content in addition to the inert components to be able to price a quantity of natural gas. The gas is transmitted under pressure in large 36" pipe lines. With this large quantity of gas that is being moved, the faster the analysis can be made the better. Current technology uses gas chromatographs (GC) and requires 80 to 100 seconds to determine the constituent concentrations at the 0.1% level. We feel that Raman could do this in times on the order of milliseconds. This improvement in speed could save the natural gas transmission industry millions of dollars. The fact that the gas is under pressure (500 psi) could be used to our advantage since the Raman signal increases directly with increased pressure. At 500 psi we could expect a Raman signal increase of roughly 35 times when compared to measuring at ambient pressure (14.8 psi).

### 1.3.2.4 Ethylene Production

Polyethylene is one of most commonly used plastics in the world today. It is generally made by dehydration of alcohols to produce the starting monomer, ethylene. The polymer is made in such large quantities that rapid, accurate analysis of the starting components is a must. Raman spectroscopy has the ability to measure the various components involved with ethylene production.

### 1.3.2.5 Ammonia Production

Since ammonia is very difficult to measure with conventional instrumentation, it requires wet chemistry. The fact that moisture is often present compounds the problem. Because ammonia is very water soluble, when moisture is removed from a sample stream, much of the ammonia is also removed. The ability of Raman to measure ammonia in the presence of water vapor makes the ammonia production application an excellent opportunity.

### Broad Application Potential

If we are successful in developing cost-effective Raman instrumentation for low detection (< 10 ppm) for one or two components, we can easily adapt the full spectrum technology to the above mentioned applications as well as many other gas phase analysis applications. We do not have to reinvent new technology for each new application.

#### 1.4 Phase II Technical Objectives

The thrust of this proposal was to develop an industrial Raman instrument that will meet the industrial gas phase environmental and process monitoring requirements. Phase I demonstrated the feasibility of using a multipass, external cavity enhancement cell coupled to a highly sensitive holographic spectrograph and inexpensive CCD array to measure a few key gases representative of environmental monitoring. Phase II continued on with the development of an actual instrument that is sufficiently rugged and "industrially hardened" to be capable of fast, remote, on-line continuous monitoring at a competitive market cost.

The overall objective of this project is to develop a reliable, competitively priced, laser-diode-pumped Raman scattering instrument capable of continuous on-line environmental pollutant monitoring. Phase I results demonstrated the feasibility to measure selected gases found in environmental and process gas analysis applications using affordable Raman instrumentation at low ppm levels in short integration times. The environmental monitoring market is not the only market opportunity, but because it is one of the largest, this is an excellent market in which to introduce this technology. The specific objectives required to accomplish our goal are geared to improving performance with increased Raman signal, reducing the overall cost of the instrument, and hardening the technology for continuous process monitoring.

We planned to focus our time and resources on one major application that involves two major market opportunities, one in the environmental pollutant analysis market and one from the process control market. More specifically, the environmental demonstration application was be the monitoring of bromine emissions in PTA production. The other was the monitoring of bromine in the process stream of PTA production. This application takes into account the best features of Raman instrumentation: 1) the ability of Raman to differentiate between many gas components including,  $\text{Br}_2$ ,  $\text{N}_2$ ,  $\text{O}_2$ ,  $\text{CO}_2$ ,  $\text{CO}$ ,  $\text{SO}_x$  and  $\text{NO}_x$  and 2) the fact that Raman can analyze these components with moisture present. The second application takes advantage of Raman's speed for use in the process side of PTA production.

The specific objectives were as follows:

1. To develop a Raman prototype process instrument capable of on-line analysis of  $\text{HBr}$  and  $\text{Br}_2$  at levels of 1 to 10 ppm at ambient pressure and temperature.
  - 1.a To incorporate our own fast, efficient, low cost, volume holographic transmission spectrograph allowing full spectral coverage while incorporating a relatively inexpensive CCD array.
  - 1.b To develop our own CCD camera control software and application specific software and graphics user interface (GUI) that will allow determination of gas phase composition.

- 1.c To develop a multipass, external cavity enhancement cell compatible with environmental analysis applications.
2. The prototype was to field tested on-line in a chemical production application for detection of HBr and Br<sub>2</sub> at ambient pressure and temperature.
3. To develop calibration procedures acceptable to the industry that assure the accuracy of the Raman analysis.

## 2.0 INSTRUMENTATION DEVELOPMENT AND TESTING

### 2.1 Introduction

The initial design for our gas-phase Raman prototype is illustrated in Fig. 5. An argon laser operating at 488 nm with a power level of approximately 2 W is used as the excitation source for the Raman measurements. Light from the laser is focused using the lens  $L_1$  to a point near the center of the mirror cavity formed by mirrors  $M_1$  and  $M_2$ . The mirrors  $M_1$  and  $M_2$  are mounted in gimbal mounts on translation stages to allow adjustment of their separation distance and orientation. Raman scattered light which emanates from the dual focal points near the center of the mirror cavity is collected by the lens  $L_2$  (Nikon f/1.2 camera lens), which is mounted on three translation stages to allow adjustment in the x, y, and z directions. For some measurements a fixed f/1.4 camera lens included with the prototype spectrometer is used for scattered light collection. The mirror  $M_3$  re-images backscattered Raman radiation from the focal points and directs it forward to be collected by the lens  $L_2$ .

The first-generation prototype spectrograph included (1) a f/1.2 camera lens for collection and collimation of the scattered light, (2) a laser-line rejection filter operating at 488 nm and placed in the collimated scattered light, (3) a f/1.4 camera lens to focus the filtered scattered light onto a slit, (4) a vertically oriented optical slit with a width of 150 micrometers, (5) a third f/1.4 camera lens to recollimate the scattered light emanating from the slit, (6) a volume holographic diffraction grating sandwiched between two aberration-correction prisms to spatially disperse the scattered light, (7) a f/1.3 camera lens to image the dispersed spectrum onto the detector, and (8) a CCD detector from Santa Barbara Instruments Group (SBIG, 7i) to convert the spatially dispersed scattered light distribution into a digitized Raman spectrum.

Figure 6 compares Raman data from ambient nitrogen obtained with this prototype system using a single pass of laser light, a double pass of laser light, and a double pass of laser light in conjunction with the rear mirror. The measured enhancement achieved with a double pass of laser light is 1.88, and that for a double pass and the rear mirror is 3.10. Similar Raman data from ambient oxygen exhibiting enhancement factors of 1.85 and 3.12 are shown in Fig. 7. This double pass configuration used in conjunction with the rear collection mirror might be suitable for many gas monitoring applications which only require gas detection at relatively high concentrations (near 0.1%). The configuration has the advantage of being easier to align and mechanically more robust.

We measured the ability of the multipass cell to enhance Raman data from ambient air by comparing signals obtained with a single pass of laser light to those obtained with the multipass cell optimally aligned. The rear mirror was again removed. Figure 8 displays the best results we were able to achieve. The Raman signals from nitrogen and oxygen are enhanced by factors of 43.9 and 53.1, respectively. We are not sure why the nitrogen and oxygen enhancement factors differ, but we suspect that the single and multipass data were obtained with different grating orientations which would cause the diffraction efficiency as a function of wavelength to shift.

## GAS PHASE PROTOTYPE

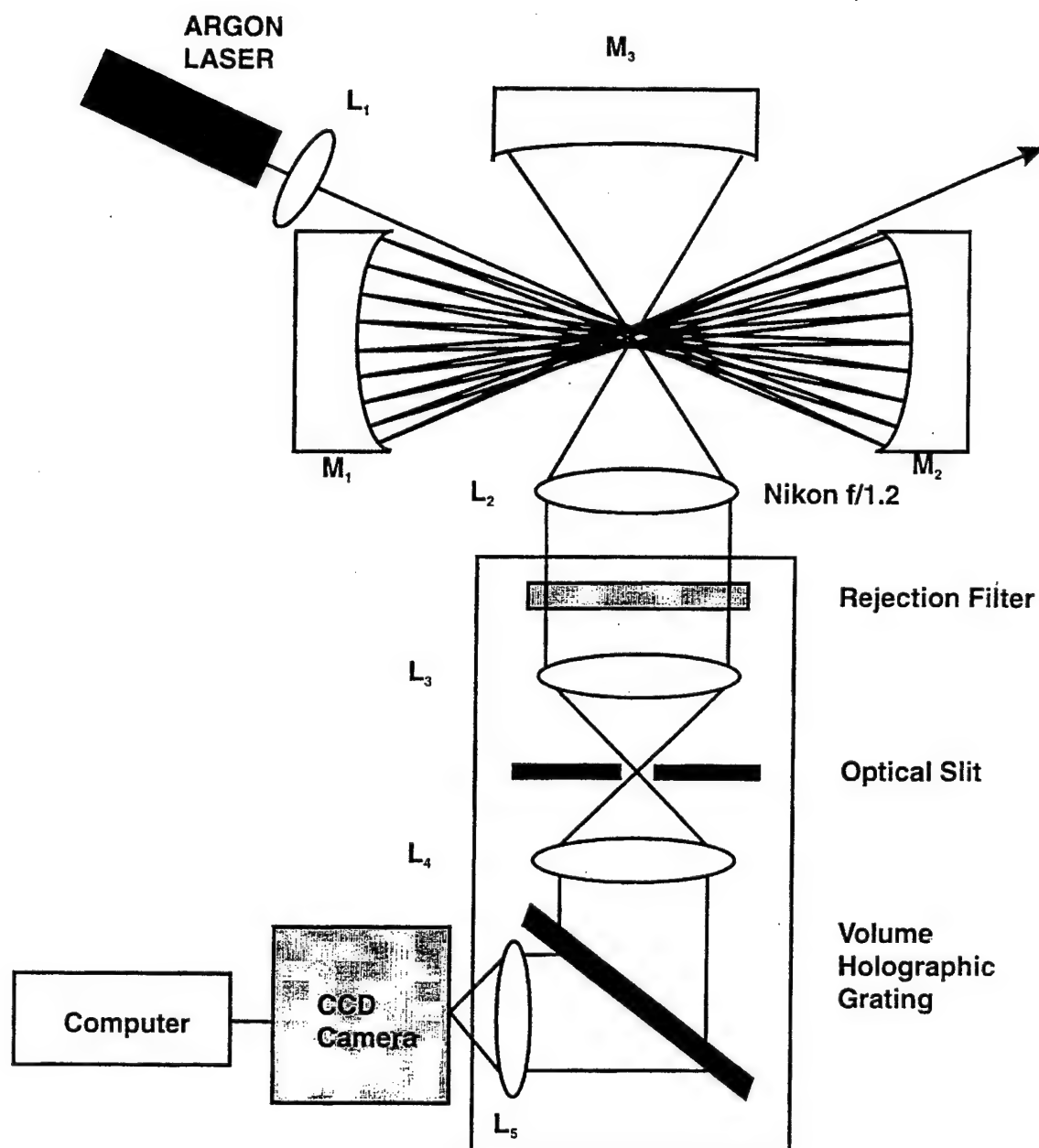


Figure 5. Initial design for our gas-phase Raman prototype. An argon laser operating at 488 nm with a power level of approximately 2 W is used as the excitation source for the Raman measurements. Light from the laser is focused using the lens  $L_1$  to a point near the center of the mirror cavity formed by mirrors  $M_1$  and  $M_2$ .



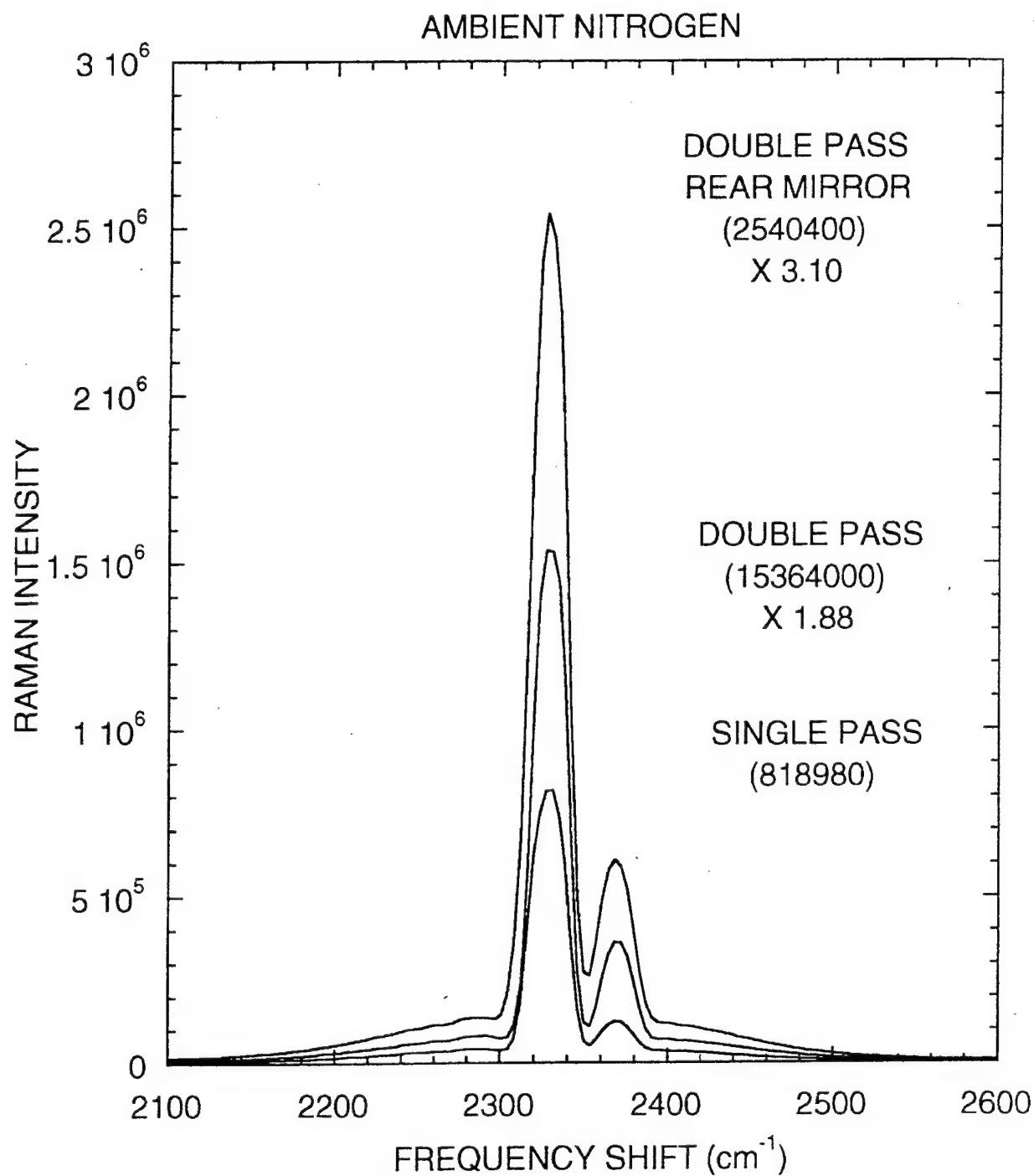


Figure 6. Raman data from ambient nitrogen obtained with this prototype system using a single pass of laser light, a double pass of laser light, and a double pass of laser light in conjunction with the rear mirror.

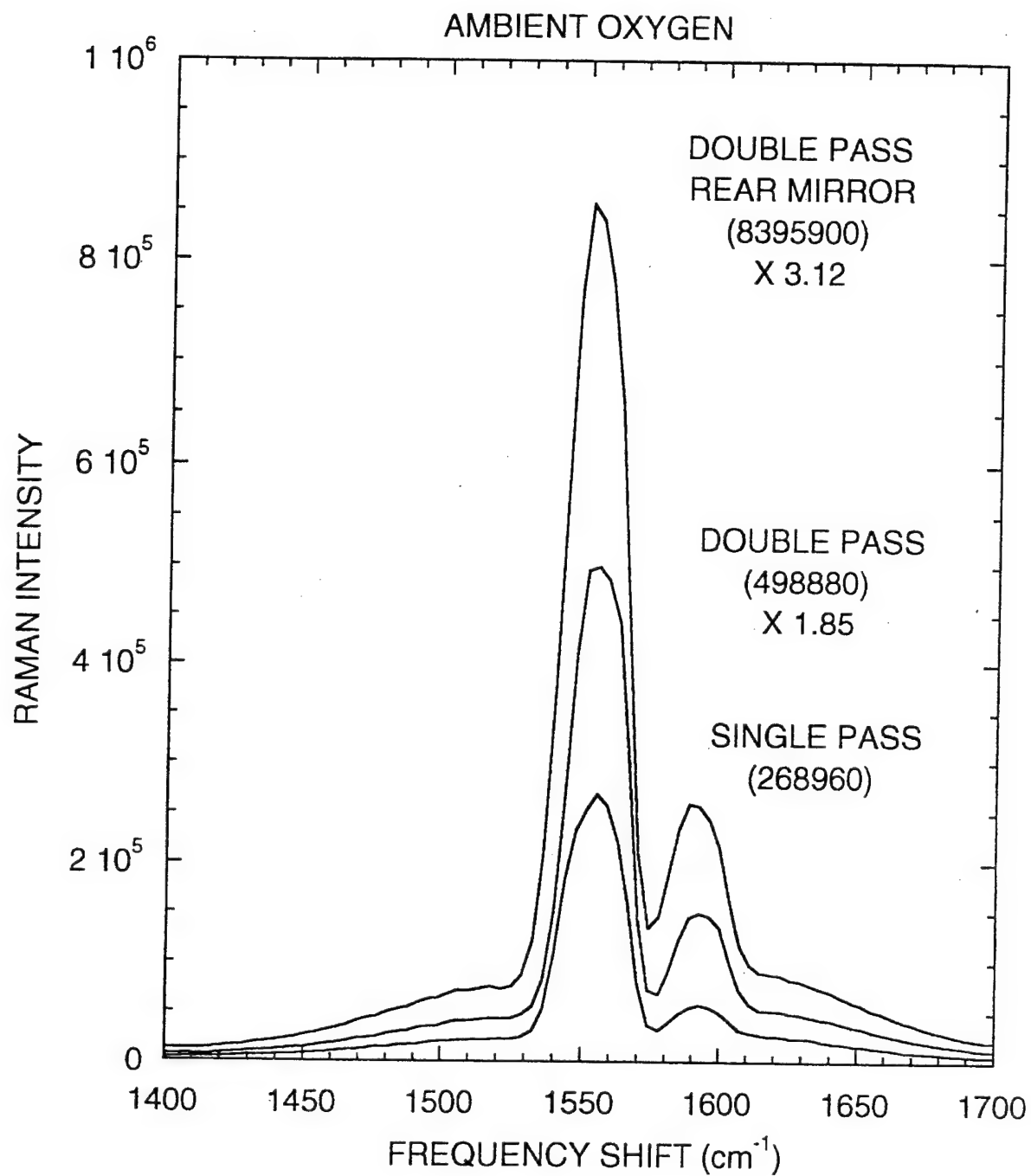


Figure 7. Raman data from ambient oxygen exhibiting enhancement factors of 1.85 and 3.12

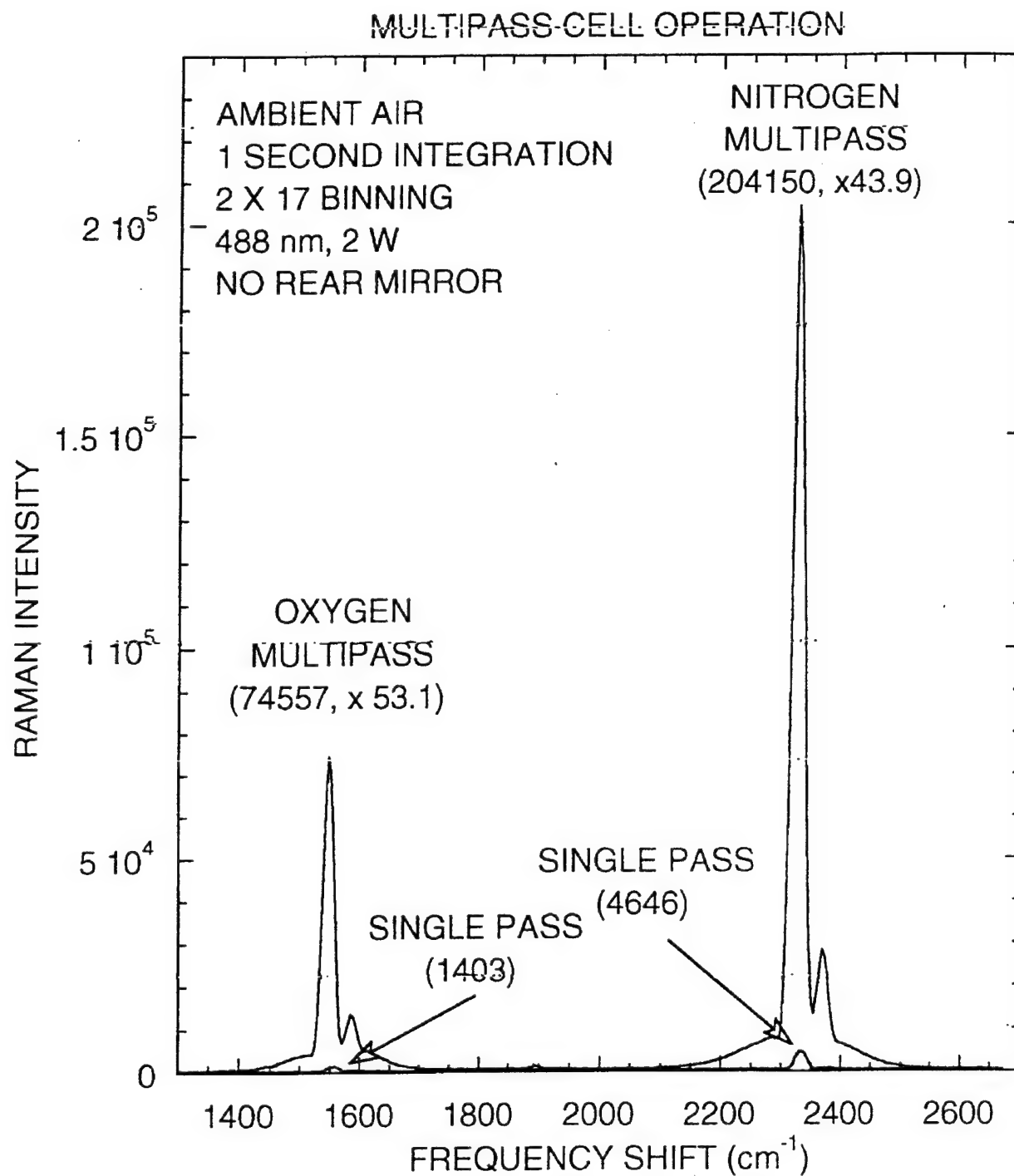


Figure 8. Measurement of the ability of the multipass cell to enhance Raman data from ambient air by comparing signals obtained with a single pass of laser light to those obtained with the multipass cell optimally aligned.

This change in grating orientation is likely since the nitrogen-to-oxygen peak ratios vary in the single and multipass data. Nevertheless, we were encouraged by the average enhancement factor of 48.5 which is very close to the factor of 50 we had originally hoped to achieve. The multipass cell alignment was rather sensitive to vibrations and to dust particles flowing through the laser beams. To test the stability of the system, we collected 100 Raman spectra from ambient air as shown in Fig. 9. The data exhibit good repeatability, but there are a few spectra with lower peak heights which may have been collected as dust particles passed through the excitation light. Figure 10. plots the nitrogen and oxygen peak heights observed in the 100 spectra. The nitrogen and oxygen signals have standard deviations of 0.93% and 0.82%, respectively.

The remaining sections of this chapter summarize work completed to improve the performance of the prototype instrument and to harden its design so that it could serve as an effective gas monitor in industrial environments. Sections are included for laser development, sample cell construction, spectrograph design, and CCD detector evaluation. A last section summarizes the performance of the final prototype.

## MULTIPASS CELL OPERATION

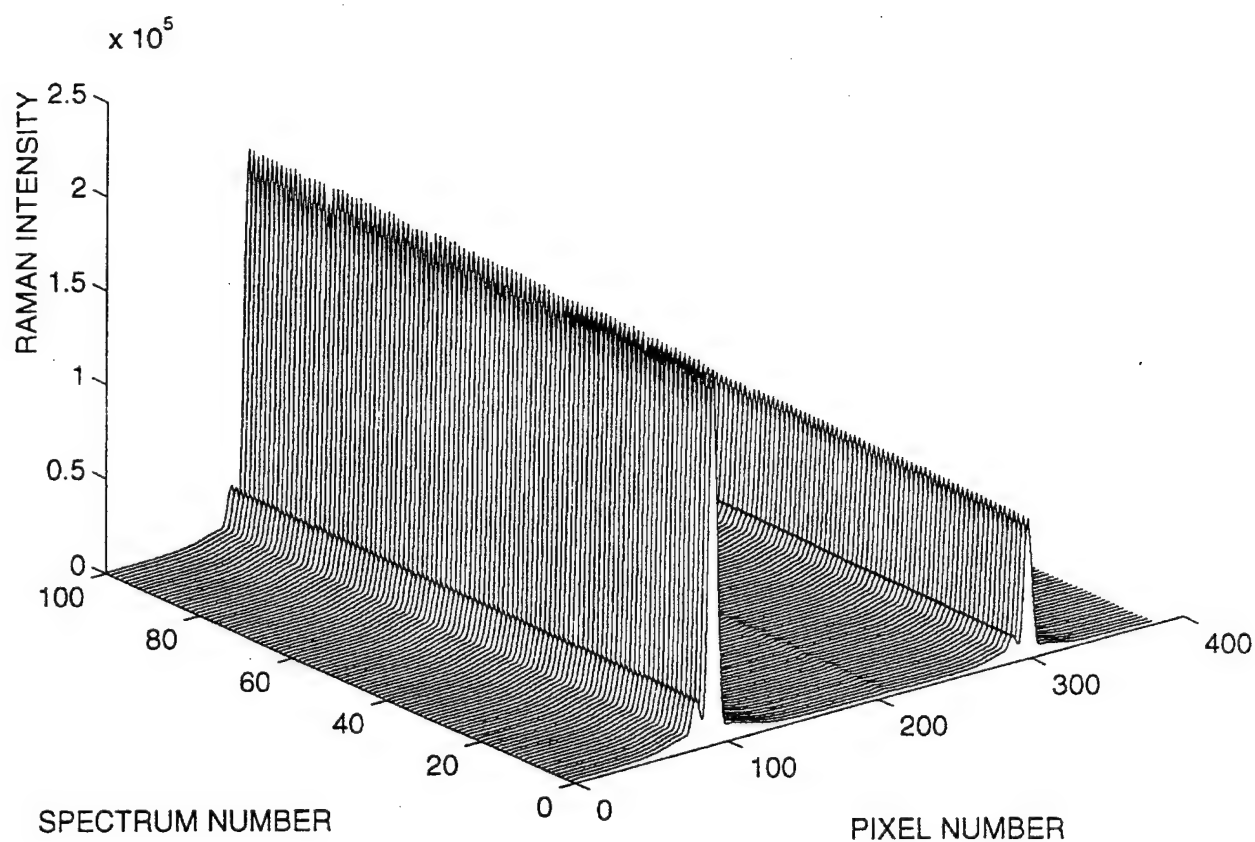


Figure 9. One hundred Raman spectra from ambient air. The data exhibit good repeatability, but there are a few spectra with lower peak heights which may have been collected as dust particles passed through the excitation light.

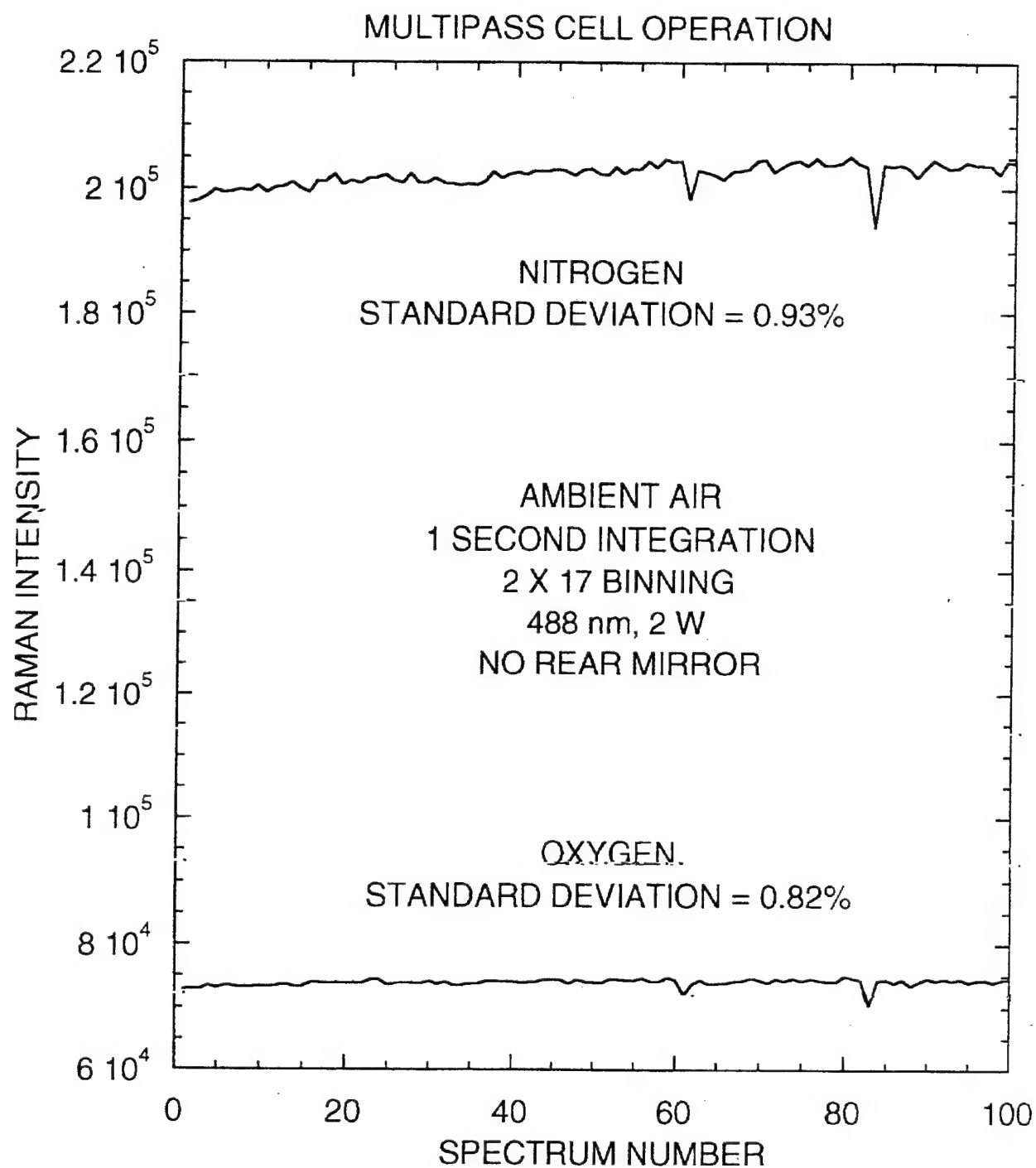


Figure 10. The nitrogen and oxygen peak heights observed in the 100 spectra. The nitrogen and oxygen signals have standard deviations of 0.93% and 0.82%, respectively.

## 2.2 Laser Sources Evaluated and Developed

The excitation source for our initial gas-phase Raman measurements was an argon ion laser operating at a wavelength of 488 nm with an output power level of approximately 2 W and vertical polarization. While this laser provided a convenient source of visible light with good beam quality for our initial feasibility studies, it was never considered to be a practical source for our portable Raman gas monitor because of its large size, high cost, high power consumption, need for water cooling, and relatively poor reliability. Use of the argon laser did, however, allow us obtain some baseline Raman data for comparison with that obtained later in the program with more practical sources and to make progress in the design of other system components such as spectrographs, CCD detectors, and sample cells while we were developing a more practical excitation source.

From the onset of the Phase I feasibility study, we had regular meetings with American Laser Corporation (Salt Lake City, Utah) about incorporating a laser diode-pumped, frequency-doubled Nd:YAG laser they were developing into our portable Raman system. Their system was expected to be relatively low cost and to provide 2-3 W of laser output at a wavelength of 532 nm in a high quality beam which would have been ideal for use with some of the multipass enhancement cells designs we were considering. However, when the laser became available for testing, we learned that the laser output stability was only controlled to within 1-2 %. We concluded that the output stability was not adequate for many industrial gas monitoring applications and that the cost of the laser (approximately \$12,000) was too high to be incorporated in a Raman gas monitor which could be sold at a competitive price.

### 2.2.1 Diode Array

We next explored the possibility of using a high-power diode array operating near 670 nm in an external-cavity-stabilized configuration to control and narrow the output line width. We also worked with our volume holographic optics supplier to develop a grating design for use in the external cavity for wavelength stabilization. The volume holographic optical element incorporated the advantages of both the Littman and Littrow cavity designs while offering improved simplicity, cost reduction, and small size. The whole system included a commercial laser diode array, two cylindrical lenses for collimating, and a retro-reflective volume holographic grating.

After testing the diode array concept, we found that in order to stabilize and narrow the 2-3 nm output line width of the diode array, we had to efficiently couple the laser energy back into the 16 individual diodes which made up our 5-W diode array. This configuration required considerably more optical components, each contributing additional losses. The combined losses severely limited the output power below the 2-3 W we required. In addition, the high cost of the diode array, \$3000, would have made its use in our Raman prototype difficult to justify.

### 2.2.2 External Cavity, Power Build-Up Cavity

As an alternative to the expensive diode array, we decided to try a passive external power build-up cavity that was pumped with a low-cost diode laser operating near 670 nm. We chose a multimode high power visible laser diode (LD2308-665-C-AR) at 665 nm, which was ordered from LDX Optronics and shipped to Blue Sky for installation of a microlens, as the pump source for the power build-up cavity. We found that the laser is actually only 75 x 1 micrometers in size rather than the advertised 90 x 1 micrometers. This laser with less than 0.3% AR coating has a threshold current of about 450 mA and output power of about 200 mW at 650 mA.

One of the mirrors for the power build-up cavity with greater than a 99.999% reflectivity was ordered from Research Electro-Optics, Inc. This "off the shelf" mirror has an AR coating on the plano side and dimensions of 7.75 mm diameter x 4mm thick. An additional mirror for the buildup cavity, with designed reflectivity of about 98%-99%, was ordered from CASIX, Inc. The dimensions of this mirror are 10 mm diameter x 5 mm thick. Both mirrors for the cavity have a 50 mm radius. We also received a half waveplate from CASIX which was used for polarization rotation.

While we were waiting for the diode laser and cavity mirrors, we did some computer simulations in order to estimate the expected buildup power and feedback strength to the diode laser. Figure 11 shows the simulation results for intracavity circulating power assuming a 300 mW input power and a 50% mode-matching efficiency. With this level of power (30-60 watts) in the visible wavelength region, parts per million concentrations of gas samples should be detectable using Raman technology. Figure 12 shows the feedback strength (or reflectivity) from the buildup cavity to the diode laser based on the same parameters used in Fig. 11. Theoretically, stronger feedback allows more stable operation of the whole system.

The multimode high power visible laser diode (LD2308-665-C-AR) with output wavelength at 657 nm sent to Blue Sky for microlens installation has a small piece of fiber attached to the laser which acts as a cylindrical lens to control the fast axis of the diode laser. With installation of the microlens, the fast axis angle is narrowed to 5.15 degrees compared to 35 degrees without the microlens. The slow axis is measured to be about 5.43 degrees. Both axes now have similar far field angles which is good for mode matching to the power buildup cavity. We also measured the wavelength of the laser. Surprisingly, we found two lobes in wavelength. Both lobes are close to 656 nm, and the bandwidth is about 1.8 nm.

We also measured three different power vs. current (L-I) curves. As shown in Figure 13, the solid-line curve represents the uncoated laser chip. At 700 mA, the power reaches 220 mW. In the same figure, the dashed-line curve represents the AR-coated laser chip (~0.3%). The threshold increases to 450 mA, and the slope efficiency increases. At 700 mA, the coated laser reaches 190 mW. The last curve (double-dash line) is from the final laser chip with both the AR coating and the microlens. Again, the threshold increases to 500 mA, and the power drops to 117 mW at 700 mA. This is the available power (~120 mW) that can be used as the pumping power



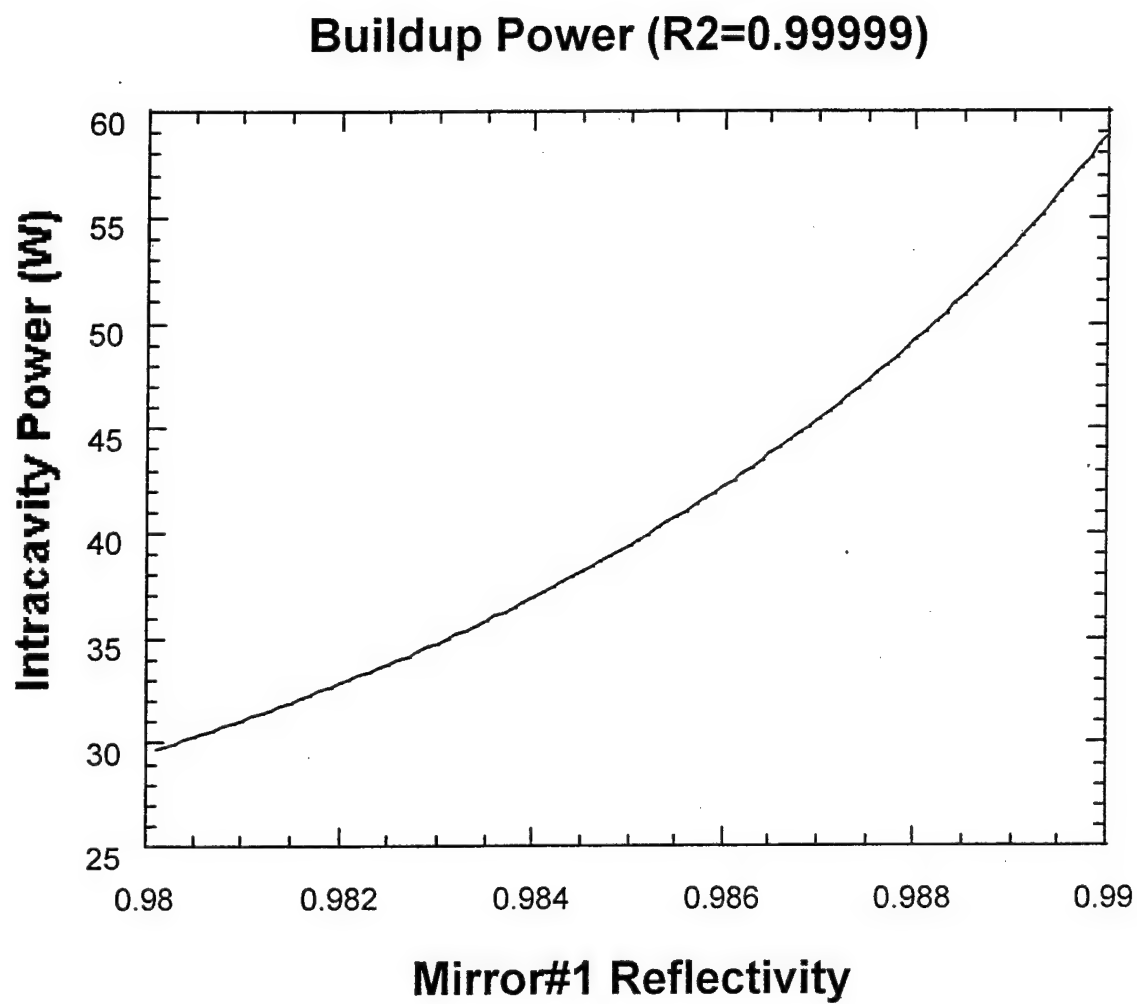


Figure 11      Circulating power inside the cavity from a 300 mW visible diode laser at 665 nm.

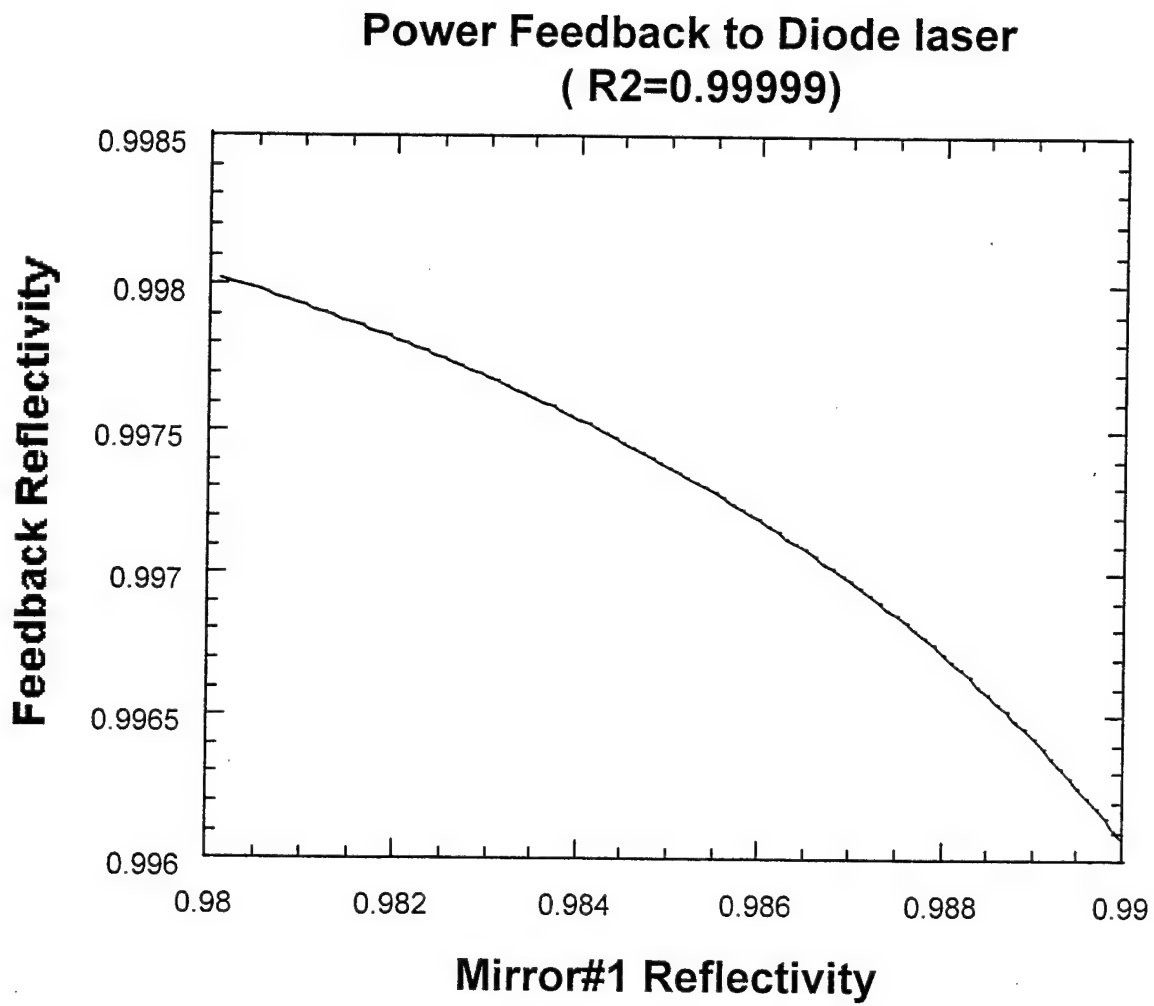


Figure 12      Simulation of Optical Feedback (OFB) from the power buildup cavity to the laser diode.

# Power vs Current

## High power visible diode laser

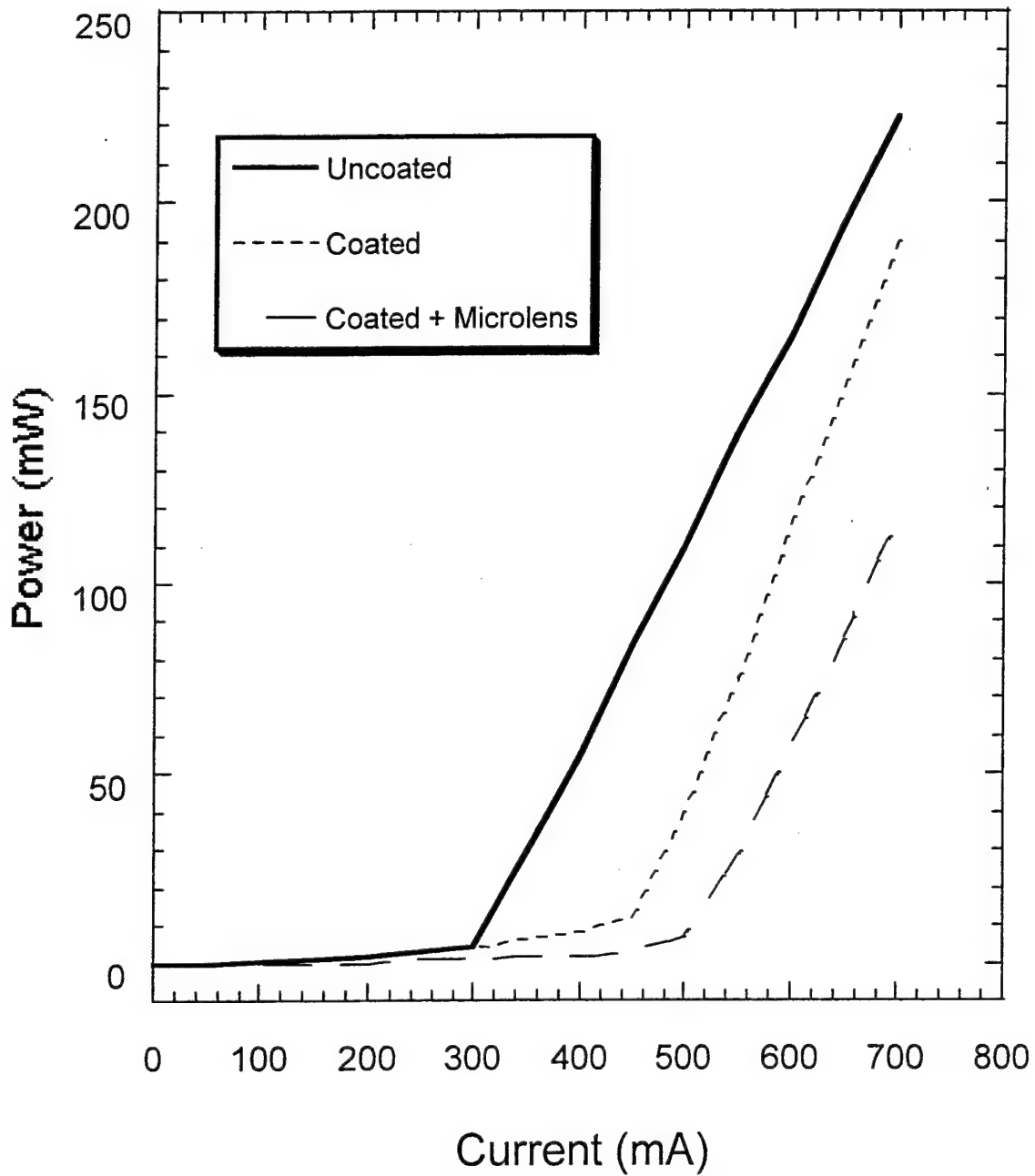


Figure 13 LI curves for diode laser in non-coated, coated, and coated plus microlens configurations.

for the power buildup cavity. While the microlens improves the beam quality, it greatly reduces the available pumping power to the build-up cavity.

We tested the multimode high power visible laser diode (LD2308-665-C-AR) with output wavelength at 657 nm in a diode-pumped cavity configuration. As indicated in Fig. 14, the 100 mW visible diode laser with a microlens installed was used as the pumping source, and a 4.5 cm spherical cavity was used as an external feedback cavity to lock the frequency of the diode laser. With proper alignment of the mode-matching lens and the cavity mirrors, output powers as high as 60 W inside the cavity were achieved. Figure 15 depicts the power achieved as a function of laser current. The device has a threshold current of about 350 mA, and the buildup power is 60 W at 700 mA. Although 60 W of optical power is very useful for gas phase Raman sensing, the bandwidth of this device is too broad ( $\sim 2$  nm) for many Raman applications. The wavelength profiles with and without optical feedback (OFB) from the cavity are shown in Fig. 16. Without OFB, the laser only shows three longitudinal modes ( $\sim 0.5$  nm). With OFB, not only does the laser shift  $\sim 3$  nm, but also its bandwidth is wider (seven longitudinal modes). For this device to be useful in Raman applications, bandwidth compression is necessary.

We also tested a laser diode without a microlens in order to increase the pumping power for the power build-up cavity from 100 mW to 200 mW. Three different mode-matching lenses were tested for use with the power build-up cavity. With the microlens removed, we found that a single lens wasn't adequate to match the optical modes inside the cavity and consequently, the mode-matching efficiency was reduced. Based on the experimental results, the average buildup power inside the cavity was only about 2.4 watts compared to the previous result of 60 watts with the microlens lens. Thus, even though the input power increases by factor of 2, the mode matching is poor and the total circulating power is much less without the microlens.

To narrow the output linewidth of the broad-area laser, we inserted a Volume-Holographic Transmission Grating (VHTG) designed for use at 670 nm between the laser diode and the buildup cavity. This grating made by Ralcon Laboratories has dimensions of 1" x 1" x 0.08" and a groove density of about 2100 grooves/mm. The first order beam appears at 45 degrees from the normal, and its efficiency is about 90 %. As calculated from theory, the grating should compress the laser linewidth from 1 THz to  $\sim 30$  GHz. This 30 GHz bandwidth is more than sufficient for most gas phase Raman applications. We can also use this grating to tune the laser wavelength. The tunability of the device allows the laser wavelength to be matched to the laser notch filter incorporated in the spectrograph which results in better laser line rejection in collected Raman spectra. The experimental setup is shown in Figure 17. In addition to the grating, we also inserted a half waveplate just in front of the cavity. This half waveplate is necessary for Raman detection because of the multimode output from the broad-area diode laser. The broad-area diode laser emits near a gaussian beam in the direction parallel to the p-n junction but emits a multimode beam in the direction perpendicular to p-n junction. Thus, in order to use a narrow slit in the spectrograph, we need to use this half waveplate to rotate the laser polarization by 90 degrees to maintain good beam quality. The cavity is about 4.5 cm long, and the distance between the laser diode and the center of the cavity is about 8 cm.

## DIODE-PUMPED POWER BUILDUP CAVITY

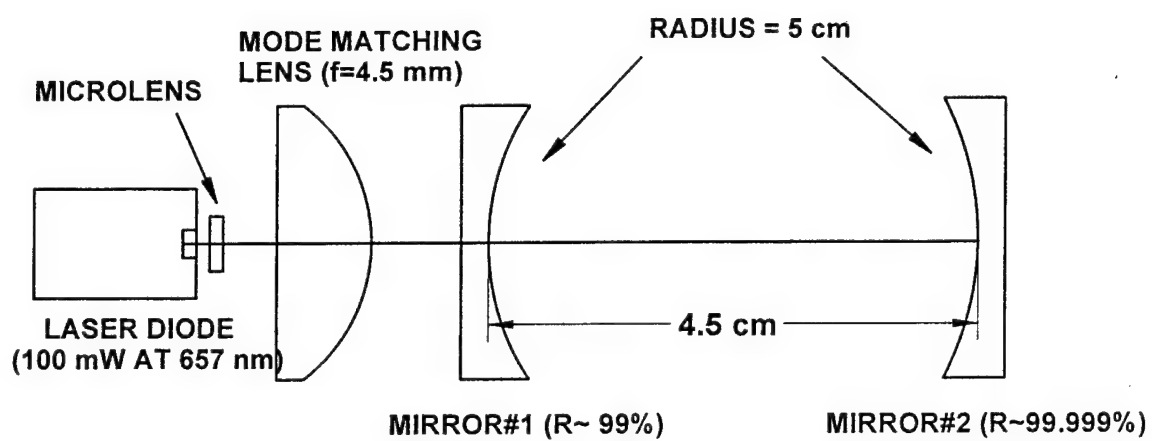


Figure 14 Process Instruments' external cavity diode laser configuration.

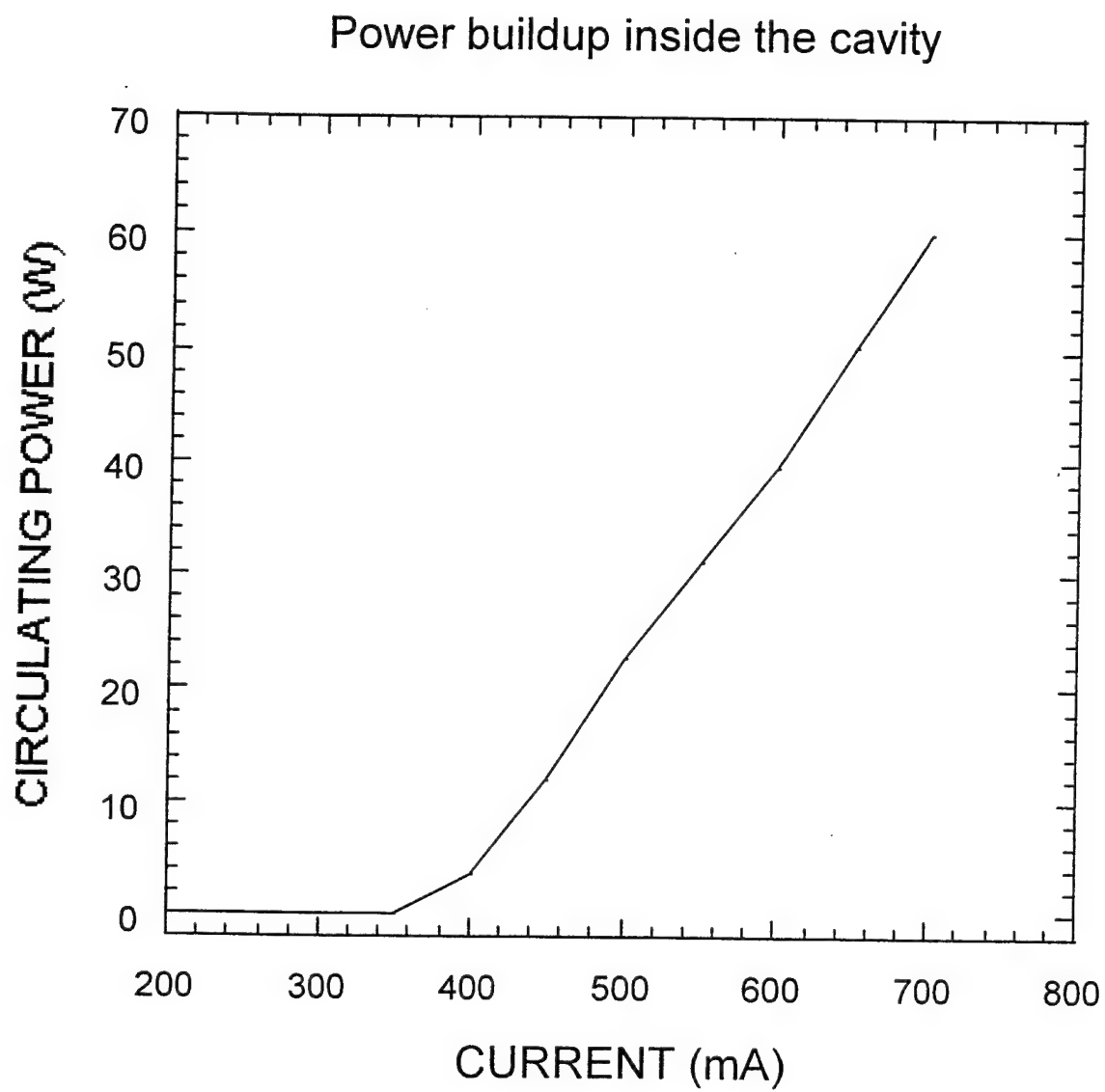


Figure 15 Power build-up curve for external cavity diode laser.

## Frequency Pulling Effect

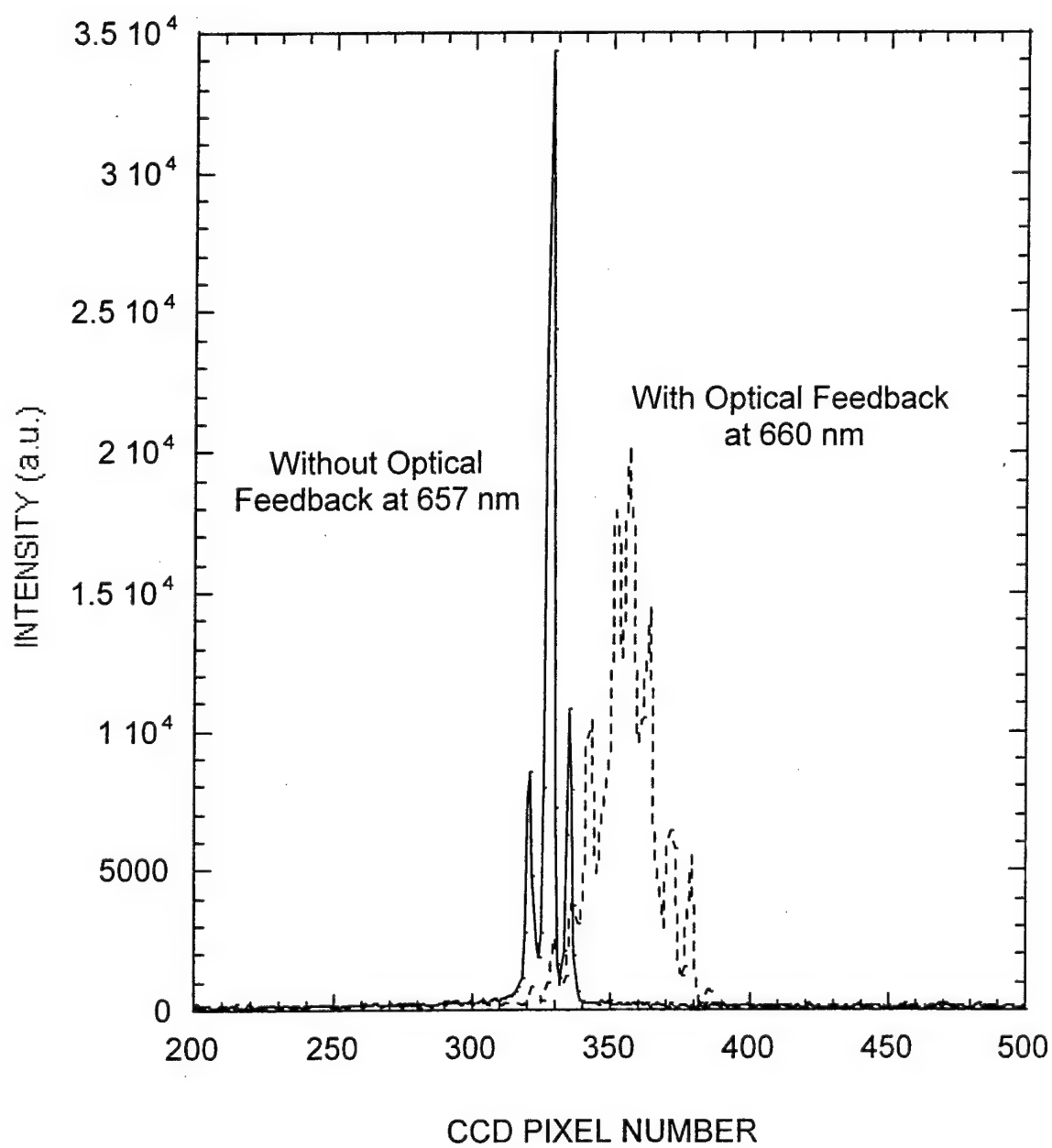


Figure 16 Laser output with and without feedback.

# DIODE-PUMPED POWER BUILDUP CAVITY WITH NARROW LINEWIDTH OUTPUT

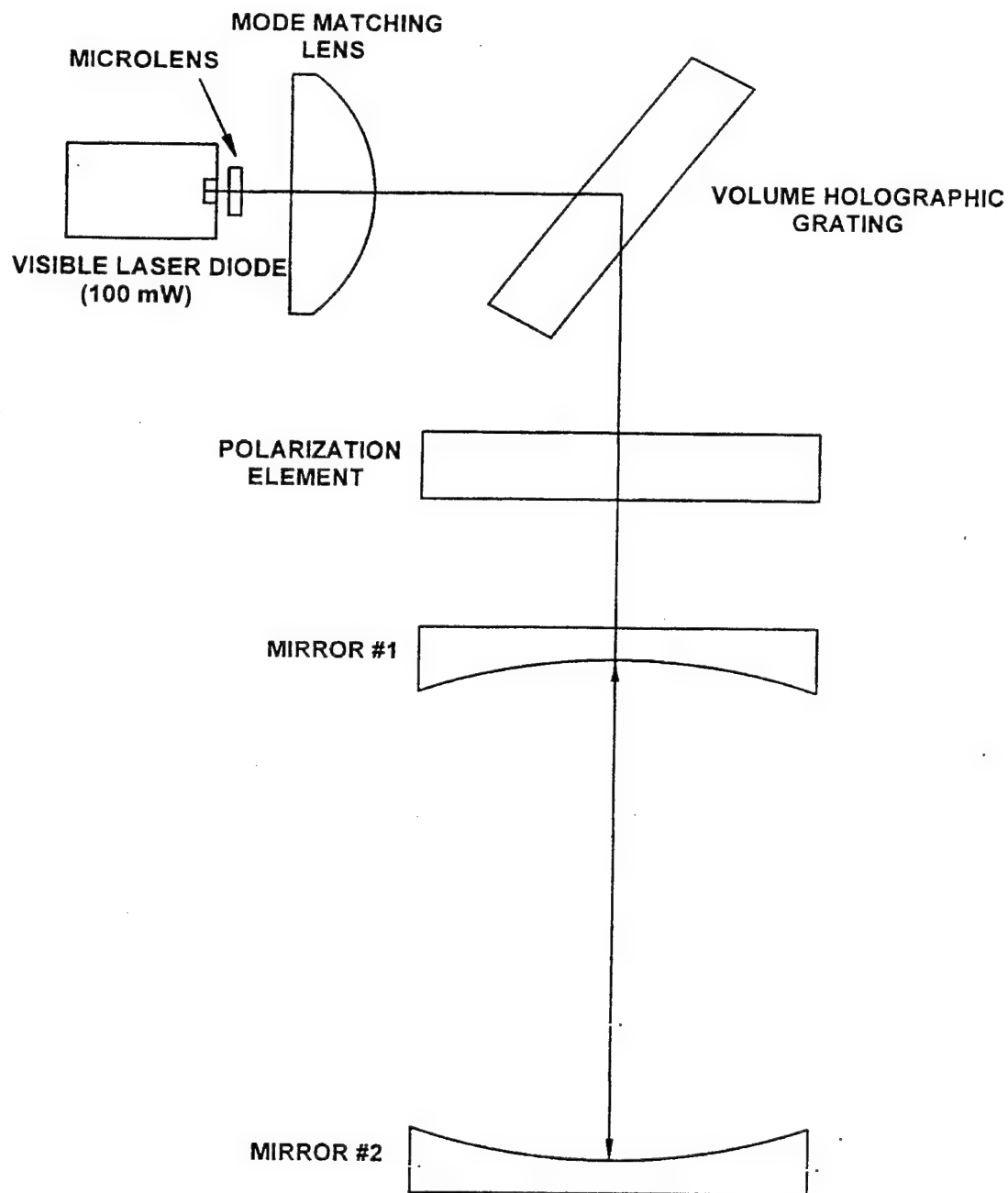


Figure 17. Experimental optical setup allowing for tunability of laser wavelength and linewidth narrowing.



### 2.2.2.1 Narrowed Line width

The results of the linewidth narrowing are depicted in Figure 18. As shown in the figure, the grating successfully selects only one longitudinal mode and compresses the laser linewidth to about 30 GHz which is better than the resolution of the spectrograph. Without the grating, the laser emits 7 longitudinal modes and covers almost 2 nm. Typically, we can tune the laser wavelength over 10 nm from 653 nm to about 663 nm. We also measured the circulating power inside the cavity versus the pumping current as shown in Figure 19. Compared to the circulating power without the grating, we only obtain about 20 % of the original optical power. This is not surprising because the grating increases the loss, and the mode matching efficiency is less when the distance between the cavity and the broad-area diode laser is greater. When the device is pumped at 700 mA, it should provide 24 watts (12 watts in each direction) of useful power for gas phase Raman sensing.

To use the Power Buildup Cavity (PBC) for Raman detection of gases, we setup the PBC in front of a f/1.4 spectrograph with a TE-cooled CCD detector. The CCD is cooled to 0 °C, and a 250 micrometer slit is used with the spectrograph. Since the PBC generates more power without linewidth narrowing, we initially only used a half waveplate between the laser diode and the PBC. We can routinely produce 30-40 watts of the intracavity power by using this configuration, although the maximum power we have obtained is 60 watts. As shown in Fig.20, the PBC is set vertically to the optical table and the laser polarization is perpendicular to the slit of the spectrograph in order to maximize the Raman signals. As calculated from the theory, a single mode beam size in the center of the PBC is ~ 150 micrometers. In the other dimension, the beam size is about 500 micrometers because of its multimode behavior. Usually, the depth of focus of the collection lens is greater than 500 micrometers, and it should still be able to collect the Raman signals efficiently. By carefully adjusting the distance between the PBC and the spectrograph, we can maximize the signals. In the spectrograph, a 1200 grooves/mm grating and a Santa Barbara 7i CCD camera were used.

Figure 21 shows the Raman spectrum obtained from ambient air with the system. For 30 watts of circulating power inside the PBC at 660 nm and with a one minute integration time, we have 182750 counts of signal for nitrogen and 76388 counts of signal for oxygen. Figure 22 depicts measured Raman spectra from ambient air with two different laser polarization directions. Without the half waveplate, the signal drops to only about 6% of its value with the optimum polarization. The bandwidth of the s-polarization signals also increases. Finally, we tested the long term stability of the device by using ambient air. As shown in Fig. 23, the nitrogen peak had a 16% Standard Deviation (SDV) and the integrated signal had a 9.25 SDV over a period of approximately 14 hours.

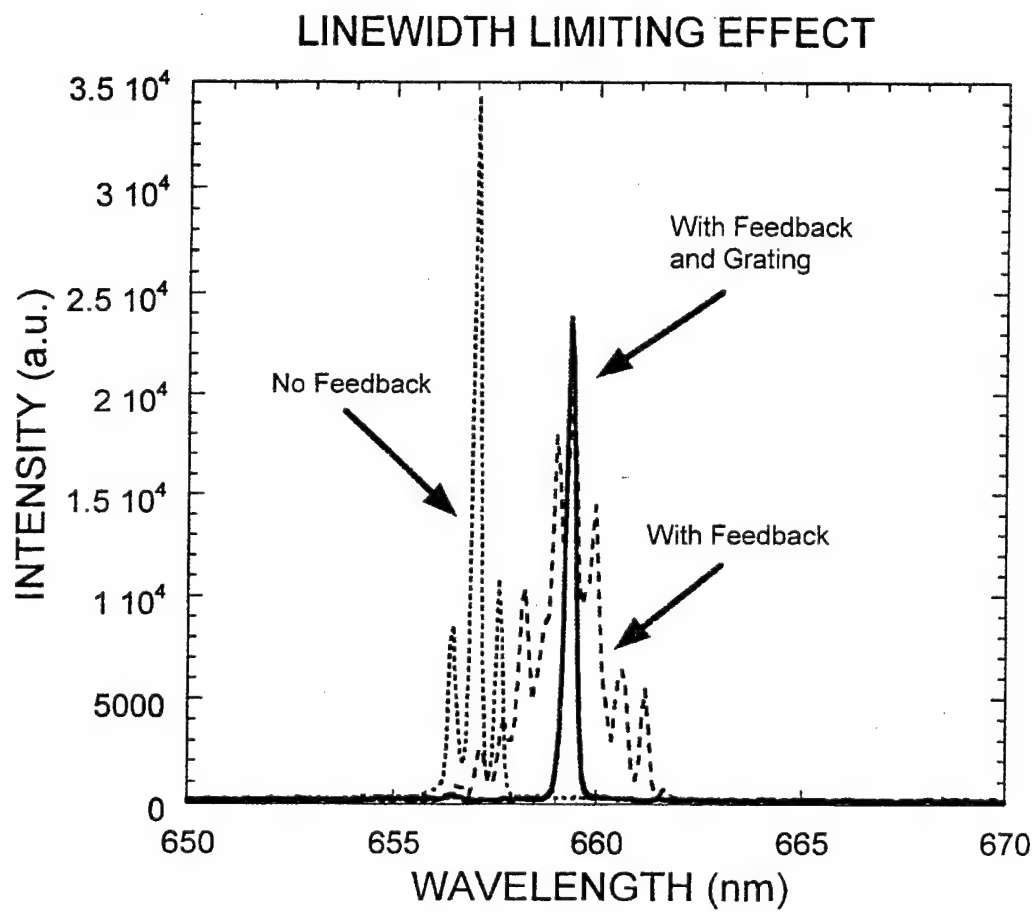


Figure 18 Results of linewidth narrowing with grating feedback.

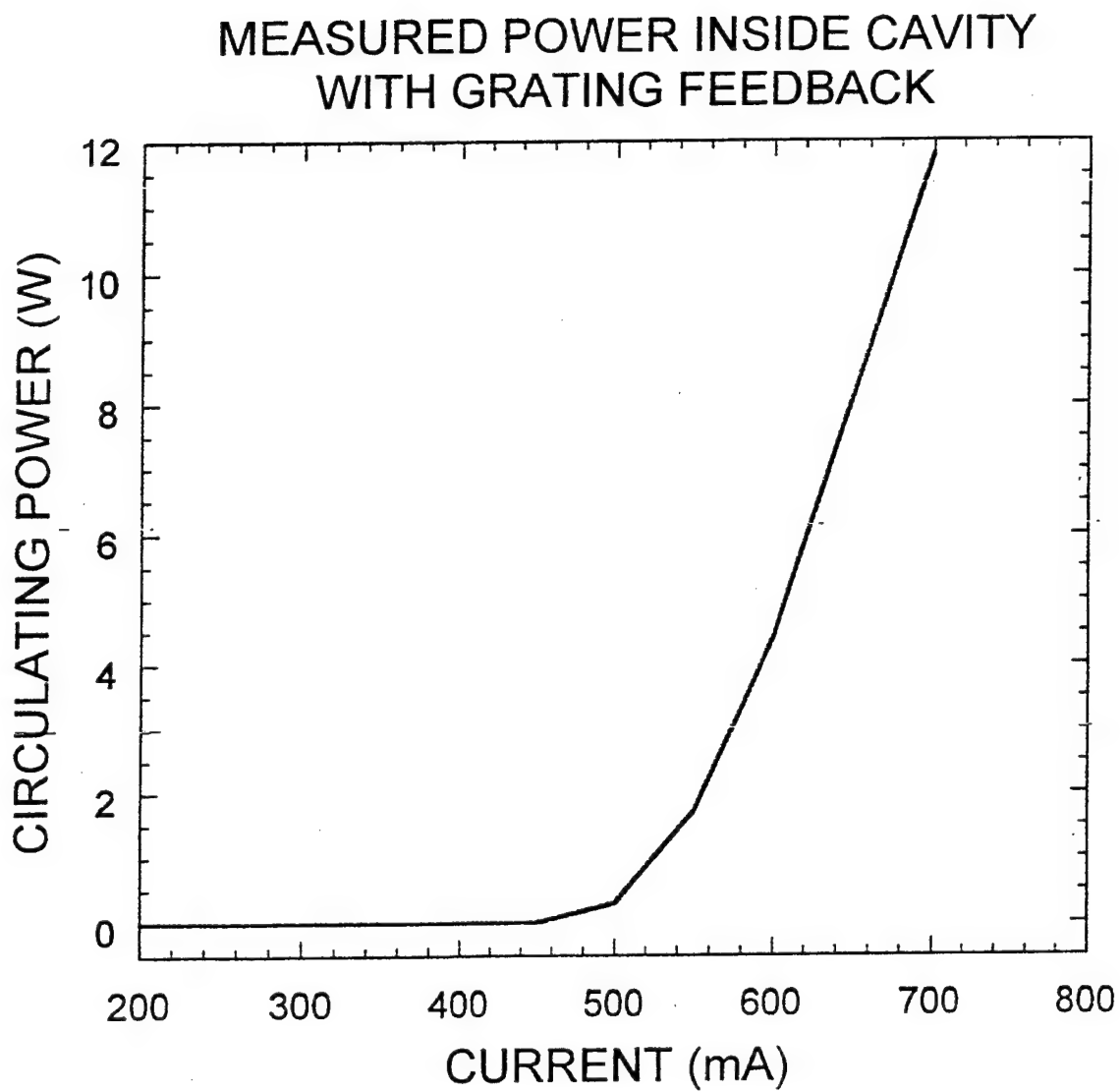


Figure 19. Circulating power inside cavity with grating feedback versus the pumping current.

## EXPERIMENTAL SETUP FOR GAS PHASE RAMAN SENSING

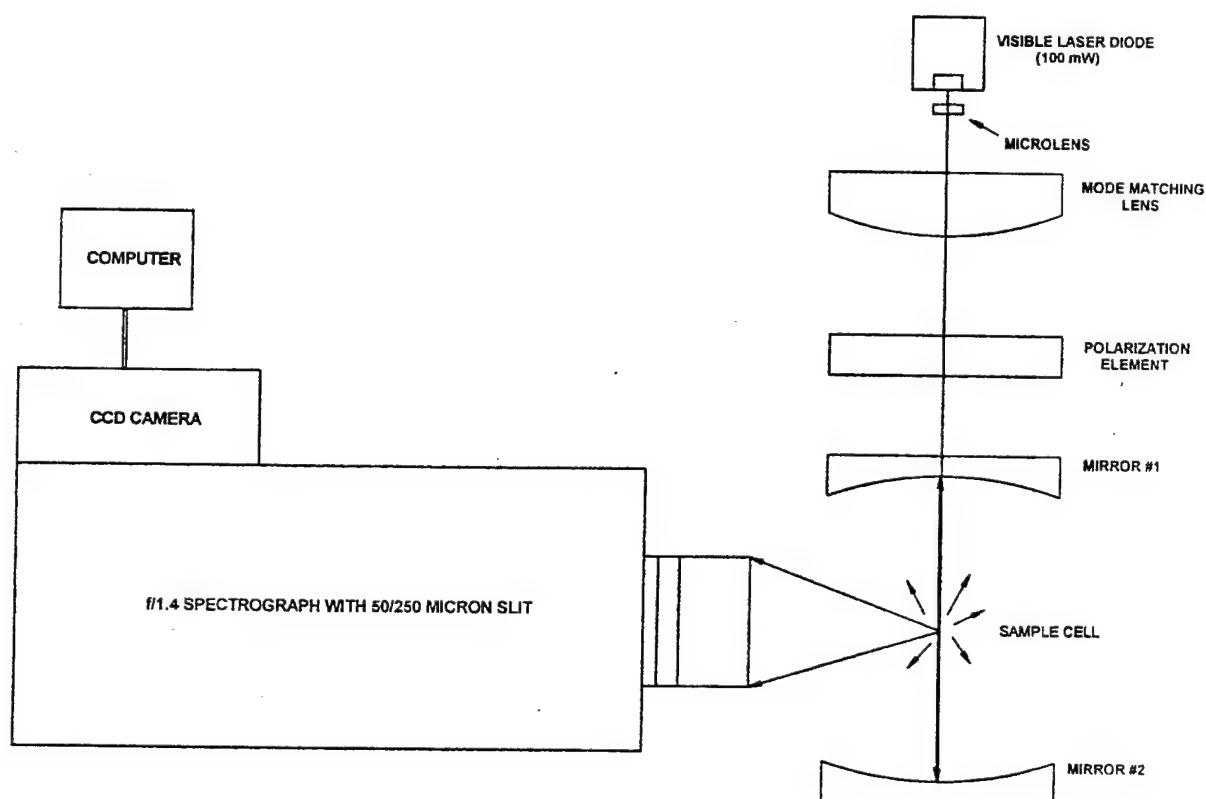


Figure 20. Experimental setup for collection of Raman data with Power build-up cavity (PBC).

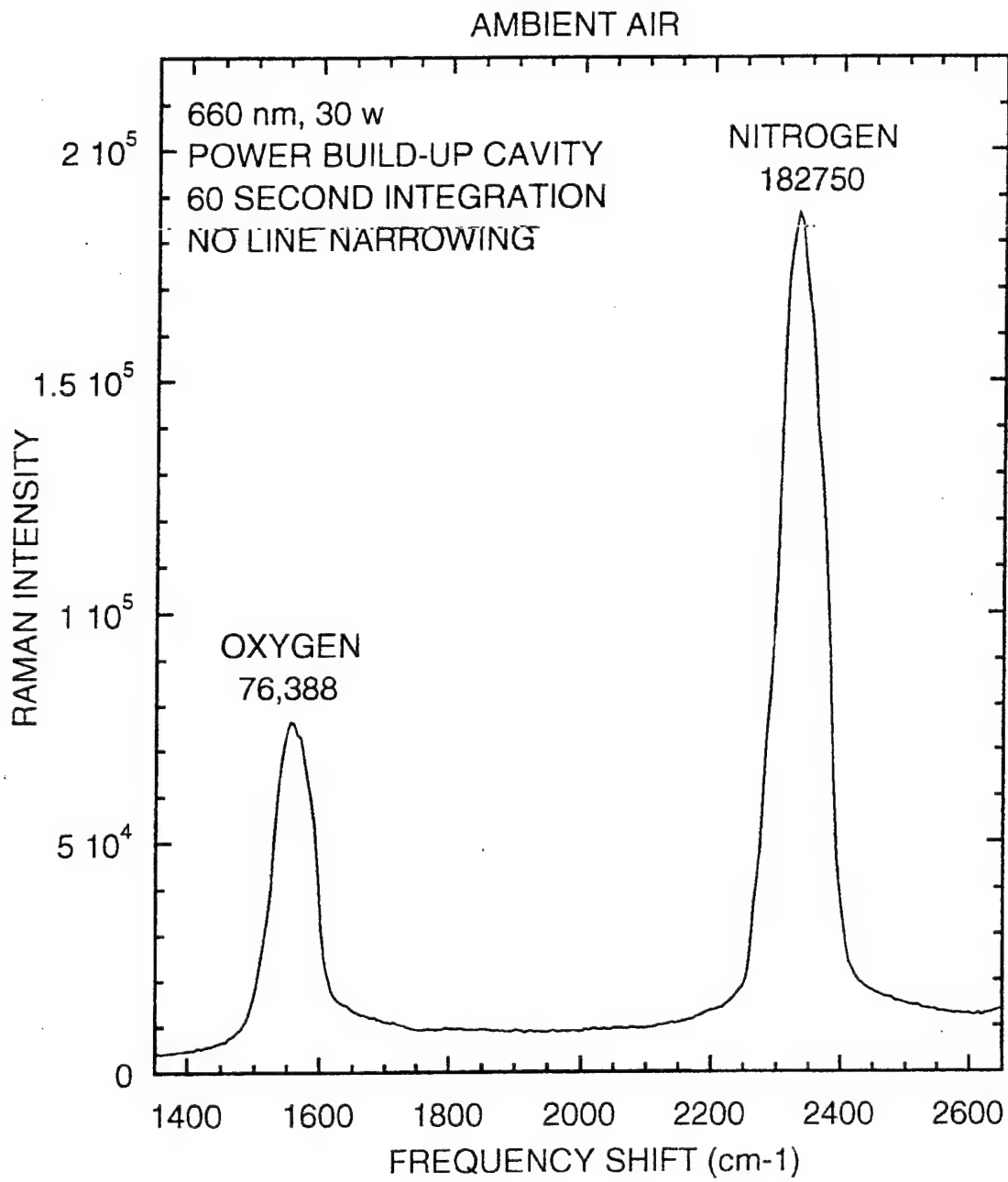


Figure 21. Raman spectrum obtained from ambient air with no laser linewidth narrowing.

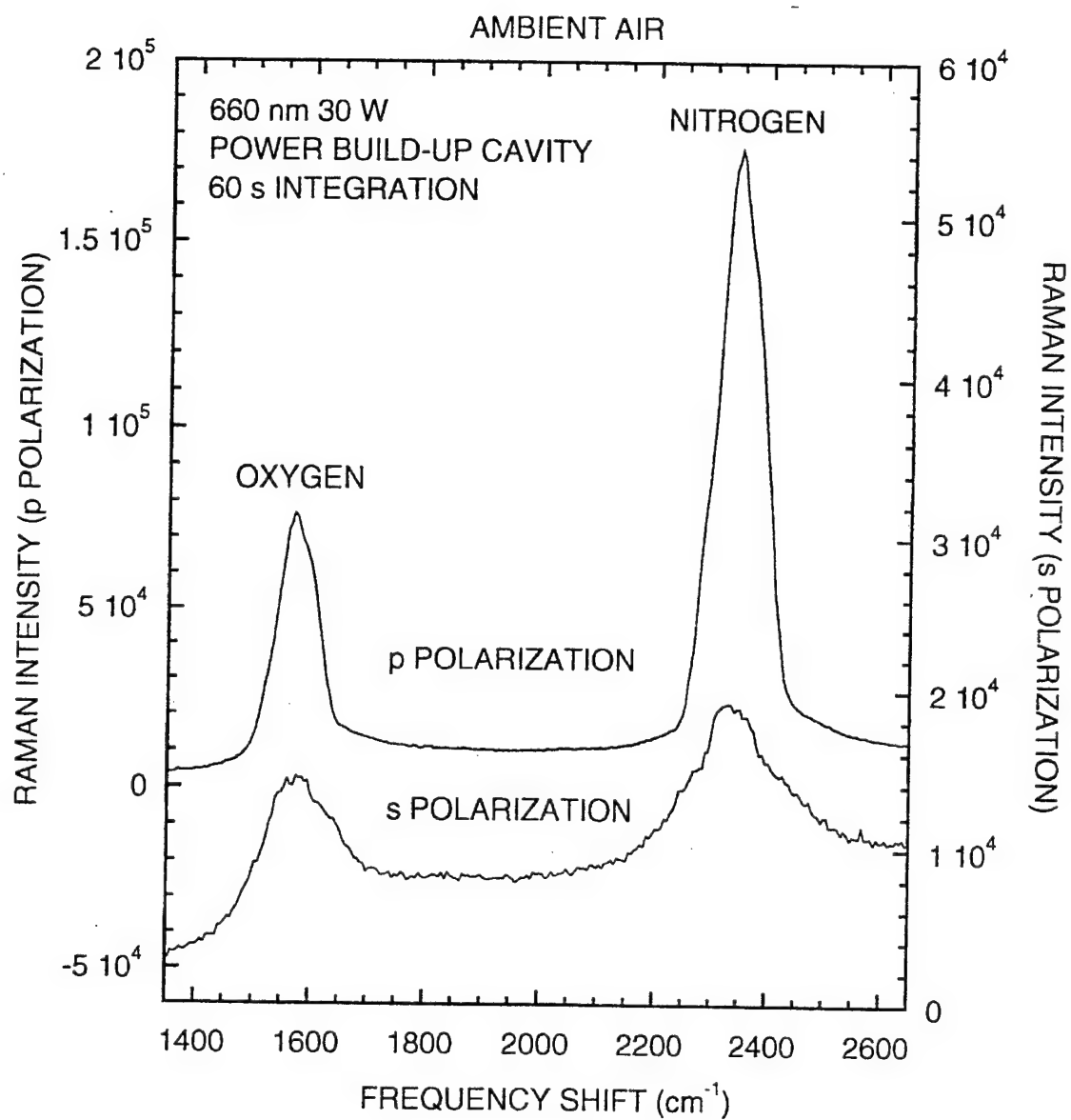


Figure 22. Raman spectra from ambient air with two different laser polarization directions.

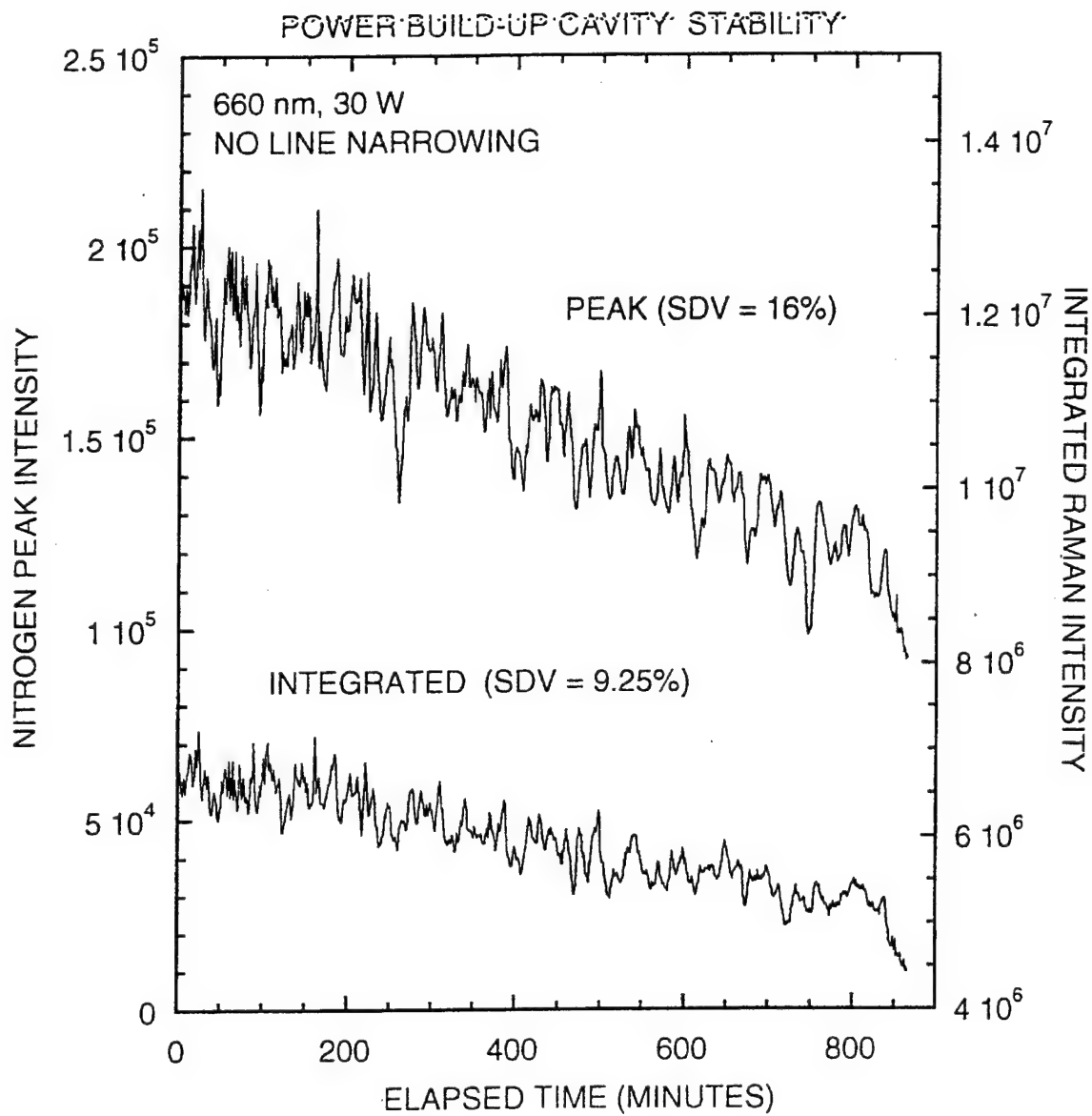


Figure 23. Nitrogen peak and integrated Raman signal stability over a period of 14 hours.

### 2.3 Sample Cells

We designed a gas flow cell that allows us to test gas mixtures when using the argon laser for excitation. Two designs were investigated. The first design uses circular windows, held in place with a washer and o-ring, to create the gas cell as shown in Fig. 24. The second design uses cylindrical glass tubing instead as shown in Fig. 25. The excitation beam is focused to a beam waist in front of the collection lens through flat circular windows in both designs. The difference in the two designs is the collection of the Raman signal. The first design images the excitation beam through a flat window while the second design images the excitation beam through cylindrical glass tubing. Both designs create a chamber for the gas samples to pass through the excitation beam and excite Raman scattering. Both designs incorporate a purge gas which acts as an air-dam, keeping the sample gases from contaminating the flat circular windows through which the excitation beam passes.

There are inherent advantages, and disadvantages of both designs. The second design, however, has many mechanical design advantages. The principal advantage of this design is cost. It is much less complicated to drill a single-sized hole to place the tube in than to manufacture specially designed washers and o-rings, and machine the ledges, within the cell on which they sit. This design will allow for a heating element to be placed within to heat the gas and simulate industrial conditions. The cell is thermally isolated from the base using washers made from polyimide, which has a low thermal conductivity. The second design is also advantageous in that it takes up less space. The width of any cell designed is limited by the focal length of the collection lens. In the flat window design, the cell must be much wider to accommodate the window thickness, o-ring, washer, and metal lip. In the tube design only the thickness of the tube and a minimal wall thickness are necessary, reducing the overall thickness of the cell. This allows for a larger margin of error and more freedom of motion in adjusting the equipment.

The potential problems with the second design are optical aberrations and fluorescence. The curved surface of the cylindrical glass tubing could cause aberrations in the image of the excitation beam. If the tube is too narrow, fluorescence could be excited in the tubing material. Therefore, tests were conducted to determine the effects of both the flat window design and the tube design on the collected Raman signal. These tests used ambient air as the control and sought to compare the measurements of ambient air without any glass to measurements made with the flat window configuration and with the tube design. Two types of glass tubes were tested: pyrex, and quartz.

To compare the fluorescence of pyrex and quartz, a sample of each material was placed at approximately a 45 degree angle in the focused laser beam in front of the spectrograph collection lens. The spot where the light passed through the glass was imaged into the spectrograph, and the collection lens was adjusted to maximize the signal. Spectra were obtained with a one second integration time for both materials. Both spectra are plotted for comparison in Fig. 26. The fluorescence background of the pyrex is eight times that of the quartz. The other narrow



# Gas Flow Cell: Design 1

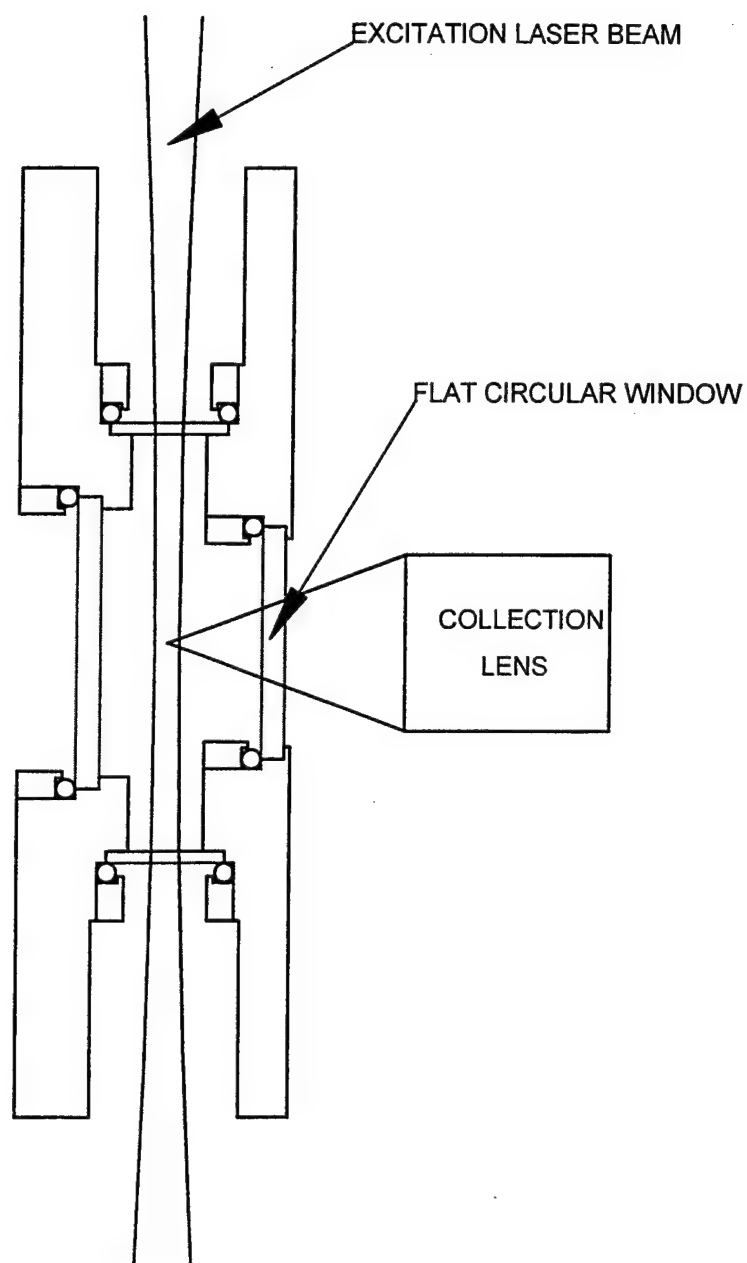


Figure 24. Flat window gas flow cell

## Gas Flow Cell: Design 2

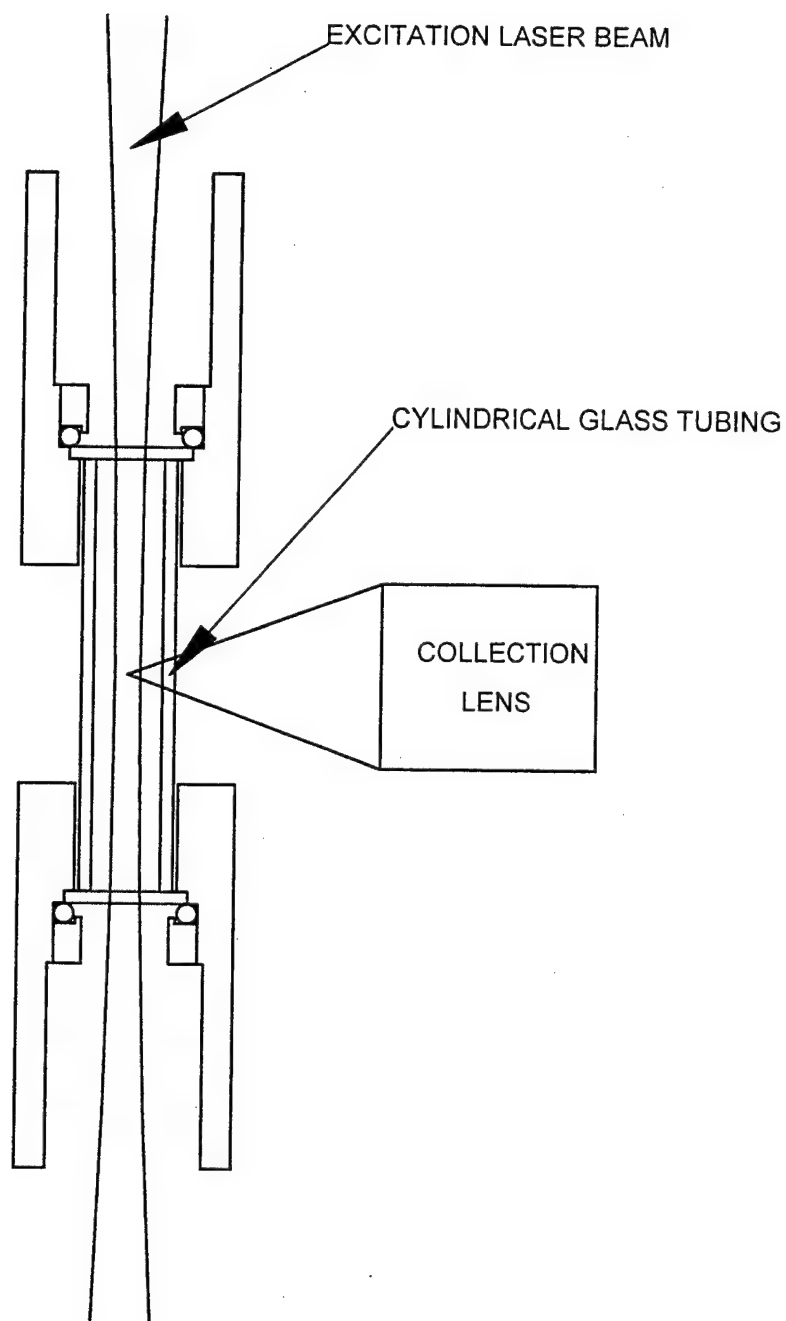


Figure 25. Glass tube gas flow cell

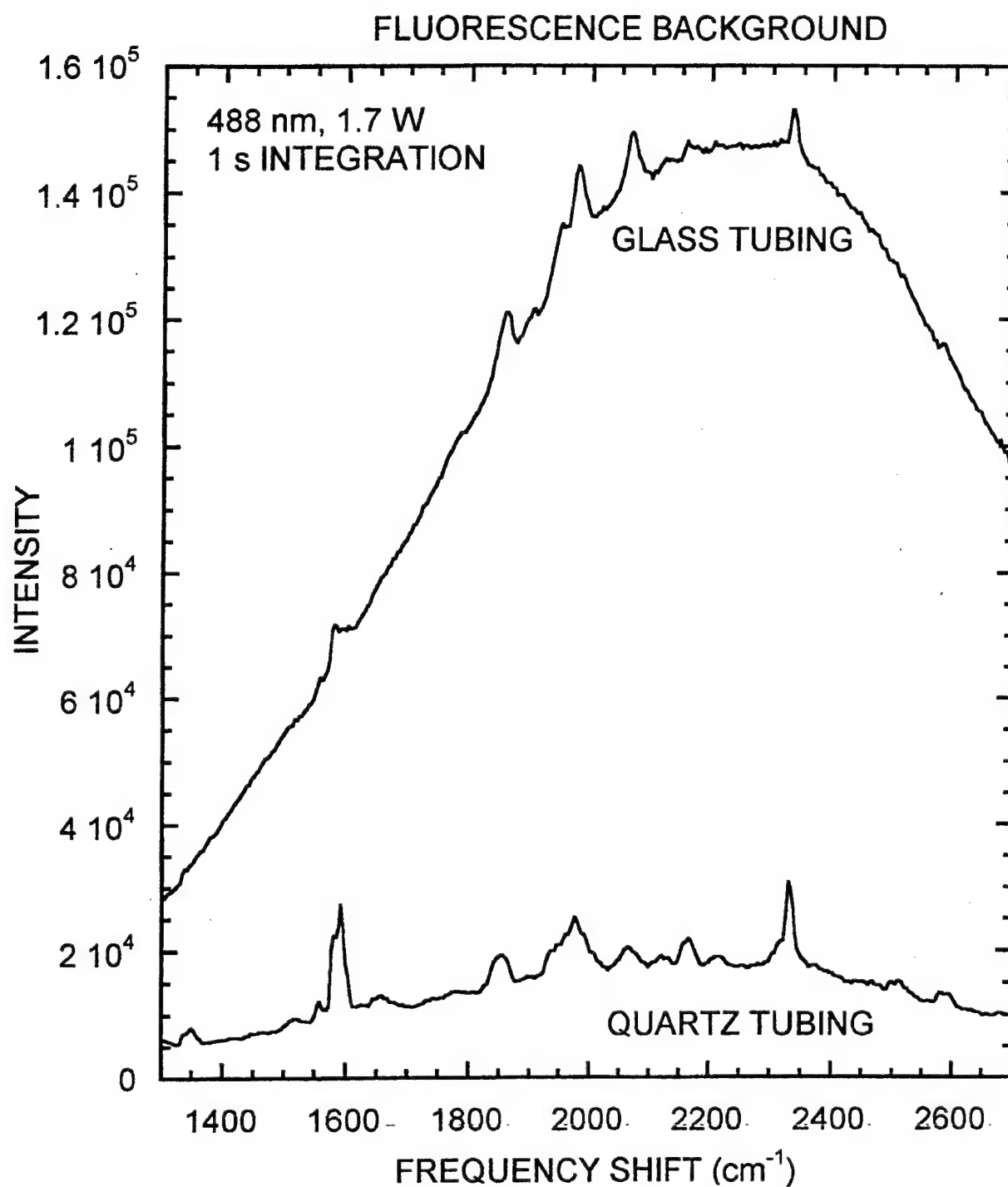


Figure 26. Spectra obtained with a one second integration time for both glass and quartz cell materials. The fluorescence background of the pyrex is eight times that of the quartz.

peaks in the spectra are likely to be plasma lines from the argon ion laser which are reflected into the spectrograph. Because of the intense fluorescence of pyrex with excitation at 488 nm, we did not use pyrex for the gas flow cell.

To test the two different gas flow cell designs, the original support plate was modified to allow space for tubing to be placed in front of the collection lens of the prototype Raman system. A temporary cell of quartz tubing was ordered to test the tubing design. B270 optical windows 30 mm in diameter by 2 mm thick were also ordered to fit over the existing one inch clearance hole in the support plate to test the window design. To reduce background light and elastic light scattering, black cardboard was placed behind the cell support, and an aperture was placed after the laser focusing lens before the cell support. These precautions proved important in reducing the background signal.

Ambient air was used as a control sample for the comparison of the two cell designs. Spectra were obtained with 1.7 to 1.9 watts excitation at 488 nm. The counts were maximized for each case, and an integration time of 90 seconds was used. The ambient air control spectrum, obtained without tubing nor windows to contain the air, shown in Fig. 27 has a nitrogen peak intensity of 1,155,300 counts, an oxygen peak intensity of 380,730 counts, and a mean background intensity of 1955 counts. With the quartz tubing in place, an ambient air spectrum, shown in Fig. 28, was obtained. No adjustment of the collection lens was needed for maximum signal through the quartz tubing. However, the quartz tubing created a loss of 50,000 counts in the peaks (nitrogen peak to 1,096,800 and oxygen peak to 330,800) as well as an increase in the background (background of 2,125). The flat glass window was first placed against the support plate at a distance of 0.0168 inches from the focused beam. With the flat window, the collection lens needed some adjustments to maximize the signal. The change in focal length measured with a micrometer was 0.035 inches. The measured change in focal length is close to the calculated change of 0.030 inches in the focal length with the addition of the optical window. The signal was maximized, and the spectrum shown in Fig. 29 was obtained. The Raman peak intensities of nitrogen and oxygen were similar at 1,161,100 and 364,800 counts, respectively compared to the signal without any window. However, the background signal also increased to 2392 counts. The increase in the background signal brought concern that the proximity of the window to the beam might be causing some fluorescence excitation in the glass. A small spacer, was inserted to move the window further away from the beam. The 0.152 inch thickness of the washer was such that the window would be at the same distance from the beam as in the preliminary design making the total distance of the window from the beam of 0.32 inches. The position of the window between the collection lens and the focused beam does not change the focal length adjustment needed to maximize the signal as expected. The spectrum, shown in Fig. 30, was obtained with 1.8 watts rather than 1.9 watts causing the signal to be slightly lower (nitrogen peak of 1142000 and oxygen peak of 350790), but the background intensity (background of 1954) is down to the same level it was without the window in place (see Fig. 27). Therefore, the gas flow cell design with the flat glass windows is best. The presence of the window does not introduce significant background if it is placed far enough from the focused beam. The window also does not introduce significant loss in Raman signal.

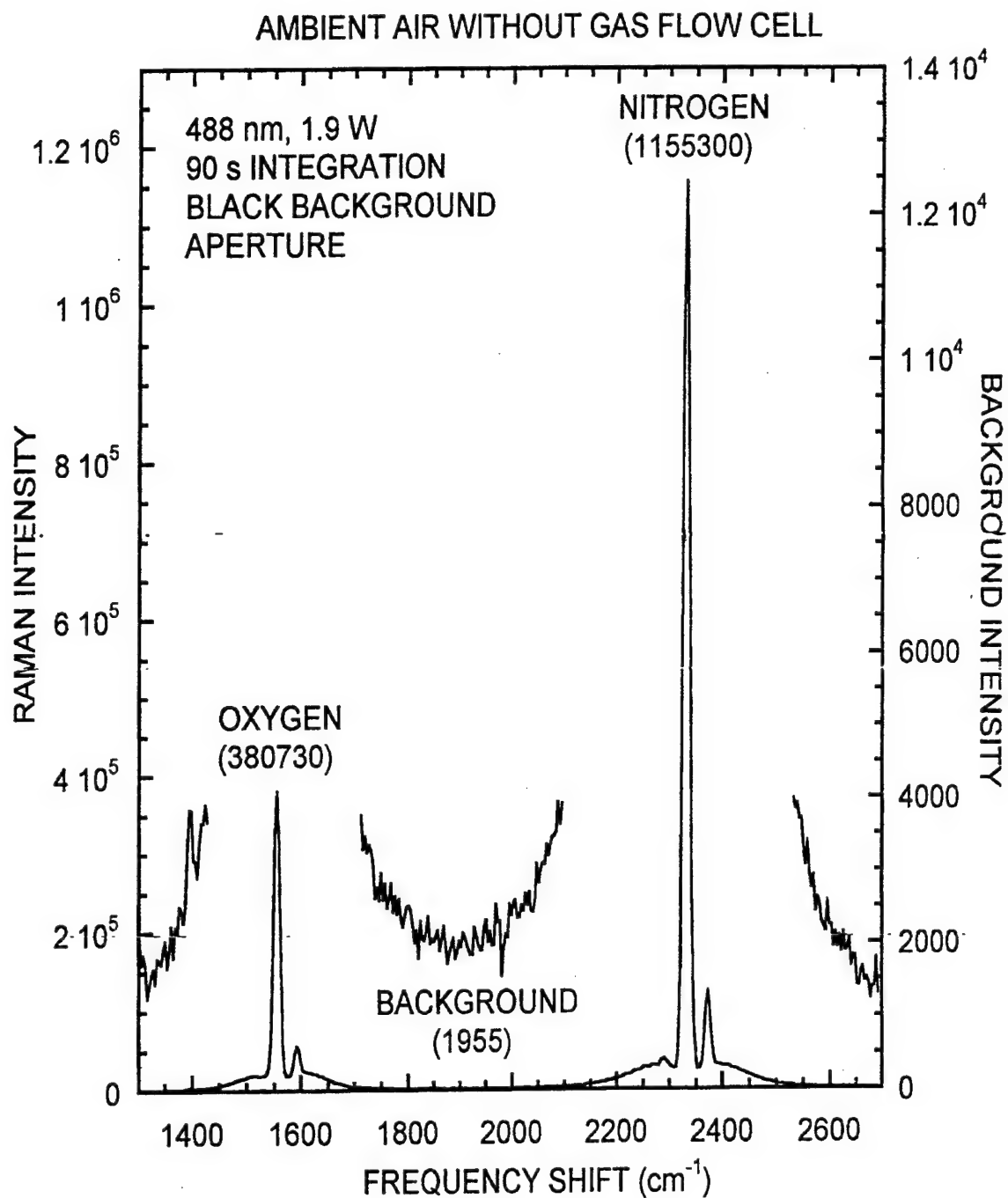


Figure 27. Ambient air control spectrum, obtained without tubing nor windows to contain the air. The spectrum has a nitrogen peak intensity of 1,155,300 counts, an oxygen peak intensity of 380,730 counts, and a mean background intensity of 1955 counts.

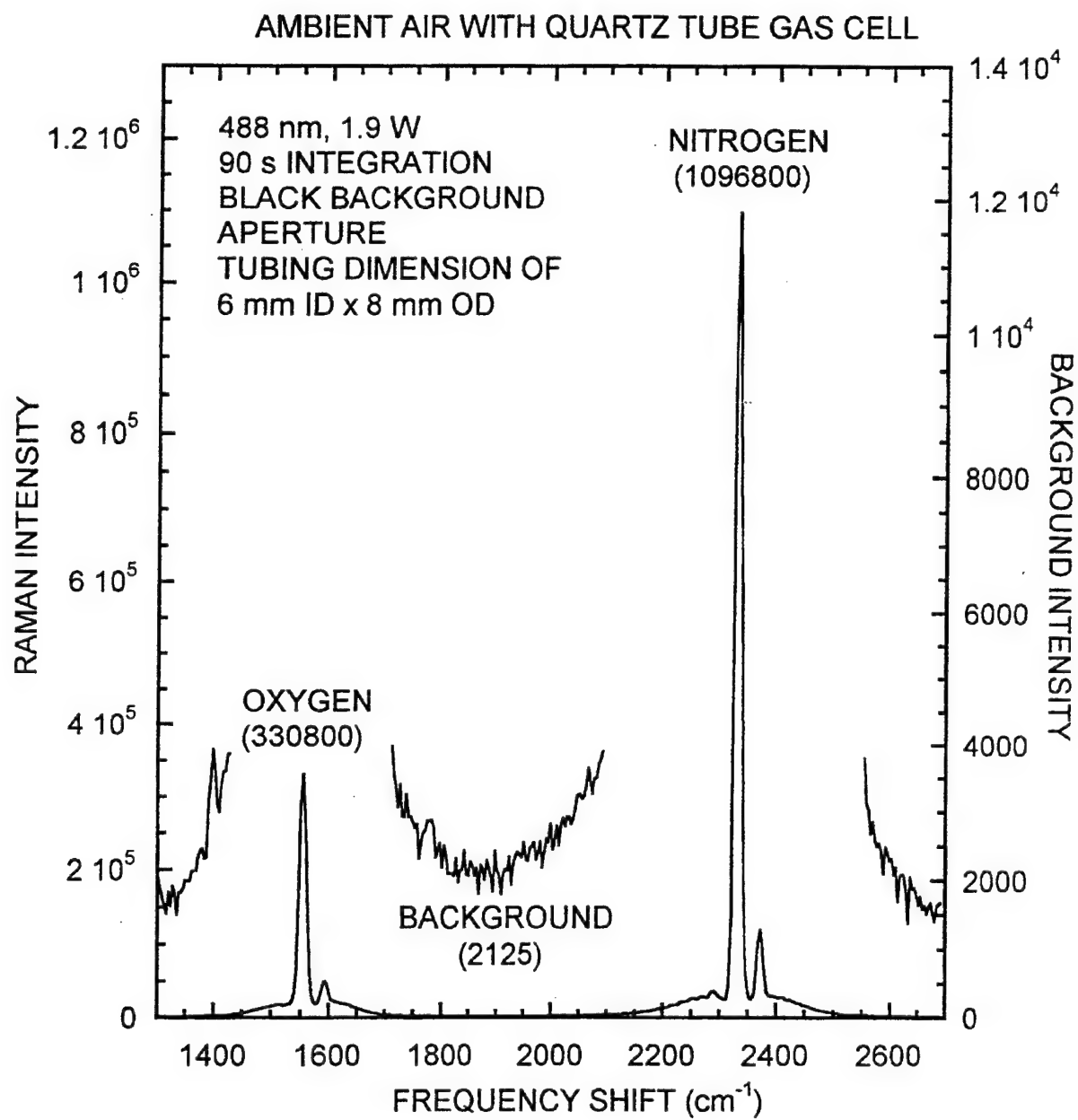


Figure 28. Ambient air spectrum with quartz tubing in place.

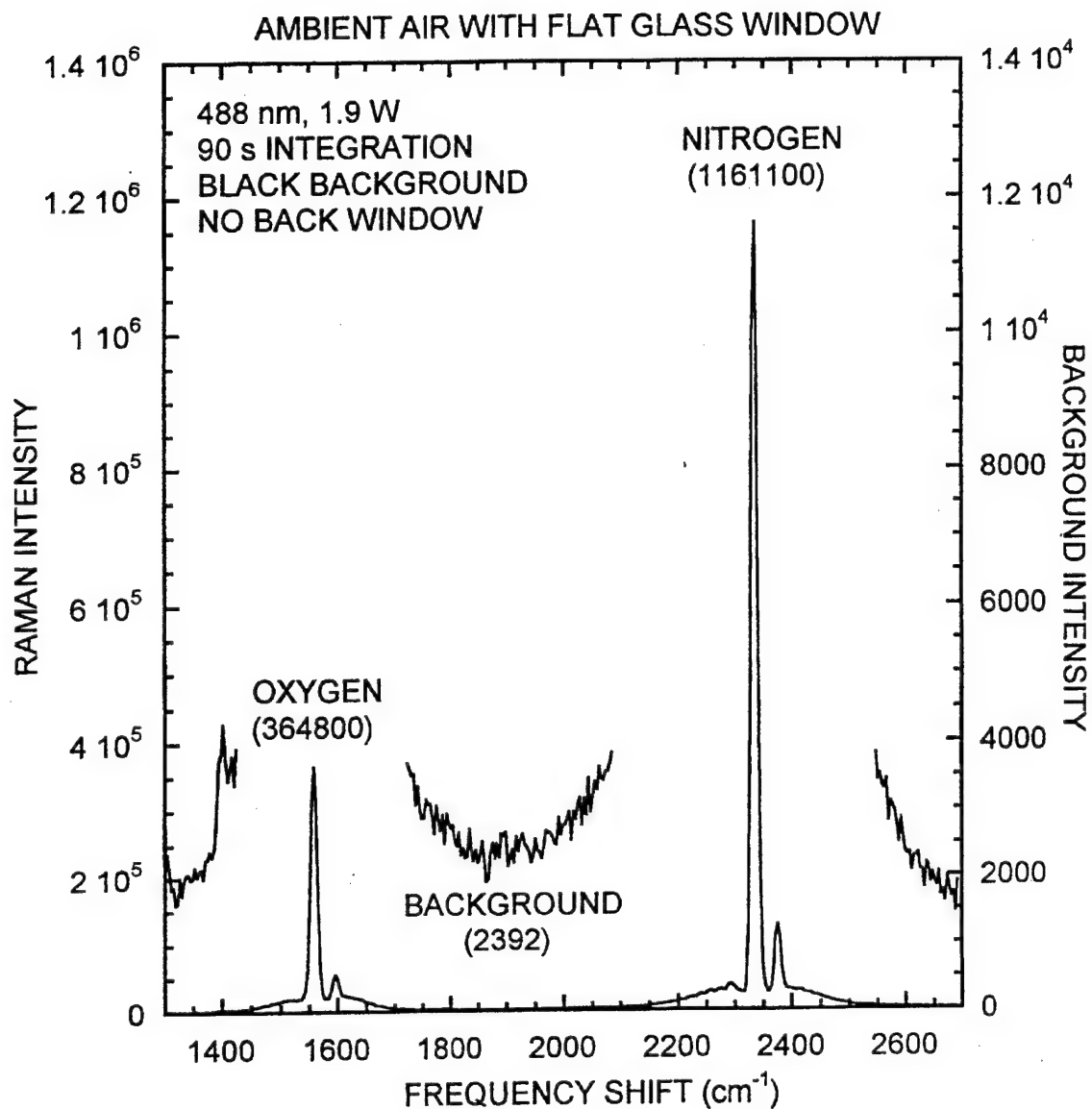


Figure 29. Raman spectrum of ambient air with flat glass window. The Raman peak intensities of nitrogen and oxygen were similar at 1,161,100 and 364,800 counts, respectively compared to the signal without any window.

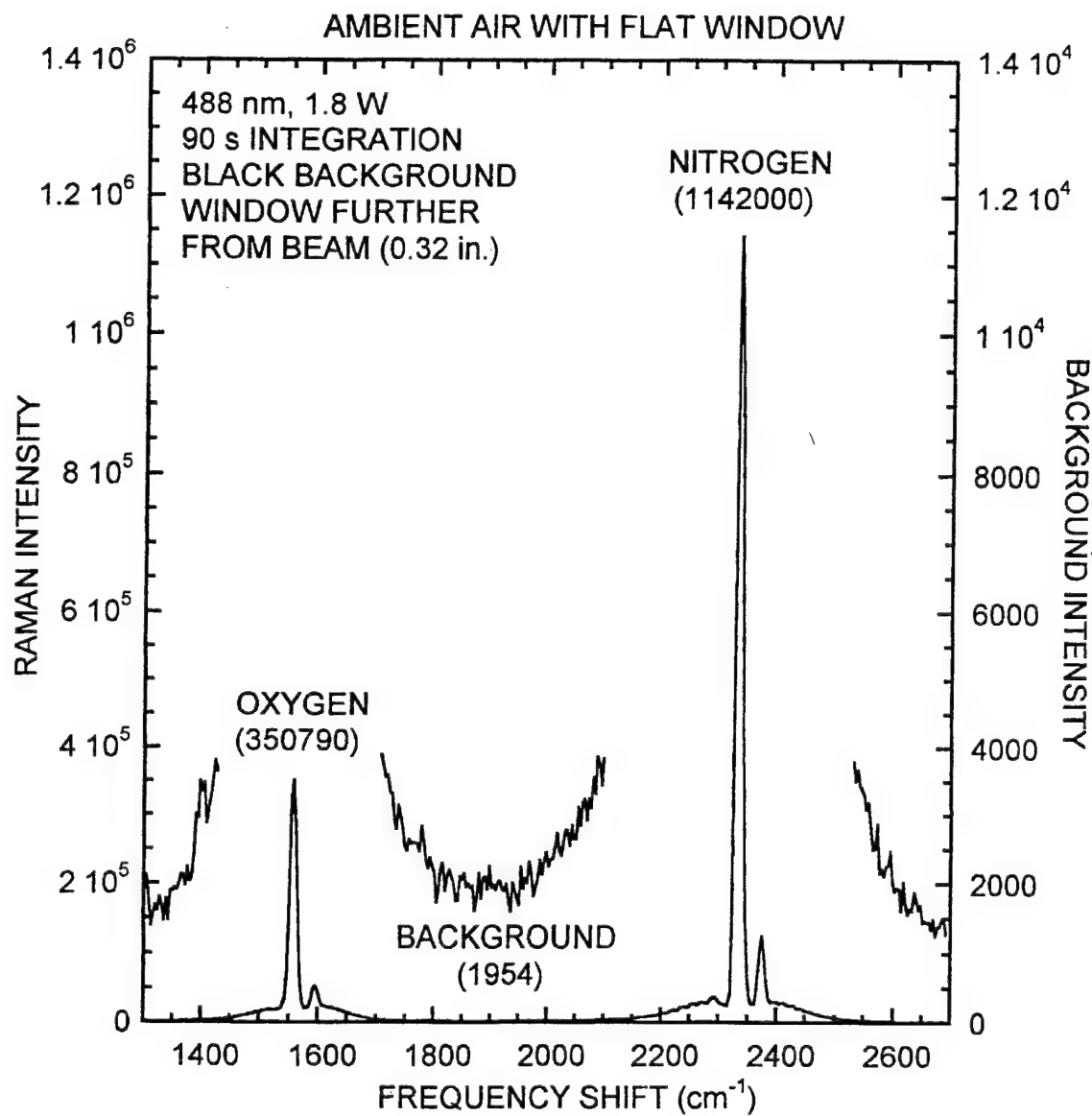


Figure 30. Spectrum obtained with 1.8 watts rather than 1.9 watts causing the signal to be slightly lower (nitrogen peak of 1142000 and oxygen peak of 350790).



The amount of background between the nitrogen and oxygen peaks was a concern. The background intensity of 1955 counts corresponds to 0.17 % of the nitrogen peak and 0.56 % of the oxygen peak. The background signal defines the gas detection limits of the instrument. A sample of one percent nitrogen in argon was obtained to measure the limits of the instrument. The spectrum of the sample found in fig. 31 shows a 48 % reduction in the background signal from 1954 to 1015. Closer inspection of the ambient air spectrum shows that the background between the nitrogen and oxygen peaks is actual Raman signal. The nitrogen and oxygen peaks are close enough together that the tails of each peak add together in the middle. The Raman signal tails limit the fundamental concentration limit of the instrument to more than 0.1 % and limit the instrument's usefulness in measuring very low concentration gases in air.

We developed the gas-phase sample flow cell illustrated in Fig. 32. The design includes provisions for heating the sample to minimize condensation, air dams to avoid window contamination, and window access to the sample from four sides to allow a 90 degree scattering geometry plus collection of both forward and backscattered Raman signals. In addition, the entire assembly has been anodized to minimize collection of elastically scattered light. There are also provisions for mounting the entire flow cell assembly directly onto the invar rod support structure of our first prototype spectrograph.

Our first tests with the flow cell involved collecting Raman spectra from ambient air with and without the cell windows installed. Spectra were recorded with 1.2 W of laser power at 488 nm in a single-pass configuration, an integration time of 120 s, and  $2 \times 17$  binning of the SBIG 7i CCD camera detector. Without the windows installed, we attained ambient air signals from nitrogen and oxygen of 1,008,500 and 317,840 counts, respectively and a background signal between the Raman peaks (near  $1900 \text{ cm}^{-1}$ ) of about 2300 counts. With the windows installed the nitrogen and oxygen peaks had counts of 890,800 and 282,570, respectively corresponding to a decrease in signal of about 11%. The background signal near  $1900 \text{ cm}^{-1}$  increased to about 5000 counts from 2300. The decrease in signal probably arises from Fresnel losses at the window surfaces, and the background increase may be caused by increased collection of fluorescence from the windows.

### 2.3.1 Diode Laser Testing in Power Build-Up Cavity

After changing excitation sources from an argon laser to the diode laser-pumped power build-up cavity, it became necessary to develop a new sample cell which was compatible with the build-up cavity. The gas cell and laser power build-up cavity we designed is illustrated in Fig. 33. The assembly includes provisions for mounting a 100 mW diode laser operating at about 665 nm, a mode matching lens, a waveplate to rotate the laser polarization, and holders for the two external cavity mirrors which form the power build-up cavity. An access hole is included to allow measurement of the leakage laser power which passes through the second cavity mirror with a reflectivity of 99.999%. This measurement allows us to estimate the laser power build-up within the cavity. A collection lens is also mounted to the gas cell assembly to collect and collimate Raman scattered light emanating from the line of laser radiation contained

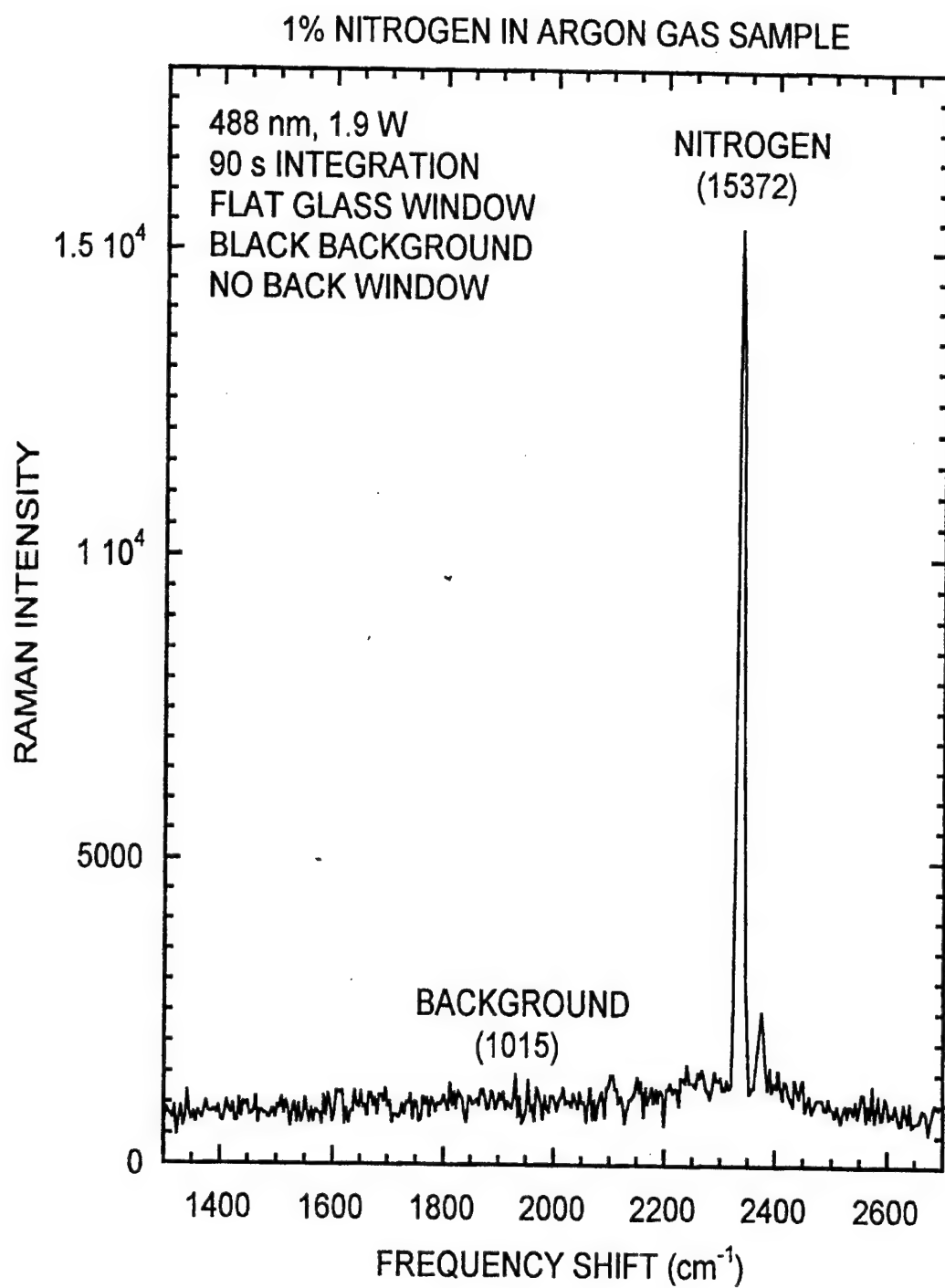


Figure 31. Raman spectrum of 1% nitrogen in argon gas

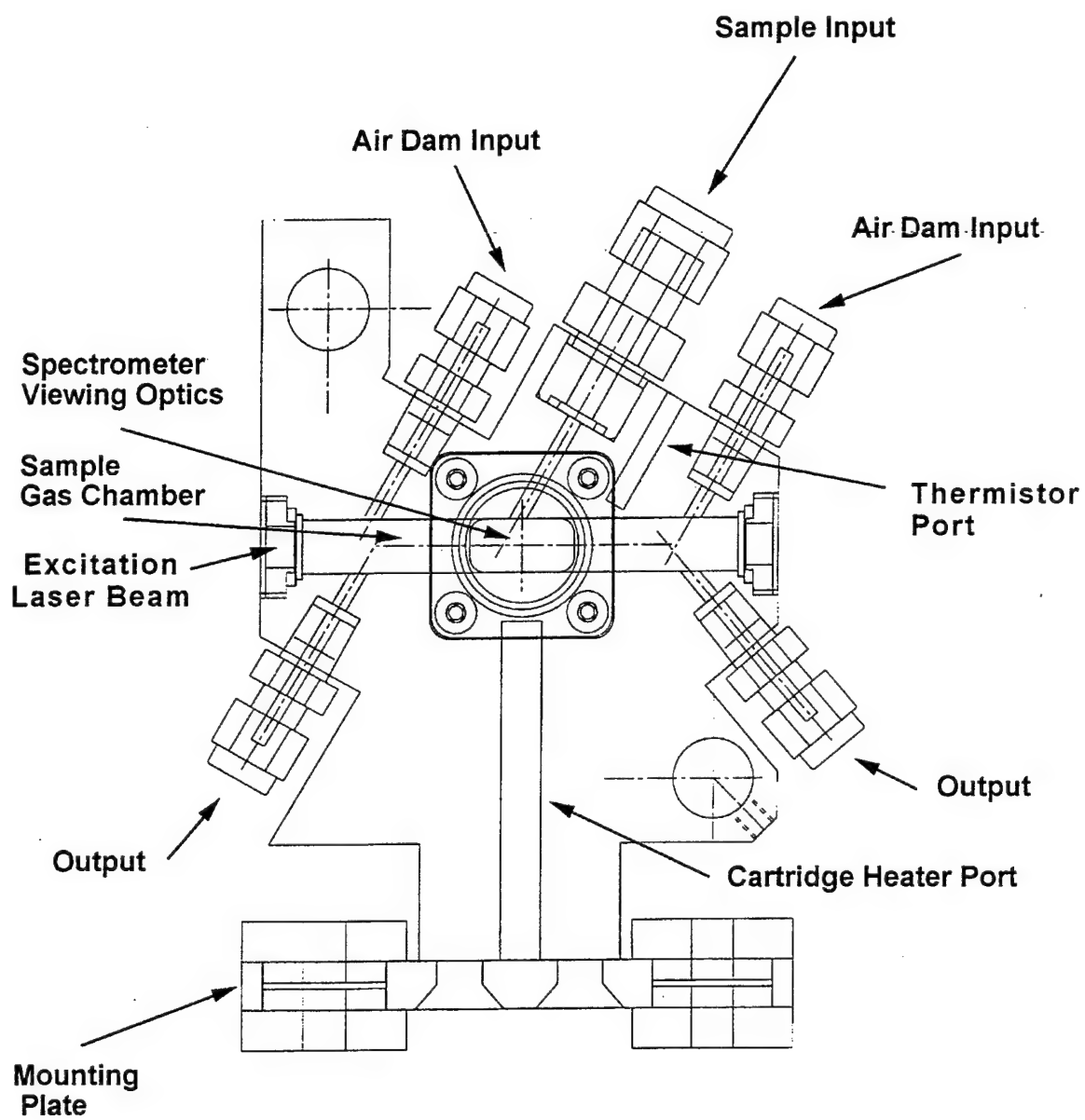


Figure 32. Gas-Phase sample flow cell for environmental monitoring.

## POWER BUILD-UP CAVITY GAS CELL

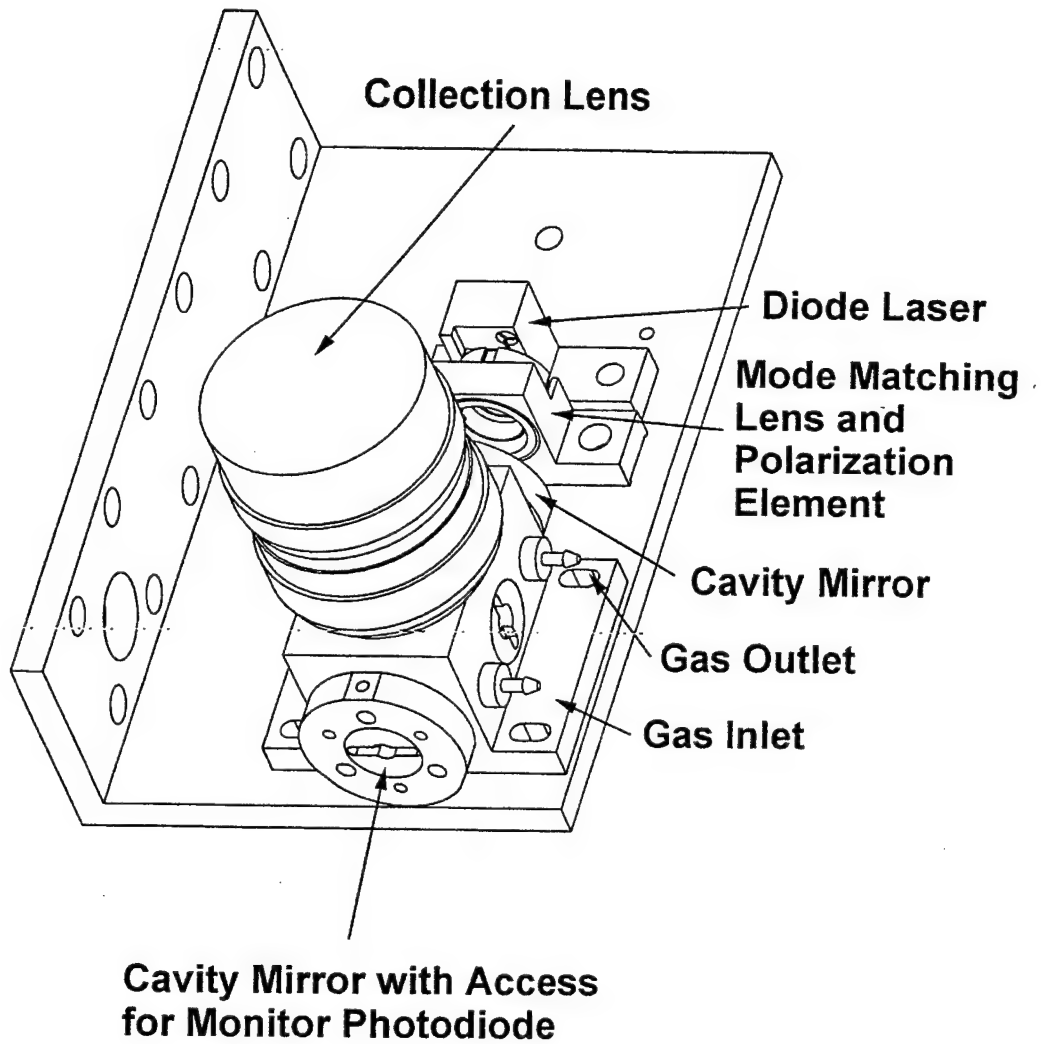


Figure 33. Power Build-up cavity gas cell.

within the gas cell. The gas cell is sealed with o-rings and has an inlet and outlet to accommodate gas flow through the cell.

The power build-up cavity was first aligned on the bench. This procedure was somewhat more difficult than it had been previously without the presence of a cell to confine the sample gas. While our current design makes it impossible to view the effects of alignment adjustments on the cavity mirror surfaces, it has the advantage that there are no additional elements such as windows in the cavity to increase the cavity loss. The alignment approach was to first optimize the feedback from the first cavity mirror to the laser diode by adjusting the mirror alignment for maximum lasing threshold reduction. The lasing threshold was measured with the second cavity mirror removed. Next, the second mirror was inserted in the gas cell mount and adjusted for lasing and maximum cavity power. The position of the mode matching lens was also adjusted to optimize the cavity. With the gas cell in place we were able to consistently achieve a total circulating cavity power of 32 W, which is less than the 60 W we had achieved previously without the gas cell in place. Reasons for the power reduction might include mirror surface contamination, the relatively narrow bore of the gas cell, or less than optimum cavity alignment. Nevertheless, 32 W of cavity power achieved from a 100 mW pump laser represents a large power build-up and is more than adequate for our Raman measurements.

We next positioned the laser assembly including collection lens in front of a spectrograph assembly consisting of a focusing lens, optical slit, collimating lens, diffraction grating with 1200 gr/mm, focusing lens, and CCD detector array. A color glass filter chosen to absorb the laser wavelength and transmit Raman-shifted light was positioned after the first collimating lens. All of the components were positioned on an optical breadboard for maximum flexibility in alignment. A box and black cloth were positioned over the spectrograph components to reduce the amount of stray light which reached the detector.

A Raman spectrum from ambient air contained within the gas cell was first obtained with the system as shown in Fig. 34. Using a slit with a width of 150 micrometers and an integration time of 60 s, we were able to obtain relatively strong signals from nitrogen and oxygen with 624,180 and 349,330 counts, respectively. The background signal away from the Raman peaks, however, was higher than expected with a value of 16,500 counts at a frequency shift of about  $1900\text{ cm}^{-1}$ . We suspected that the background signal was caused by laser light which was elastically scattered from the bore of the sample cell, transmitted through the color glass filter, and eventually reached the CCD detector. The background light could either be light at the primary lasing wavelength or spontaneous emission from the laser diode which extends over a relatively broad wavelength range near the primary lasing wavelength. To look at the spectral dependence of the background signal, we filled the gas cell with argon which doesn't have any Raman peaks in the spectral range of interest. With argon in the cell, we collected the spectrum shown in Fig. 35, which varies significantly with frequency shift from the laser line. Based on Fig. 35, we attribute much of the background to spontaneous emission from the laser diode which is modulated by the transmission function of the color glass filter. There may also be a significant component which arises from elastic scattering at the primary laser wavelength.

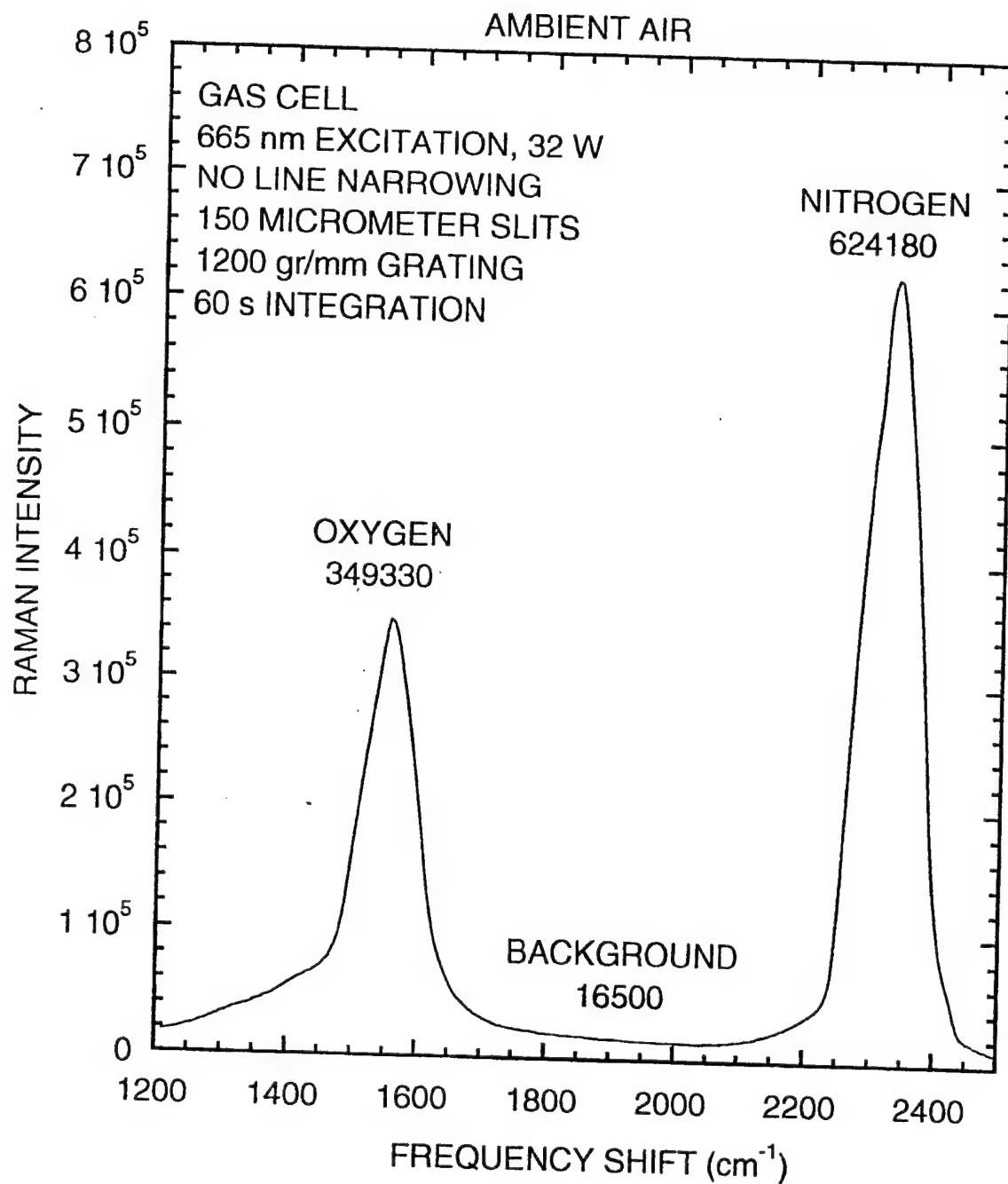


Figure 34. Raman spectrum from ambient air contained within the gas cell.

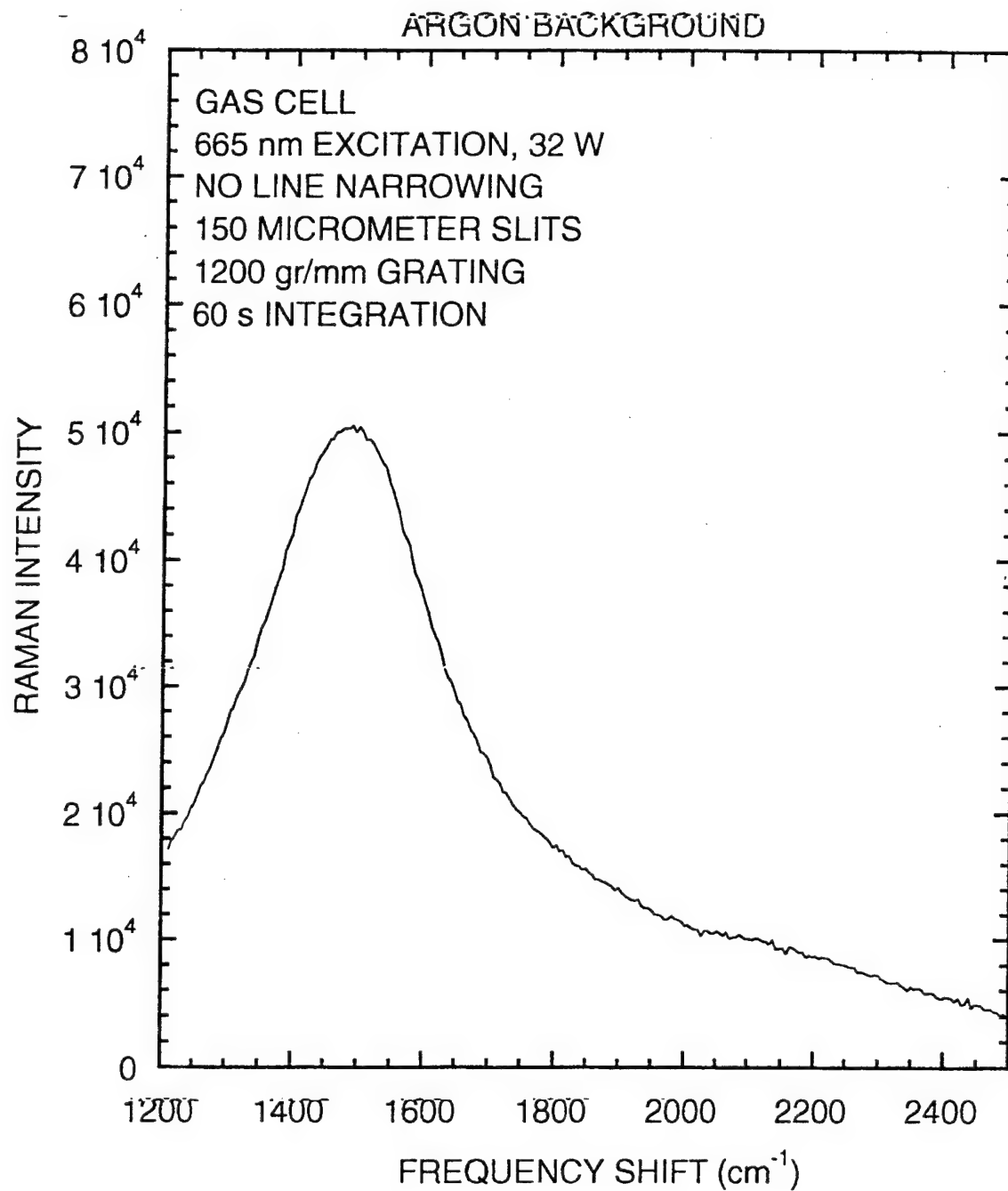


Figure 35. Raman spectrum from argon contained within the gas cell.

### 2.3.2 Determination of Prototype Detection Limits

As shown in Fig. 36, we were able to improve the ambient air spectrum by subtracting the measured background (Fig. 35) from the air spectrum (Fig. 34). After the subtraction, the background signal at  $1900\text{ cm}^{-1}$  was reduced to 2500 counts from 16,500. As a first estimate of detection limits with the power build-up cavity, we assume that a Raman peak with a signal level equal to the background should be easily detectable above the background. With this assumption, we should be able to detect a nitrogen concentration equal to  $2500/617,560$  times the ambient concentration value ( $\sim 80\% \text{ N}_2$ ), which results in a detection limit for nitrogen of 0.3 %. A similar approach to calculating the detection limit for oxygen ( $\sim 20\%$  in ambient air) leads to an oxygen detection limit of 0.16%. We were quite pleased with these preliminary detection limits which apply for an integration time of 60 seconds. Lower detection limits could be obtained with longer integration times.

We next filled the gas cell with a commercial gas mixture containing 95%  $\text{CO}_2$ , 4%  $\text{N}_2$ , and 1%  $\text{O}_2$ . The Raman spectrum we obtained from the mixture with peaks from all three components is shown in Fig. 37. The  $\text{CO}_2$  molecule has two Raman peaks near  $1350\text{ cm}^{-1}$  compared to one each for  $\text{O}_2$  and  $\text{N}_2$  at  $1555\text{ cm}^{-1}$  and  $2331\text{ cm}^{-1}$ , respectively. Figure 37 illustrates the capability of our preliminary system to detect the presence of oxygen at the 1% level in the presence of an interfering signal from carbon dioxide at the 95% level. The peaks from the two gases would be much better separated, however, if the laser line width were narrowed to improve the overall spectral resolution.

To demonstrate the ability of our Raman system to monitor gas concentration changes with time, we next recorded Raman spectra as the gas within the sample cell changed from the carbon dioxide mixture to ambient air with the cell inlet and outlet open. The results are plotted in Fig. 38 where each spectrum was recorded with an integration time of 60 seconds. As expected the carbon dioxide peaks at high pixel number decrease with increasing spectrum number (time) while the oxygen and nitrogen peaks increase. Relatively large amounts of noise, which we attribute to shifting of the laser mode structure, are also observed, especially in the nitrogen peak at low pixel number.

The first gas sample cell for the power build-up cavity had a small diameter for the sample region. We found that this small diameter tube was too close to the beam path, and thus, increased the elastic scattering background. We modified the sample cell by increasing the sample cell diameter. With the modified sample cell, the elastic scattering signal was reduced significantly.



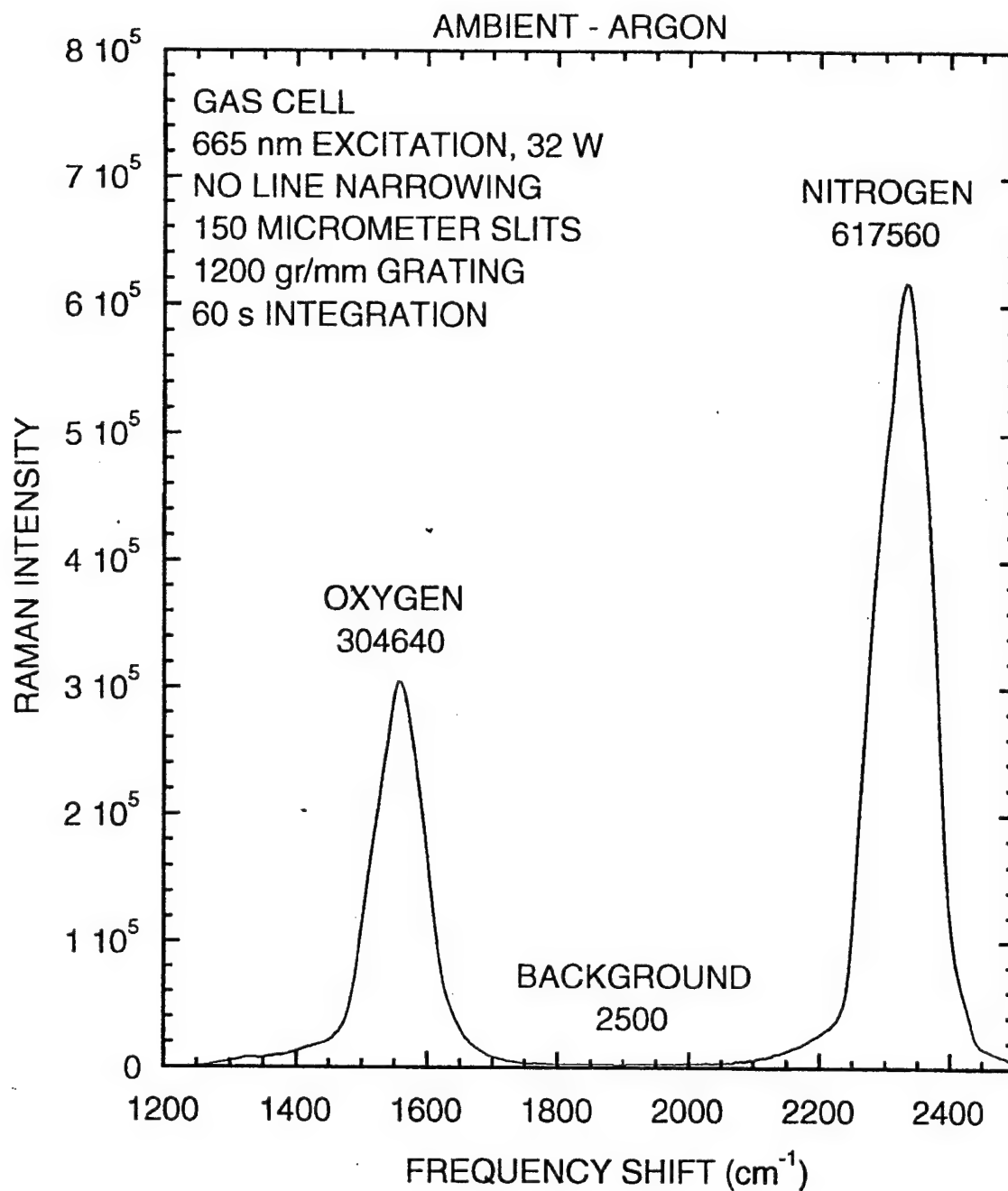


Figure 36. Improved ambient air spectrum obtained by subtracting the measured background in (Fig. 31) from the air spectrum in (Fig. 30).

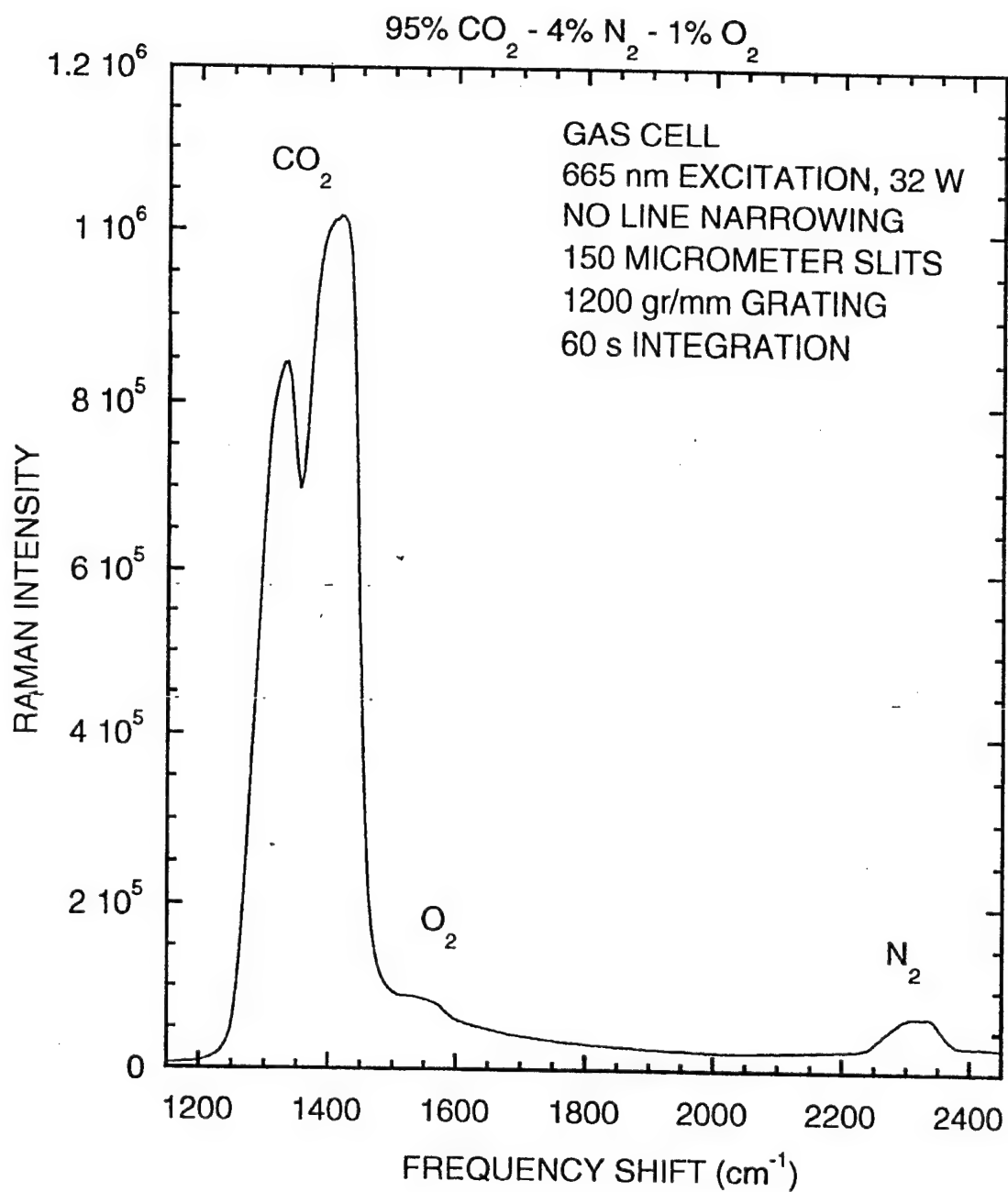


Figure 37. Raman spectra obtained from a commercial gas mixture containing 95% CO<sub>2</sub>, 4% N<sub>2</sub>, and 1% O<sub>2</sub>.

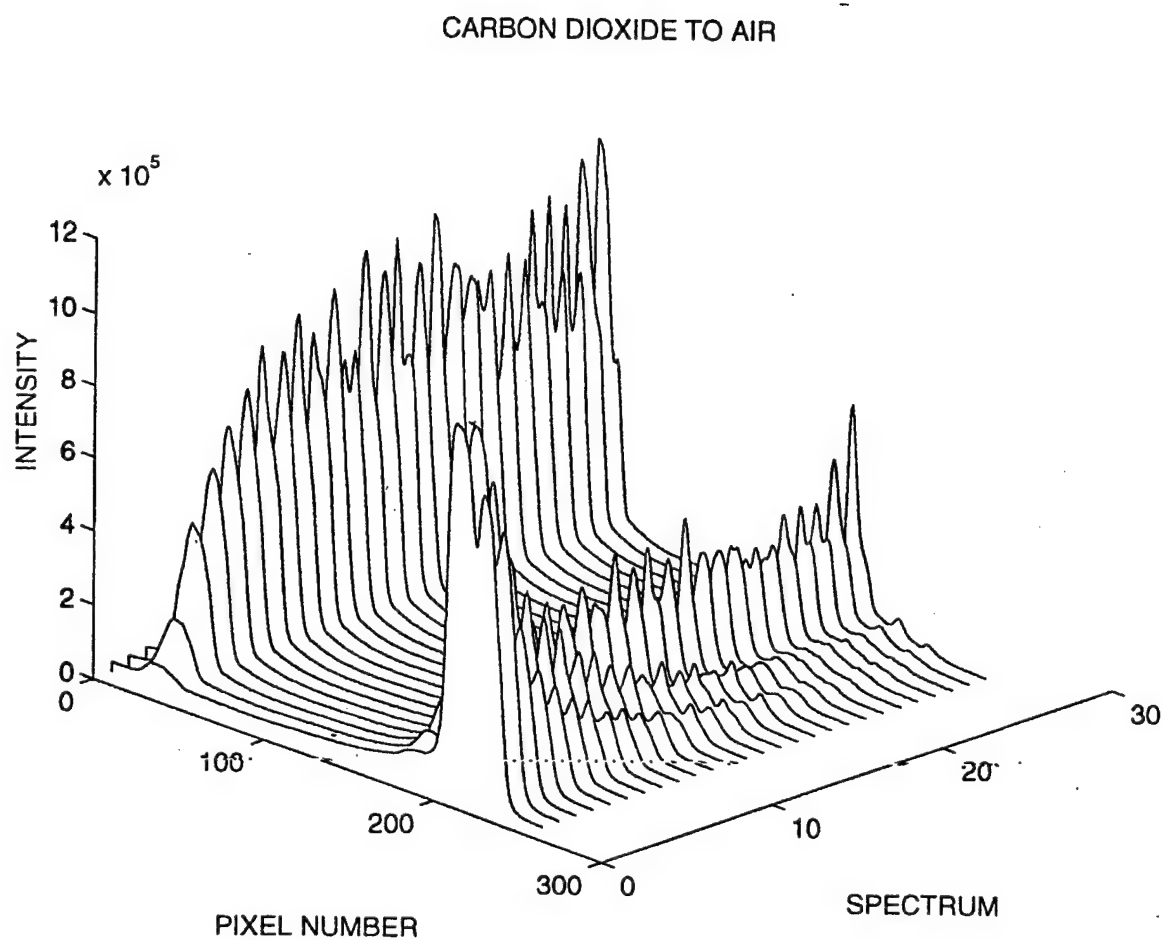


Figure 38. Raman spectra obtained as the gas within the sample cell changed from the carbon dioxide mixture to ambient air with the cell inlet and outlet open.

## 2.4 Spectrograph Development and Patent Application

We developed a new simplified compact and robust spectrograph design for Raman applications which do not require large amounts of elastic light rejection. As shown in Fig. 39, the new design includes provisions for fiber input, a  $f/1.4$  collimating lens, a conventional reflective diffraction grating, a  $f/1.3$  focusing lens, and a cooled CCD array detector. The new design also includes some alignment targets which make it relatively easy to achieve proper alignment of the grating and lenses. Resistive heaters are included to allow the spectrograph to be temperature controlled. Compared to our previous design utilizing invar rods and volume holographic filters and gratings, the new system is easier to machine, more compact, and much easier to align. It is also compatible with a variety of commercially available diffraction gratings which will allow us to tailor the spectral coverage and resolution for a variety of gas or liquid phase applications. A patent application was submitted in June 1999.

Our newly designed spectrograph with the slit assembly installed (as shown in Fig. 40) is normally used for gas phase studies with a 600 grooves/mm grating which gives about  $3000\text{ cm}^{-1}$  coverage and  $60\text{ cm}^{-1}$  resolution when using a  $150\text{ }\mu\text{m}$  slit. The laser diode (without line width narrowing) has a line width of about  $45\text{ cm}^{-1}$ . Since the bandwidth ( $45\text{ cm}^{-1}$ ) of the laser source is less than the bandwidth ( $60\text{ cm}^{-1}$ ) of the spectrograph, the spectrograph produces a smooth line shape at the output rather than the mode structure of the laser source itself. With this compact spectrograph, we can align the setup and measure the Raman signal easily. During our initial experiments, when the collection lens of the gas sample cell was first aligned with the input lens #1 of the spectrograph, we instantly saw the Raman signal of the room air ( $\text{N}_2$ ,  $\text{O}_2$ ). No additional adjustment was needed. We also found that the system produced lower background noise when the laser line rejection filter was placed after the input lens #2 (rather than input lens #1). The slits used in the experiments were 50, 100, 150, and  $250\text{ }\mu\text{m}$  and their corresponding resolutions are 20, 40, 60, and  $100\text{ cm}^{-1}$ . We chose a  $150\text{ }\mu\text{m}$  slit for most of our experiments because its resolution ( $60\text{ cm}^{-1}$ ) is greater than the  $45\text{ cm}^{-1}$  source line width and also because it gives better throughput.



## Spectrograph for gas-phase Raman sensing

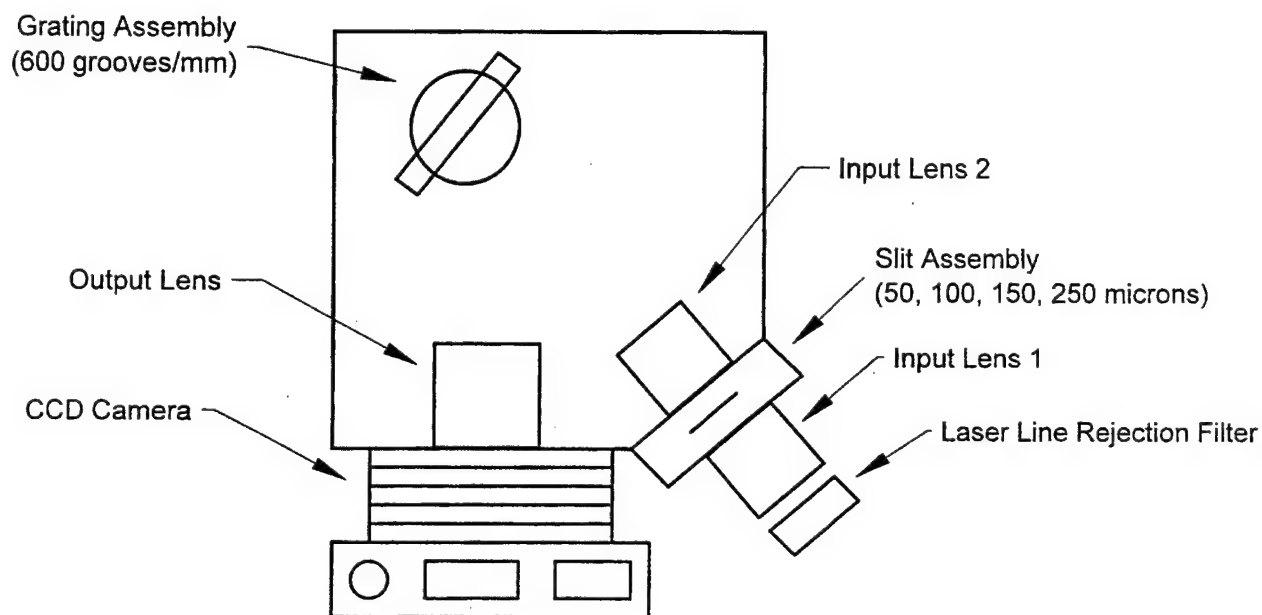


Figure 40 Newly designed spectrograph using s a 600 grooves/mm grating which gives about  $3000\text{ cm}^{-1}$  coverage and  $60\text{ cm}^{-1}$  resolution

## 2.5 CCD Detectors

### 2.5.1 Santa Barbara Instruments Group Camera

A CCD camera (Models 6i, 7i, or 8i) manufactured by Santa Barbara Instruments Group (SBIG) was used to obtain most of the Raman spectra recorded in this study. These cameras have the advantage that they are low in cost and still have relatively good performance specifications. During the development program, we attempted to characterize the performance of the SBIG cameras, compare their performance with several other commercial CCD systems, and to explore the feasibility of developing our own CCD camera system.

In early studies using a 7i CCD camera we had borrowed from SBIG, we had observed substantial nonlinearities between signal strength and integration time at high signal levels approaching about 30% of the full-well capacity of the CCD. This problem was associated with the anti-blooming feature included with the camera. Consequently, when we purchased our own 7i camera, we ordered it without the anti-blooming feature. Figure 41 shows linearity results for our new 7i camera without anti-blooming based on Raman data from ambient air. Using the 2 x 17 binning, the full-well capacity of the CCD corresponds to about 1.96 million counts. Based on the data of fig. 41, the new camera appears to have a linear relation between signal level as long as the signal is below about 1.7 million counts or about 85% of full-well capacity.

While we were waiting for some of the spectrometer modifications and changes to the multipass enhancement cell to be completed, we began some additional studies of the noise characteristics of the SBIG 7i CCD camera. Our first goal was to better characterize the pixel-to-pixel variations we have previously observed with the camera in the dark. These variations, which we termed pattern noise, are illustrated in Fig. 42. The camera was operated at 0 degrees C in the dark using a 2 x 17 binning mode, and spectra were recorded for integration times ranging from 1 to 120 seconds. For short integration times the variations across the pixel number axis are small, and the CCD array response appears to be uniform. However, for long integration times the pixel-to-pixel signal variations become much more pronounced. Since our normal data collection procedure is to subtract a "dark" frame obtained with a shutter in front of the CCD closed from a "light" frame obtained with the shutter open and the CCD exposed to a light signal, some of these pixel-to-pixel variations are removed by the subtraction process. However, we still observe a tendency for the standard deviation of the signals associated with the individual spectra to increase with increasing integration time. Figures 43 and 44 summarize the data of Fig. 42 obtained at 0 degrees C by plotting the mean and standard deviation signals for the "light" and "dark" frames as well as their difference as a function of integration time. The equations of linear fits to the various signals are also indicated. Although the mean value of the difference signal (Fig. 43) is not strongly dependent on integration time, the standard deviation of the difference (Fig. 44) increases with increasing integration time and has a slope of 1.3671 counts/second.

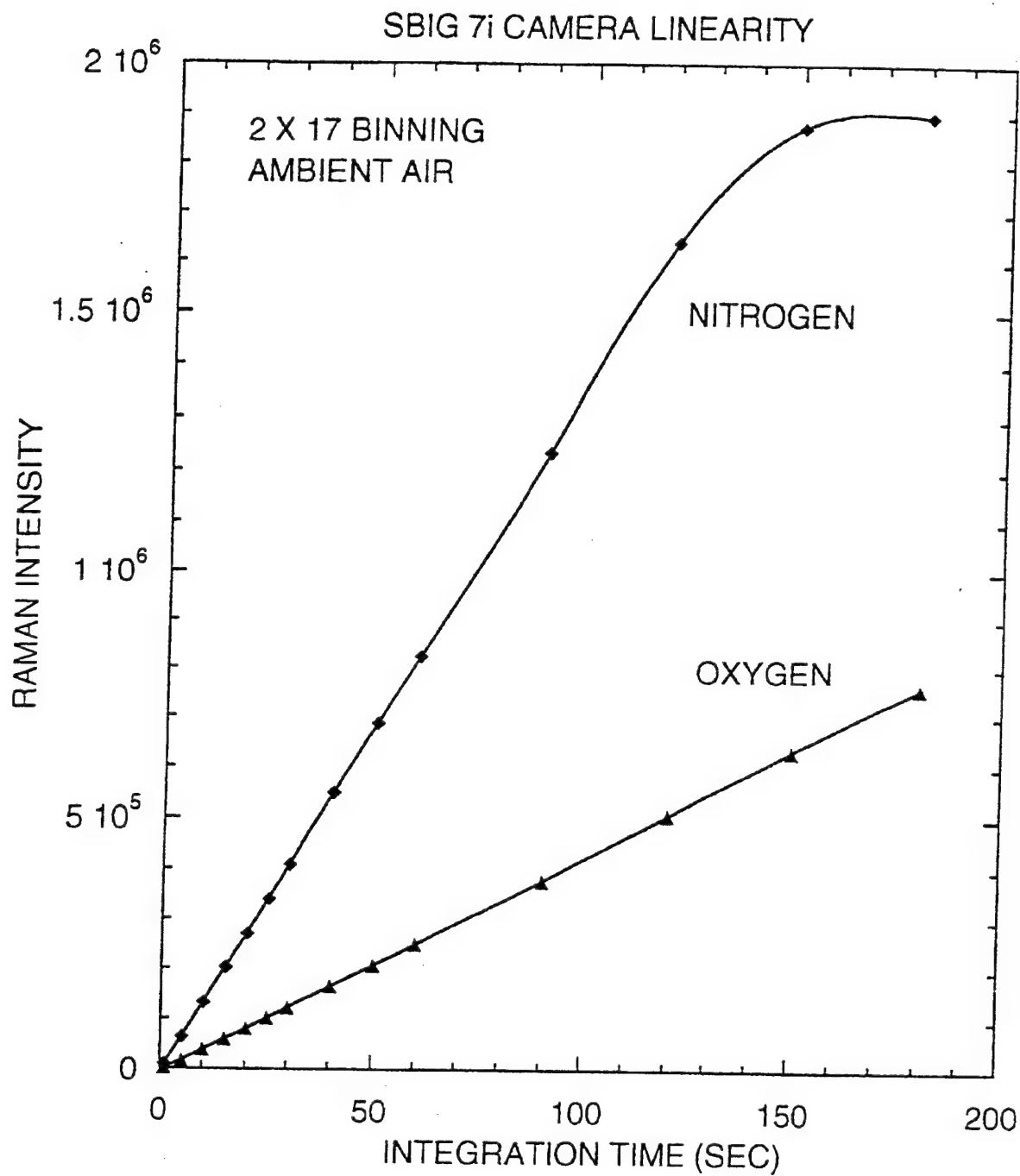


Figure 41      Linearity results for our new 7i camera without anti-blooming based on Raman data from ambient air.



**SBIG 7i DARK FRAME - T = 0 DEGREES C**

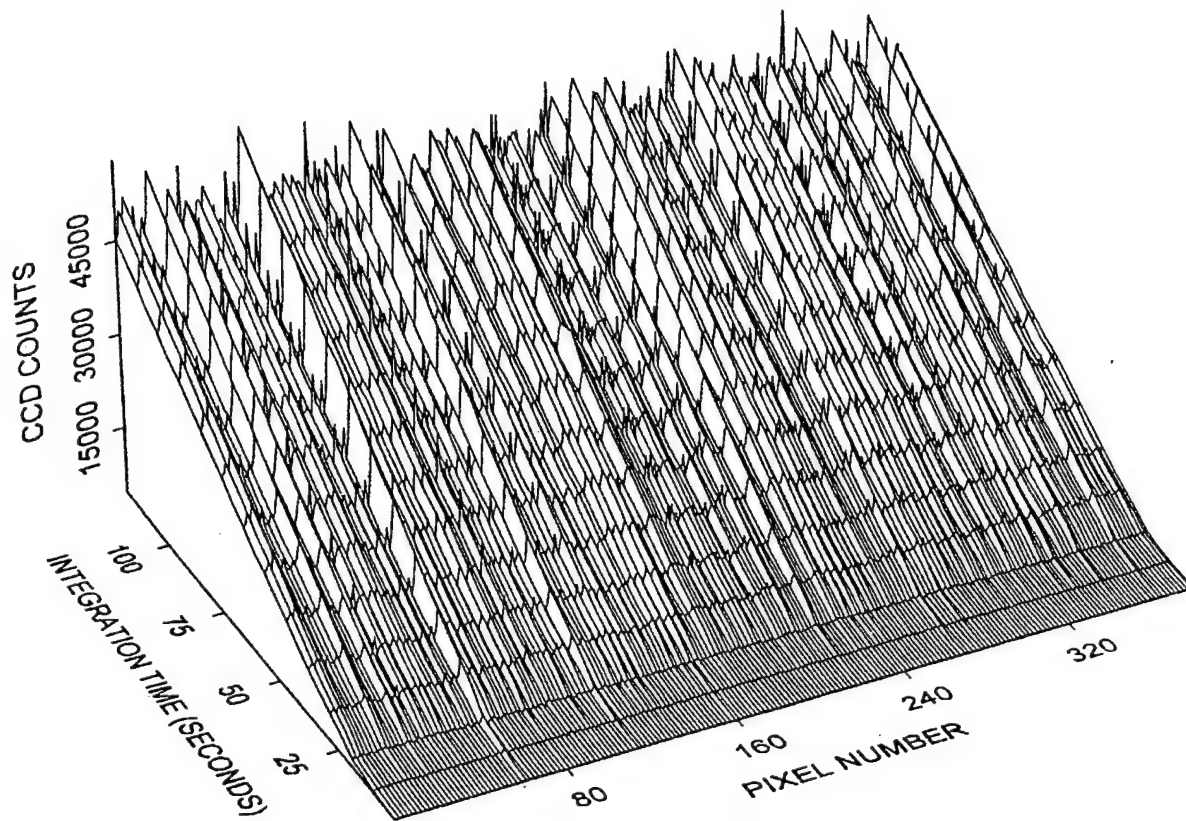


Figure 42. Pixel-to-pixel variations observed with the camera in the dark.

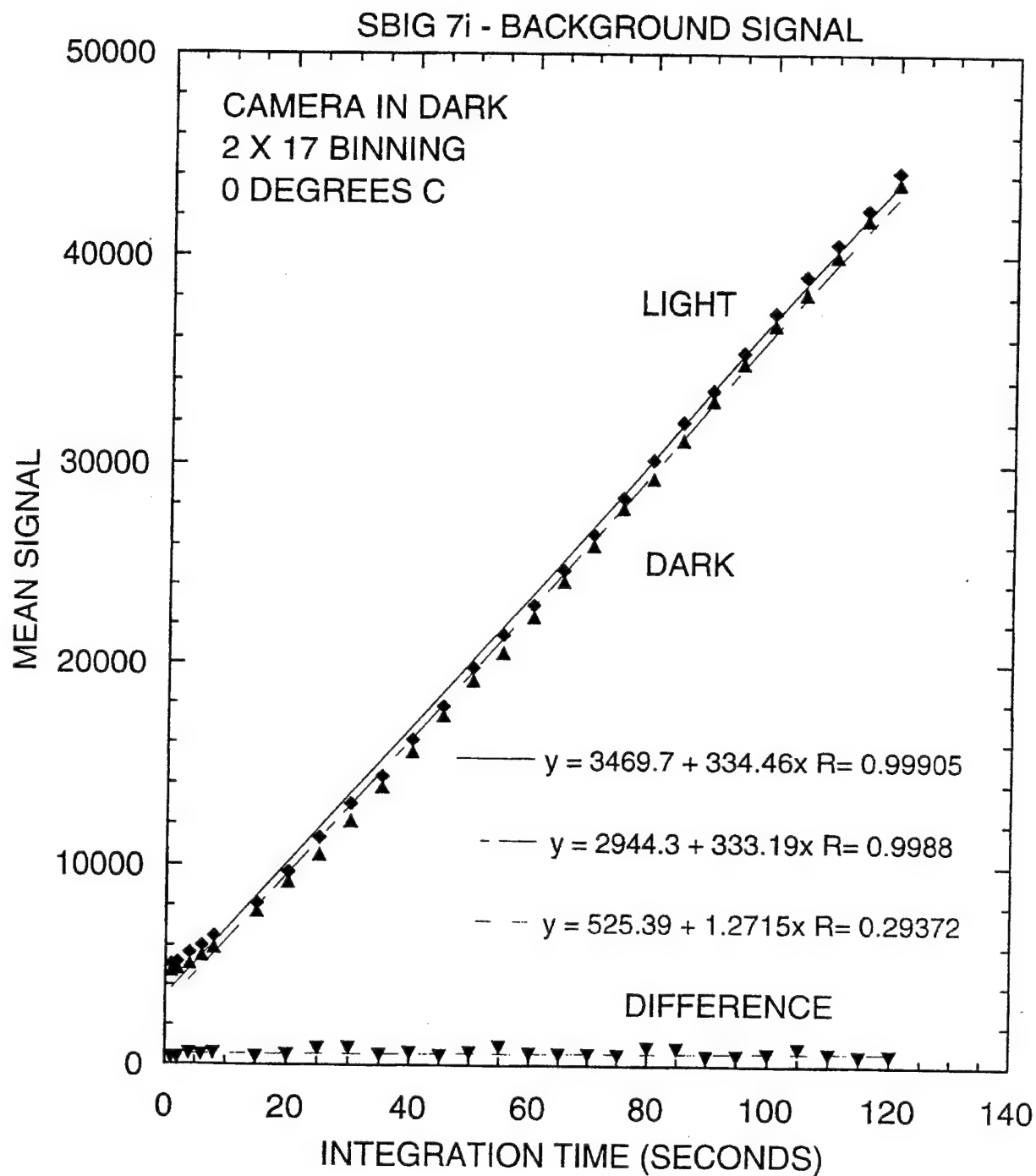


Figure 43. Summary of the data of Fig. 38 obtained at 0 degrees C.

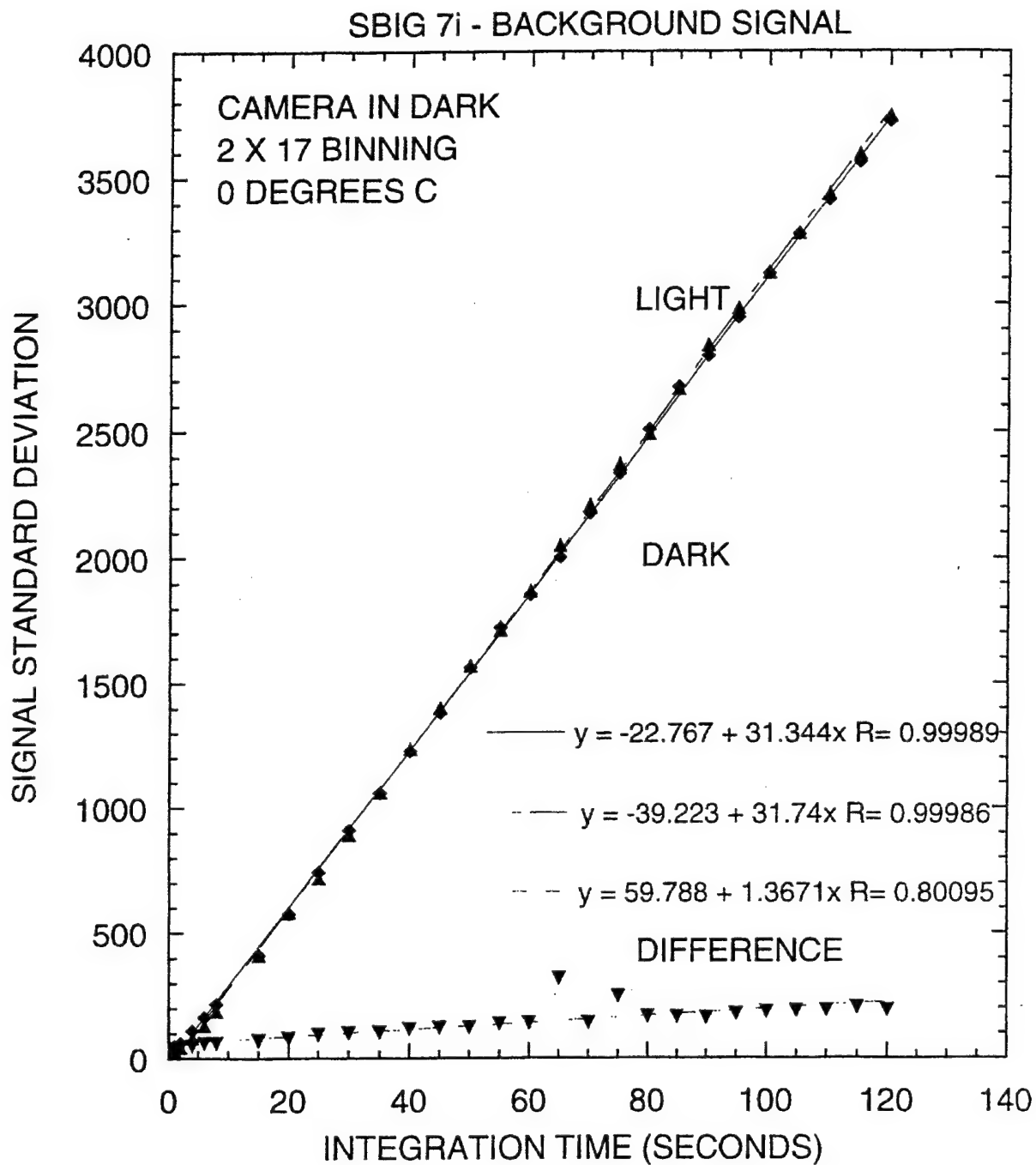


Figure 44. Summary of the data of Fig. 38 obtained at 0 degrees C by plotting the standard deviation of the signals for the light and dark frames.

A possible explanation for the pattern noise effects is a pixel-to-pixel variation in the dark count. For longer integration times, pixels with higher dark count rates would accumulate significantly larger signals than pixels with lower dark count rates. To test this possibility, we recorded additional data similar to that presented in Figs. 43 and 44, for CCD temperatures of -10 and -20 degrees C. The SBIG 7i camera only has a single stage-TE cooler and normally is only capable of reaching temperatures near 0 degrees C when cooled from room temperature. To obtain the lower camera temperatures, we placed the camera in our cooled instrument enclosure which was maintained near 0 degrees C. Figures 45 and 46 display mean and standard deviation data as a function of integration time obtained with the camera at a temperature of -10 degrees C, and Figs. 47 and 48 display mean and standard deviation data as a function of integration time obtained with the camera at a temperature of -20 degrees C. As temperature is decreased, the mean "light" and "dark" signals have an increasing zero-time intercept and a decreasing slope. In addition, as shown in Figs. 44, 46, and 48, the standard deviation of the difference signal also decreases with decreasing temperature.

### 2.5.2 Photometrics SENSYS CCD Camera System

We borrowed a Sensys CCD camera from Photometrics in order to compare its performance with that of our SBIG 7i camera. Both cameras use the same Kodak CCD chip (KAF0400) we are considering for the CCD camera system we are developing. The Photometrics camera is more expensive but comes with a complete software control package. Photometrics only utilizes a 12-bit A/D convertor for reading the CCD, which they justify based on noise considerations, compared to the 16-bit D/A used by SBIG. In addition, the Photometrics system is intended primarily as a microscope imaging camera and only has provisions for cooling the temperature of the CCD to a temperature of 10 degrees C rather than to 0 degrees C as with the SBIG 7i. One of our goals in evaluating the Photometrics camera was to separate performance characteristics inherent in the CCD chip from those associated with the control electronics and software interface.

Our initial tests with the Photometrics camera utilized a binning mode which combined two pixels horizontally in the dispersion direction and all of the pixels vertically in the direction parallel to the spectrograph slit (2 x full vertical binning). Because of the higher operating temperature of the Photometrics camera which causes a higher dark count rate, we were concerned that the 12-bit A/D convertors might reach saturation in relatively short integration times even with the camera in the dark. Photometrics provides a partial solution to this problem by including provisions for three gain factors to be used in converting accumulated CCD charge to ADJ counts. Figure 49 displays dark spectra obtained with the camera in the dark and at 10 degrees C with a 10 ms integration time for the 3 gain factors of 5, 20, and 40 electrons/count. With the highest gain (5 electrons/count) the dark signal approaches the 12-bit saturation value (4095 counts) in the 10 ms integration time, which is much shorter than the normal integration times we utilize for collection of Raman data. With the short 10 ms integration time much of the accumulated charge might be readout noise rather than dark count. Figure 50 shows the dependence of the mean dark signal on integration time with the camera gain set at its lowest

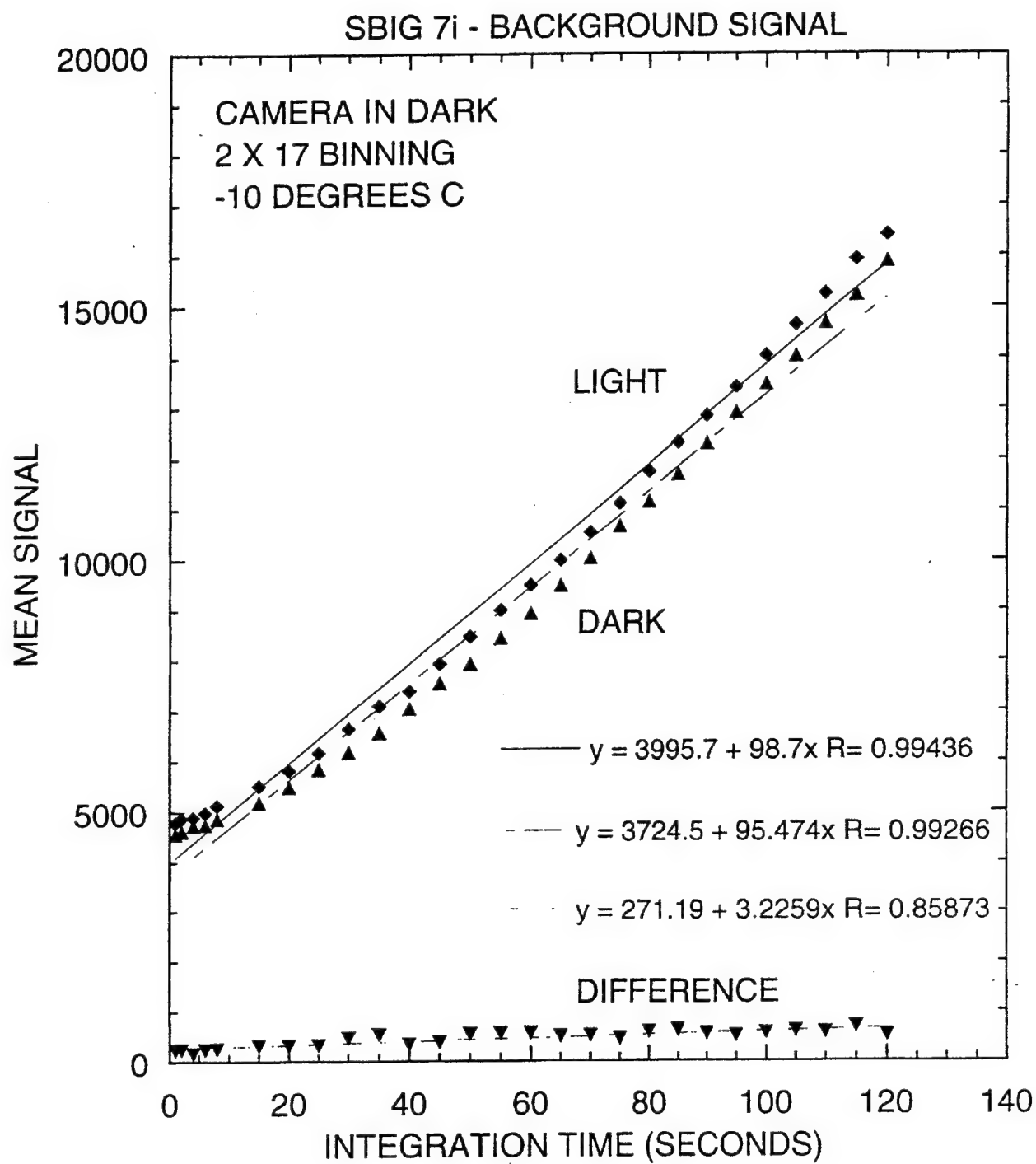


Figure 45. Mean signal data as a function of integration time obtained with the camera at a temperature of - 10 degrees C.

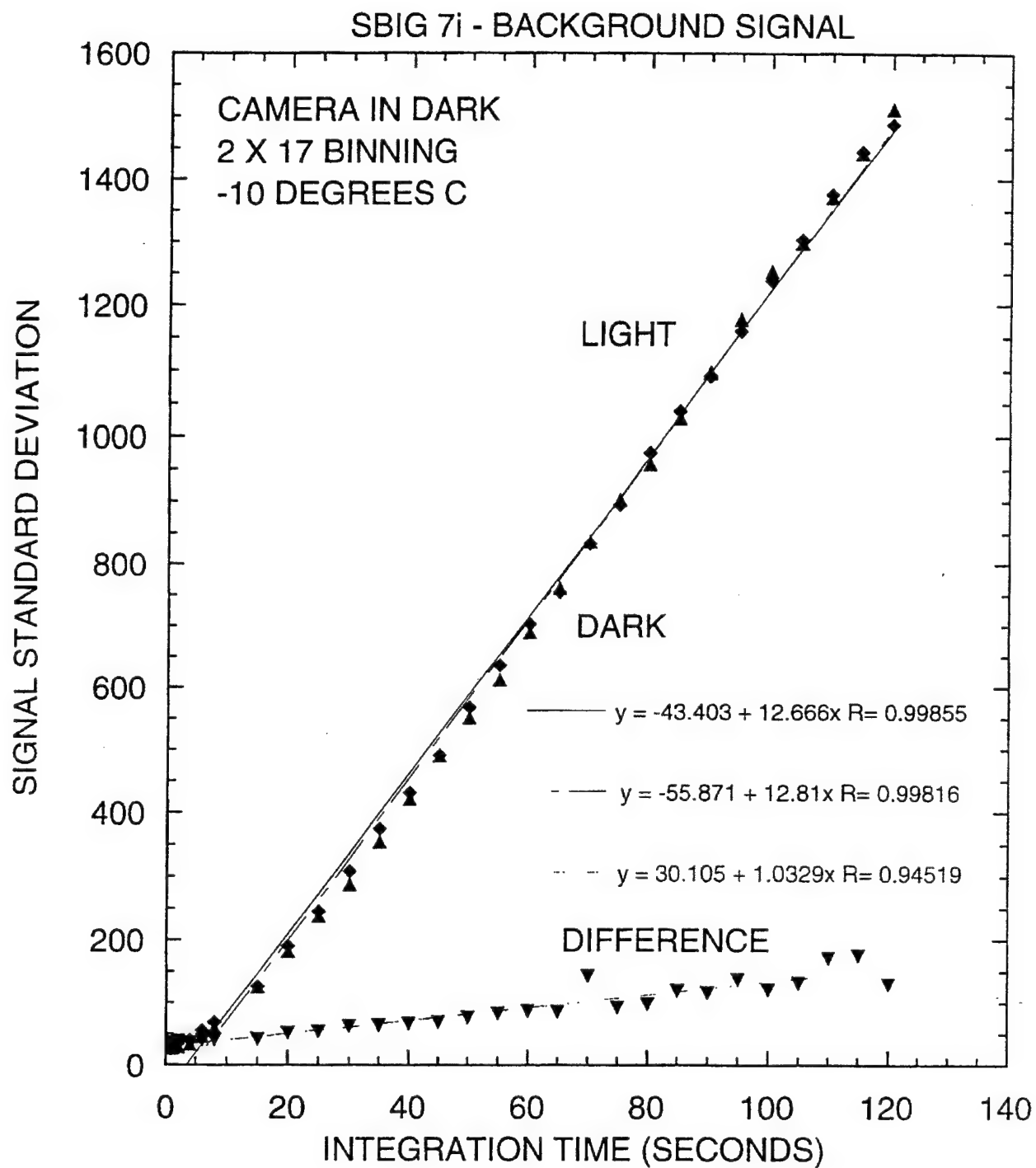


Figure 46. Signal standard deviation as a function of integration time obtained with the camera at a temperature of - 10 degrees C.

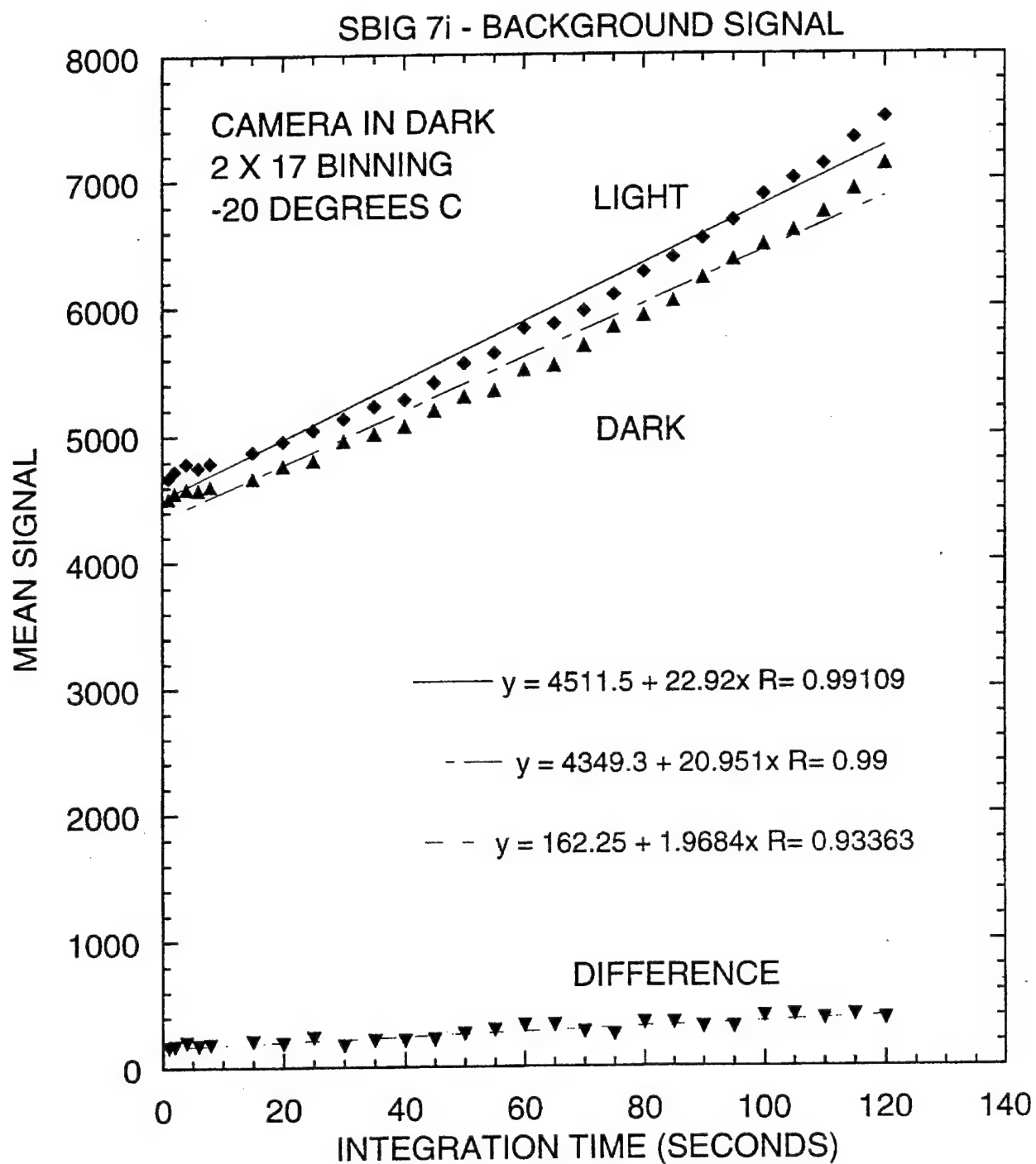


Figure 47. Mean signal data as a function of integration time obtained with the camera at a temperature of - 20 degrees C.

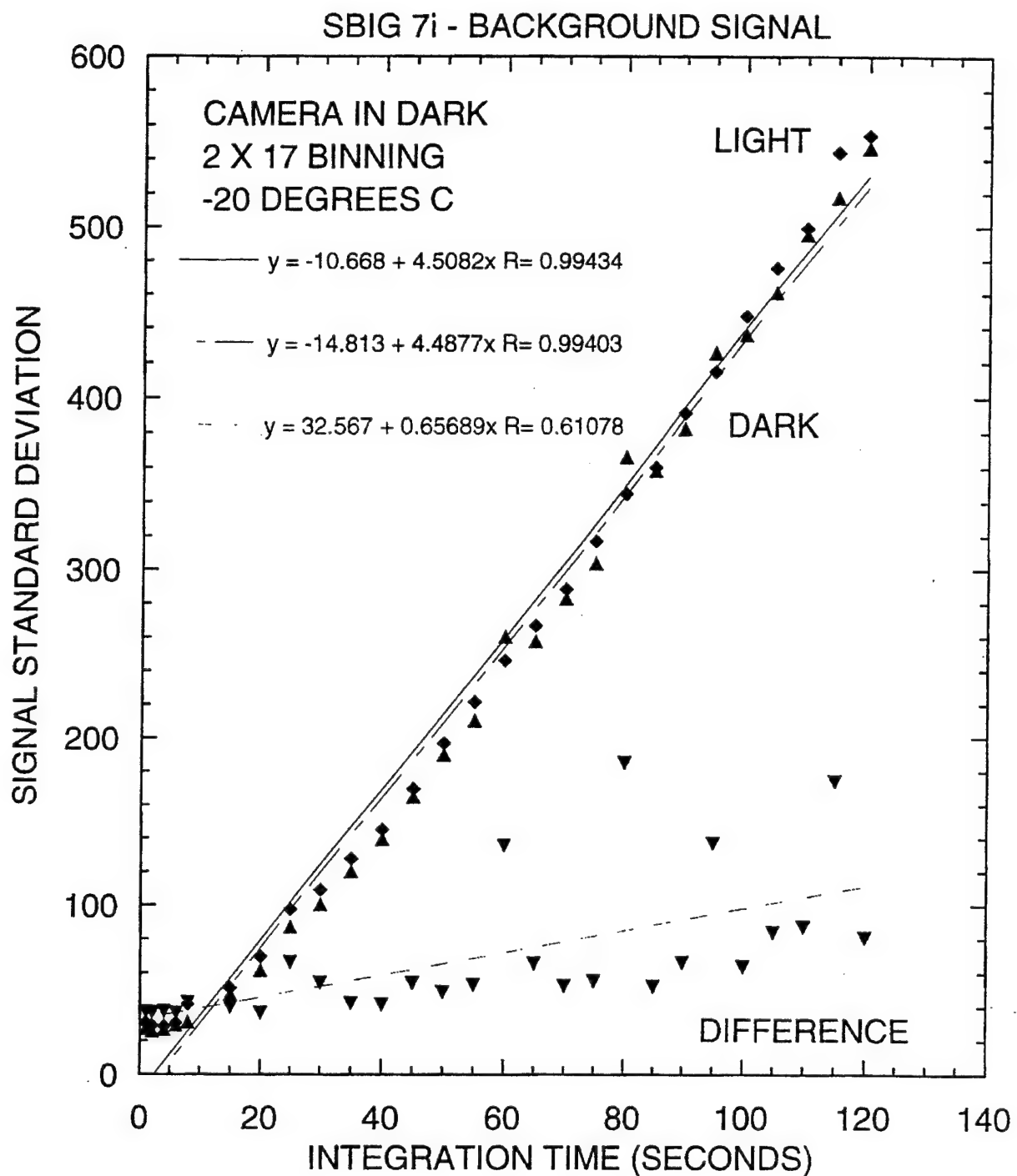


Figure 48. Signal standard deviation as a function of integration time obtained with the camera at a temperature of - 20 degrees C.



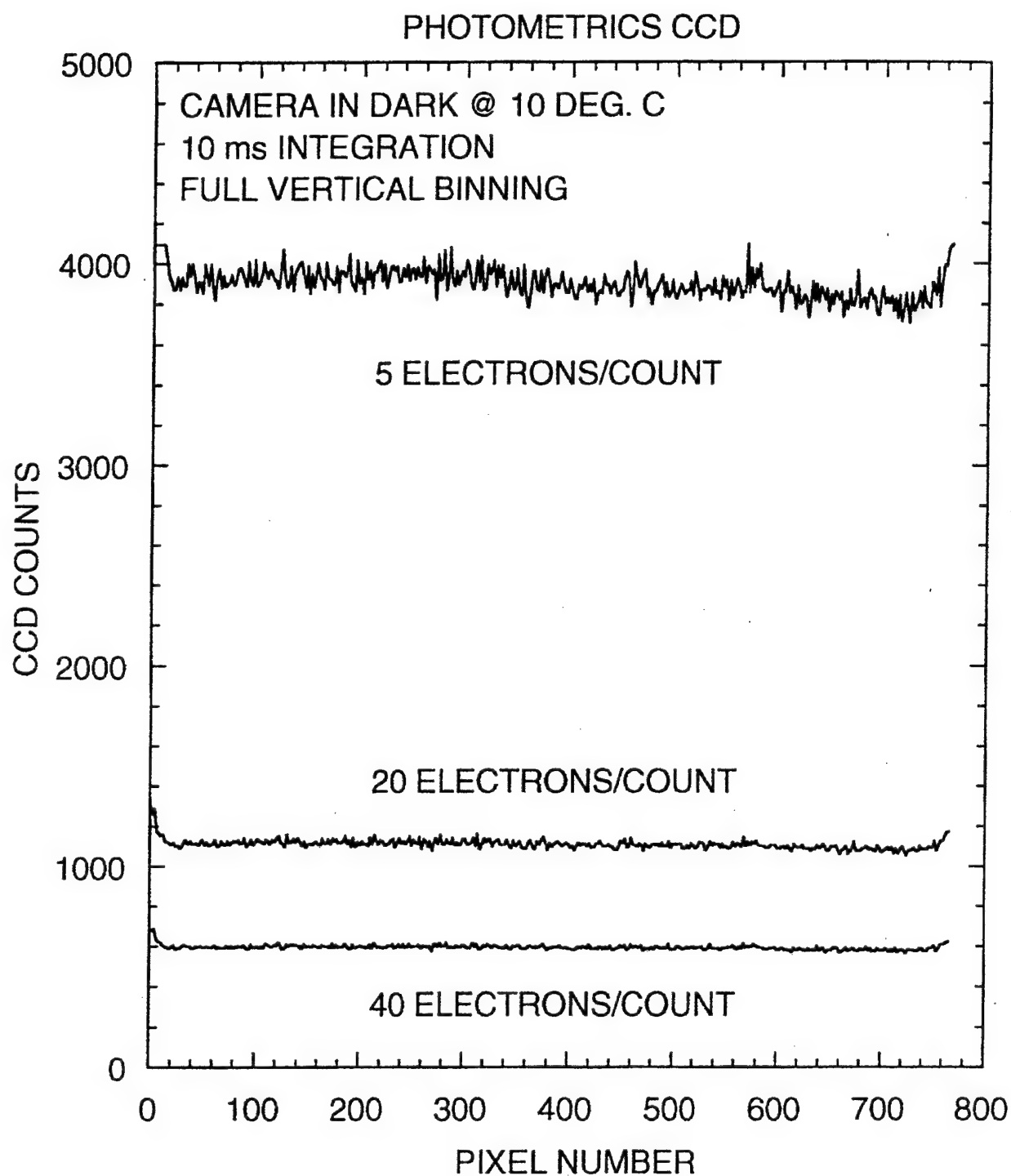


Figure 49. Display of the dark spectra obtained with the camera in the dark and at 10 degrees C with a 10 ms integration time for the three gain factors.

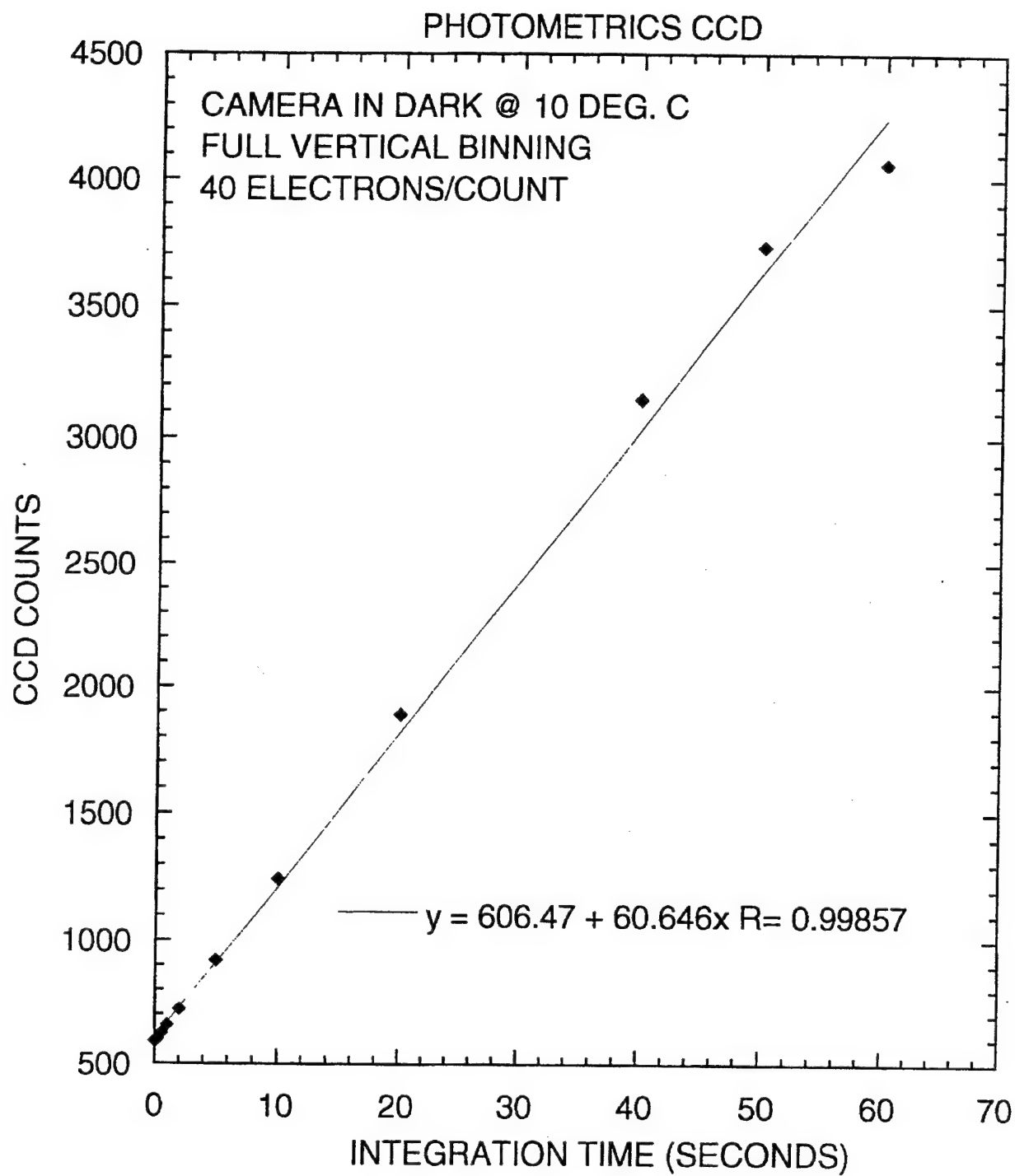


Figure 50. The dependence of the mean dark signal on integration time with the camera gain set at its lowest value.

value of 40 electrons/count. Saturation begins to occur at integration times longer than 40 seconds in the 2 x full vertical binning mode. Figure 51 displays some of the spectra associated with the data in Fig. 50. The percentage standard deviations of the spectra increase with increasing integration time contrary to expectations. We attribute this effect to pattern noise or pixel-to-pixel variations in dark count across the CCD array. For longer integration times the variations between pixels become more pronounced.

Overall, we find that the SBIG 7i CCD system performs better than the Photometrics Sensys system for Raman spectroscopy applications even though both cameras use the same CCD chip. Possible explanations for the improved performance of the SBIG camera include its lower operating temperature and higher resolution D/A convertors.

### 2.2.3 Andor CCD Camera Evaluation

We evaluated a CCD camera system from Andor Technology to determine the extent to which the use of a more expensive CCD would improve our Raman detection limits. The system we borrowed from Andor included an EEV 30-11 front-illuminated CCD chip with a 256 x 1024 array of 26 micrometer square pixels, a three-stage TE-cooler which was capable of lowering the CCD to a temperature of -60 degrees C without water cooling (even lower with water cooling), and complete software for use with the Windows operating system. Our initial tests with the system involved recording data with the camera in the dark to quantify background noise levels. Figure 52 displays the mean signals recorded as a function of integration time for full vertical binning and with the CCD at -60 degrees C. The signal intercept at zero integration time can be thought of as read noise, and the signal component which increases with time is dark current. After an integration time of more than five minutes, the dark component is only about 60 counts out of the 16-bit (65,536) count capacity. In terms of background noise, the more important quantity is the standard deviation of this mean signal across the 1024-point axis of the array. Figure 53 plots the signal standard deviation as a function of integration time. For a 5-minute integration time, the measured standard deviation was only 9 counts. The dark characteristics of the Andor CCD were excellent. In contrast, the less-expensive SBIG camera we have been using has signal standard deviations which are more than 1000 times greater after a five minute integration time (see Fig. 54).

Overall, we were very much impressed with the operation of the Andor camera system and are considering using it for applications which require very high sensitivity and can justify the higher price.

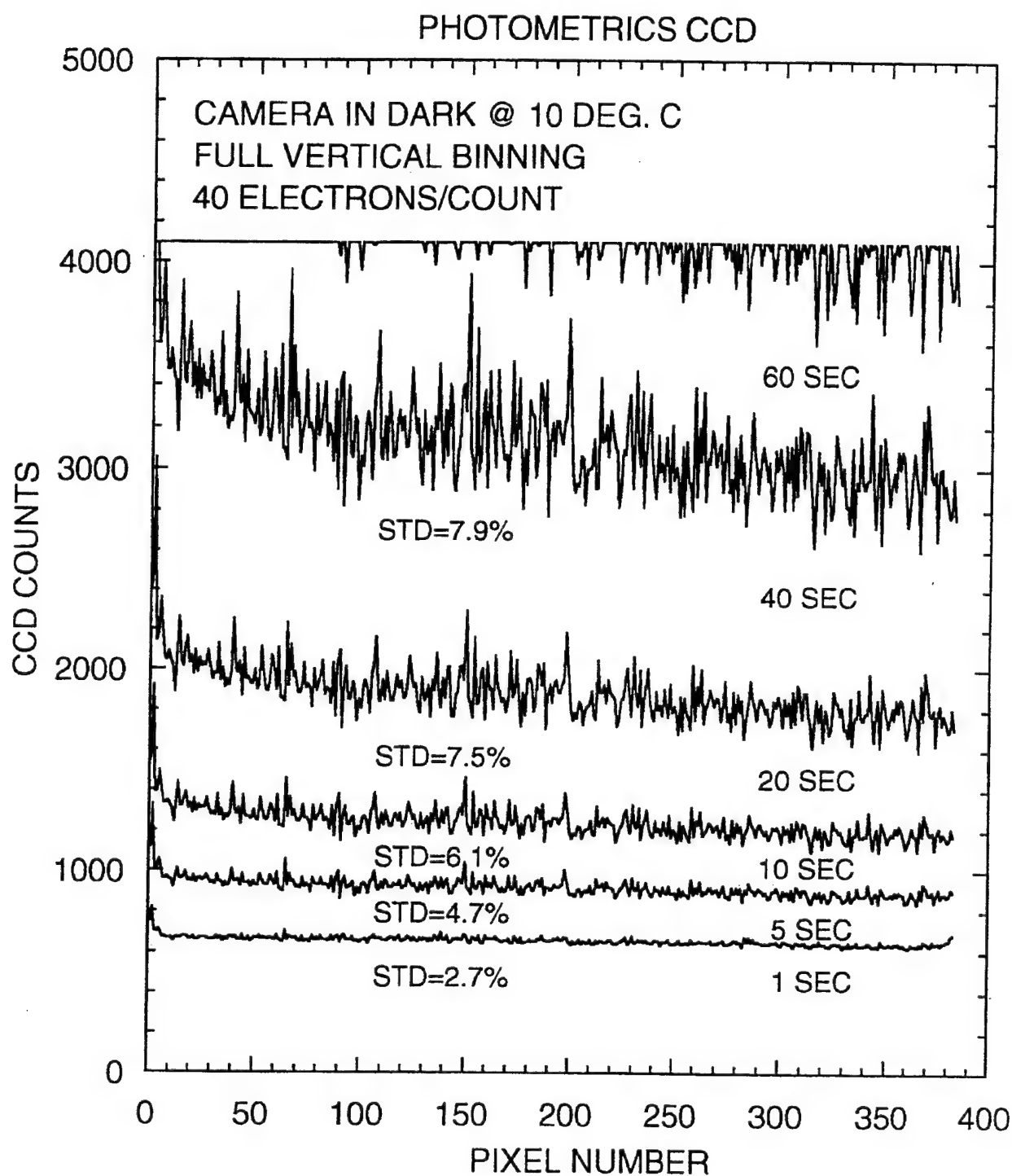


Figure 51. Display of some of the spectra associated with the data in Fig. 46.

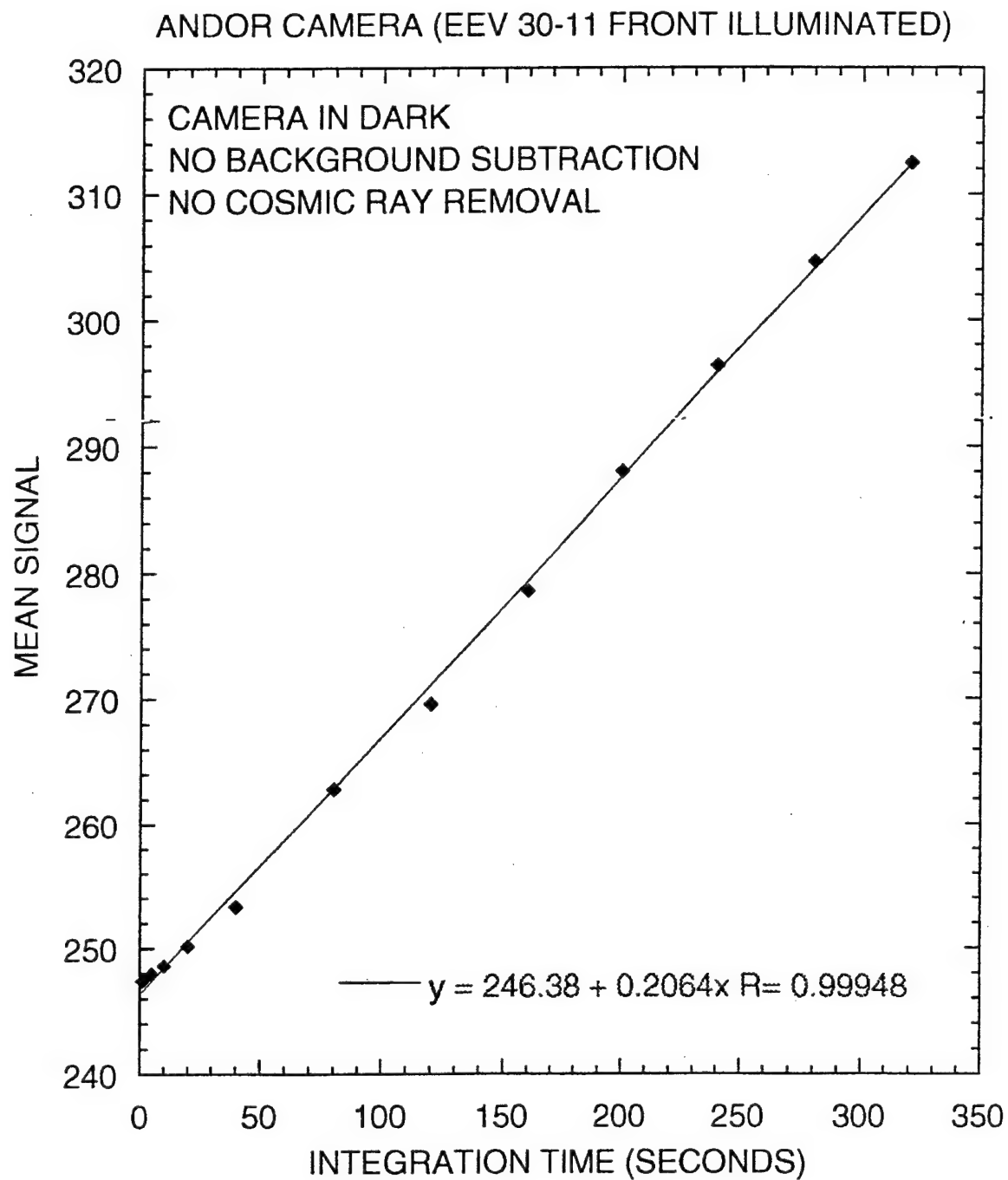


Figure 52. The mean signals recorded as a function of integration time for full vertical binning and with the CCD at -60 degrees C.

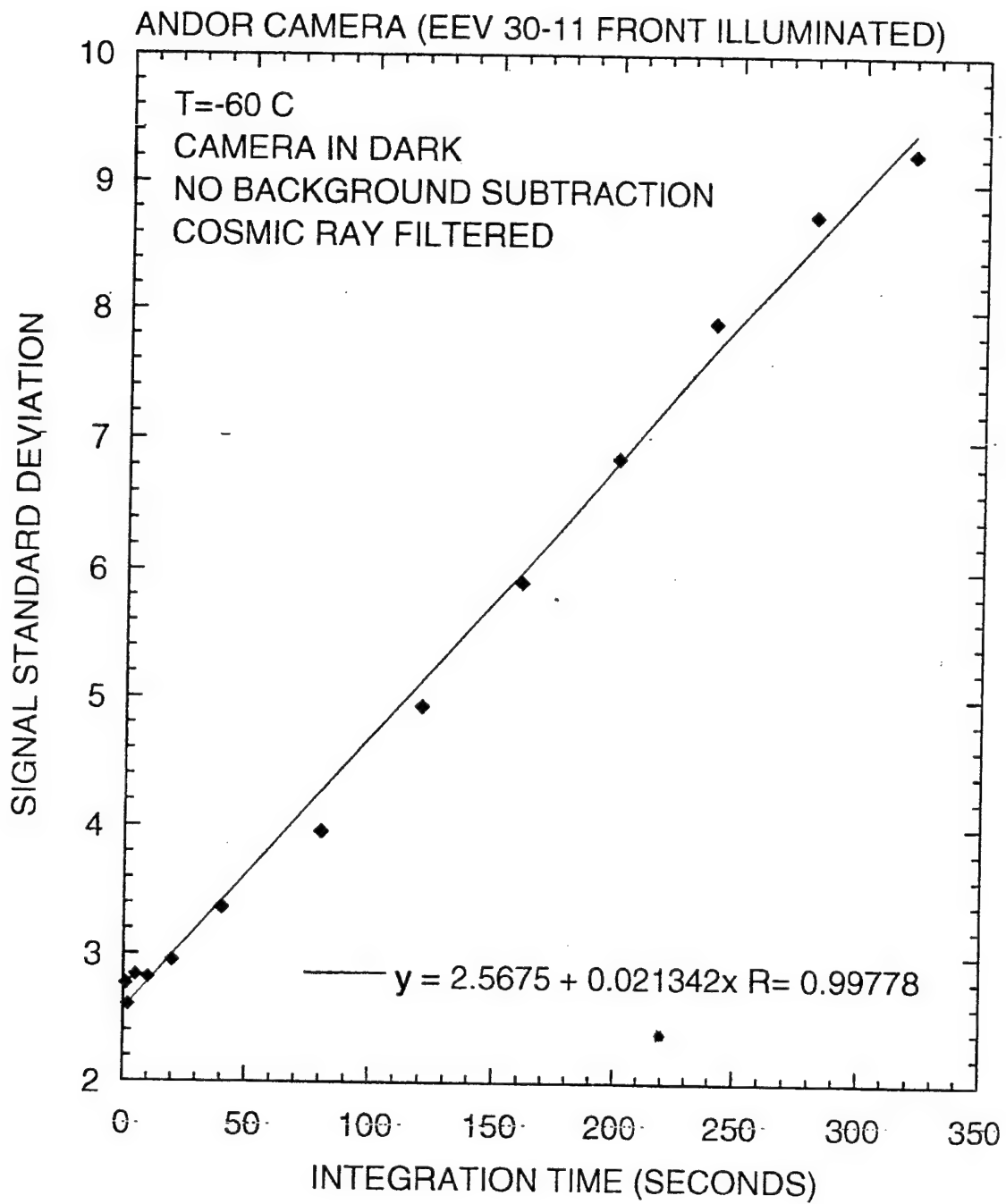


Figure 53. Signal standard deviation as a function of integration time. For a 5-minute integration time, the measured standard deviation was only 9 counts.

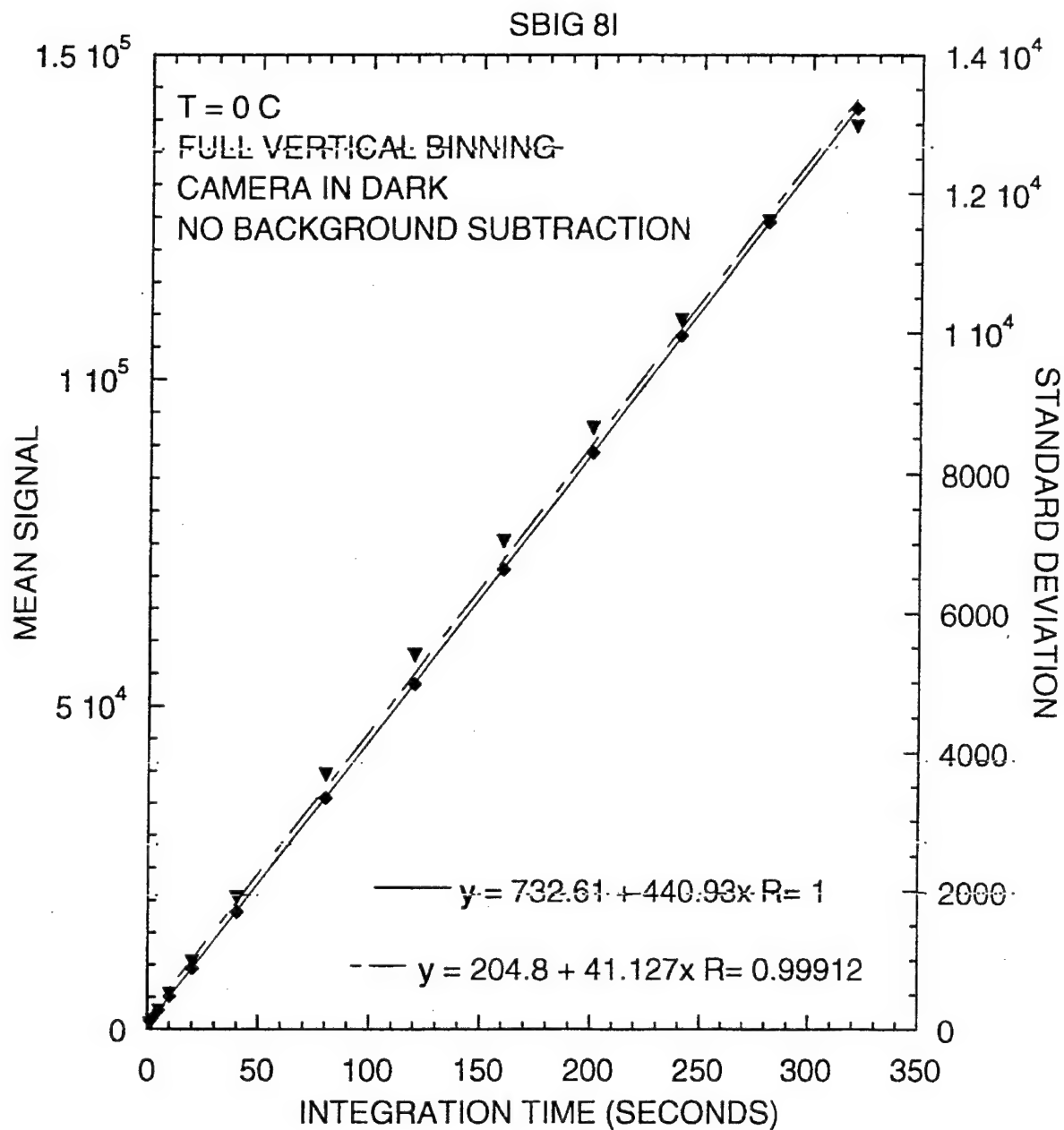


Figure 54. Mean signal and standard deviation as a function of integration time for a SBIG camera. SBIG camera signal standard deviations are more than 1000 times greater after a five minute integration time.

## 2.6 Performance of Current Prototype Instrument

The current gas-phase Raman prototype includes the following components:

1. Diode laser-pumped power build-up cavity with or without line width narrowing operating at a wavelength near 660 nm.
2. Compact sample cell incorporating power build-up cavity.
3. F/1.4 spectrograph with conventional grating and laser line rejection filter.
4. SBIG 7i CCD detector.
5. Windows 95/98 control software.

For final prototype testing and characterization, the power build-up cavity was realigned and its mirrors were carefully cleaned. The circulating power inside the cavity was about 32 W again, indicating that this power may be the limit of the current design. The previous prototype could reach over 60 W of power but was not as robust as the current design and its dimensions were also larger. We first measured the background intensity with argon inside the cell. Figure 55 shows that when the laser rejection filter was placed inside the spectrograph, the background intensity was lower. This may indicate that we have a stray light rejection problem associated with zeroth order grating reflections which may be partially absorbed by the filter. We plan to order a holographic grating with 1200 gr/mm which should improve the stray light rejection. We also plan to use a better dielectric laser line rejection filter rather than the color glass filter we are currently using and hope that we can reduce this background intensity.

We next collected a Raman spectrum from ambient air with the background subtracted as shown in Figure 56. Using a slit width of 150  $\mu\text{m}$  and an integration time of 30 s, we were able to obtain relatively strong signals from nitrogen and oxygen with 735,820 and 246,780 counts, respectively indicating that we have about 2.5 times more signal than in our previous results. We next filled the gas cell with a gas mixture containing 95%  $\text{CO}_2$ , 4%  $\text{N}_2$ , and 1%  $\text{O}_2$ . As shown in Figure 57, we obtained all the peaks from the three components. There are two Raman peaks for  $\text{CO}_2$  near 1350  $\text{cm}^{-1}$  and one each for  $\text{O}_2$  and  $\text{N}_2$  at 1555  $\text{cm}^{-1}$  and 2331  $\text{cm}^{-1}$ , respectively. Compared to our previous results, we obtained about twice the signal. Also, we were able to detect the 1% level of oxygen.

To demonstrate the resolution from different slit sizes, we have done a series of experiments by using slit widths of 50, 100, 150, and 250  $\mu\text{m}$ . Figure 58 depicts the nitrogen peaks obtained using these slits. It is obvious that the peak intensities do not increase linearly with the slit sizes. Especially, from 150 to 250  $\mu\text{m}$ , we found that the peak intensity only went up by 15% which indicates that the beam size of the laser was between 150 to 250



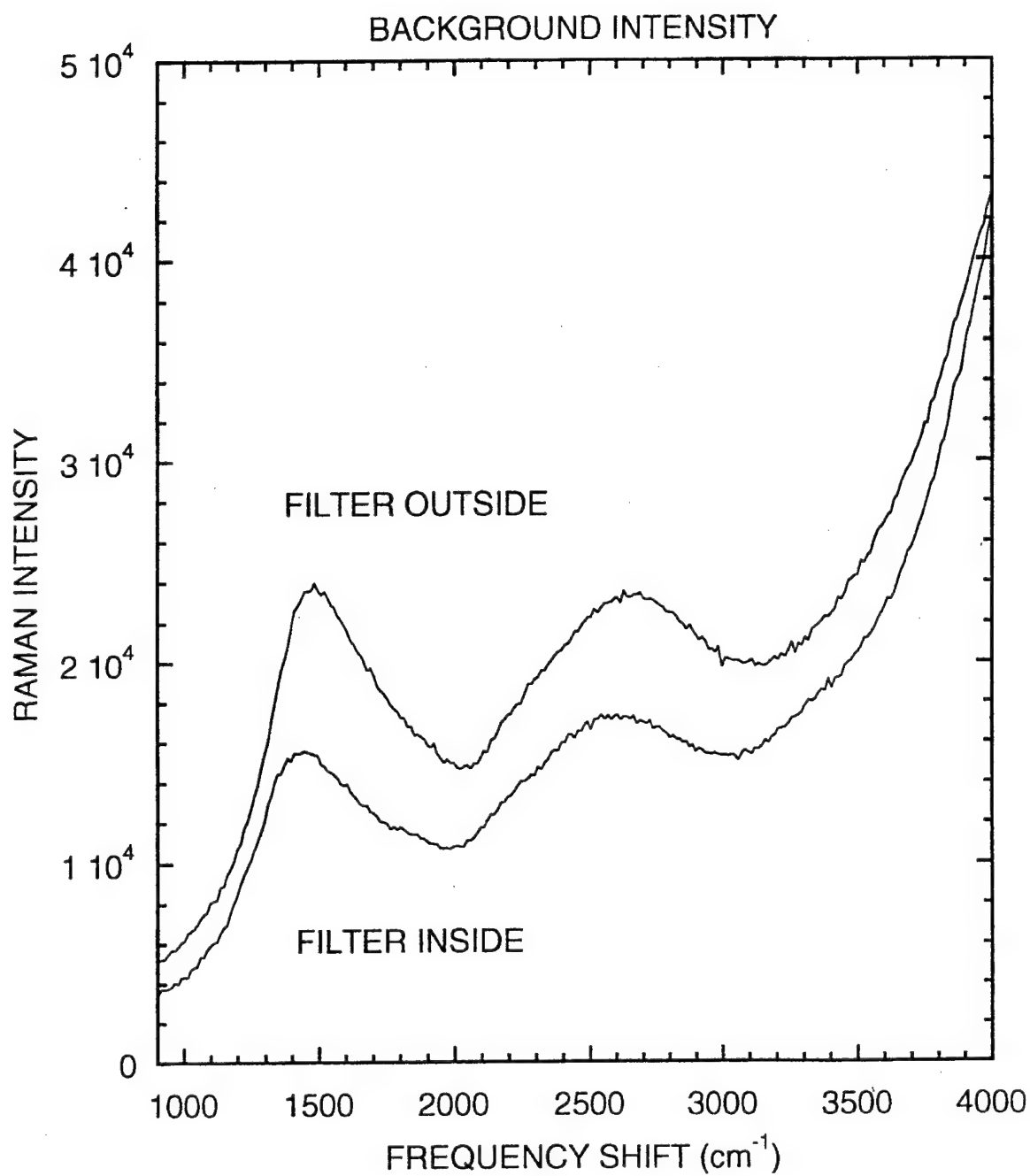


Figure 55. Effects of filter placement on background noise.

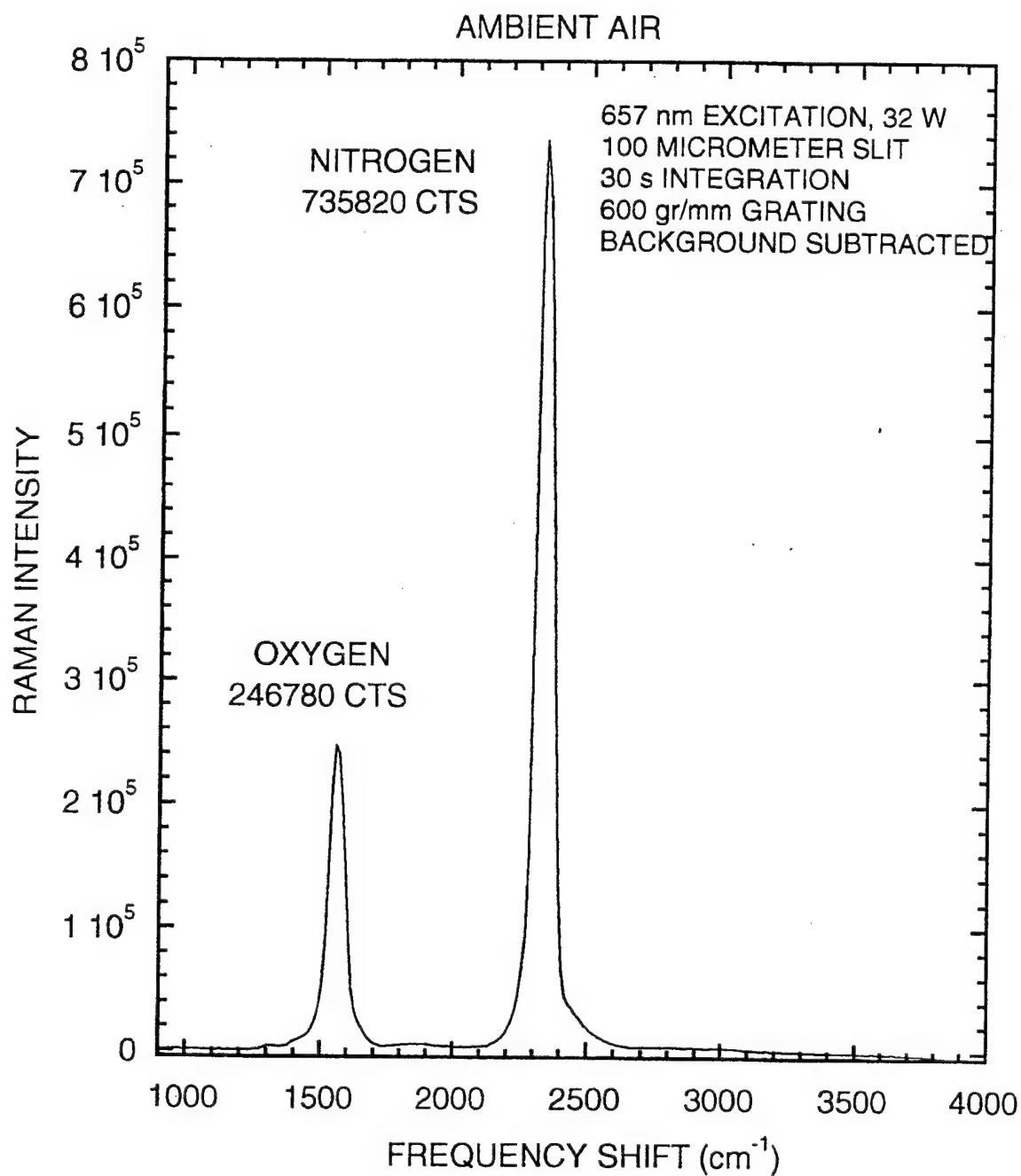


Figure 56. Raman spectrum from ambient air with the background subtracted .

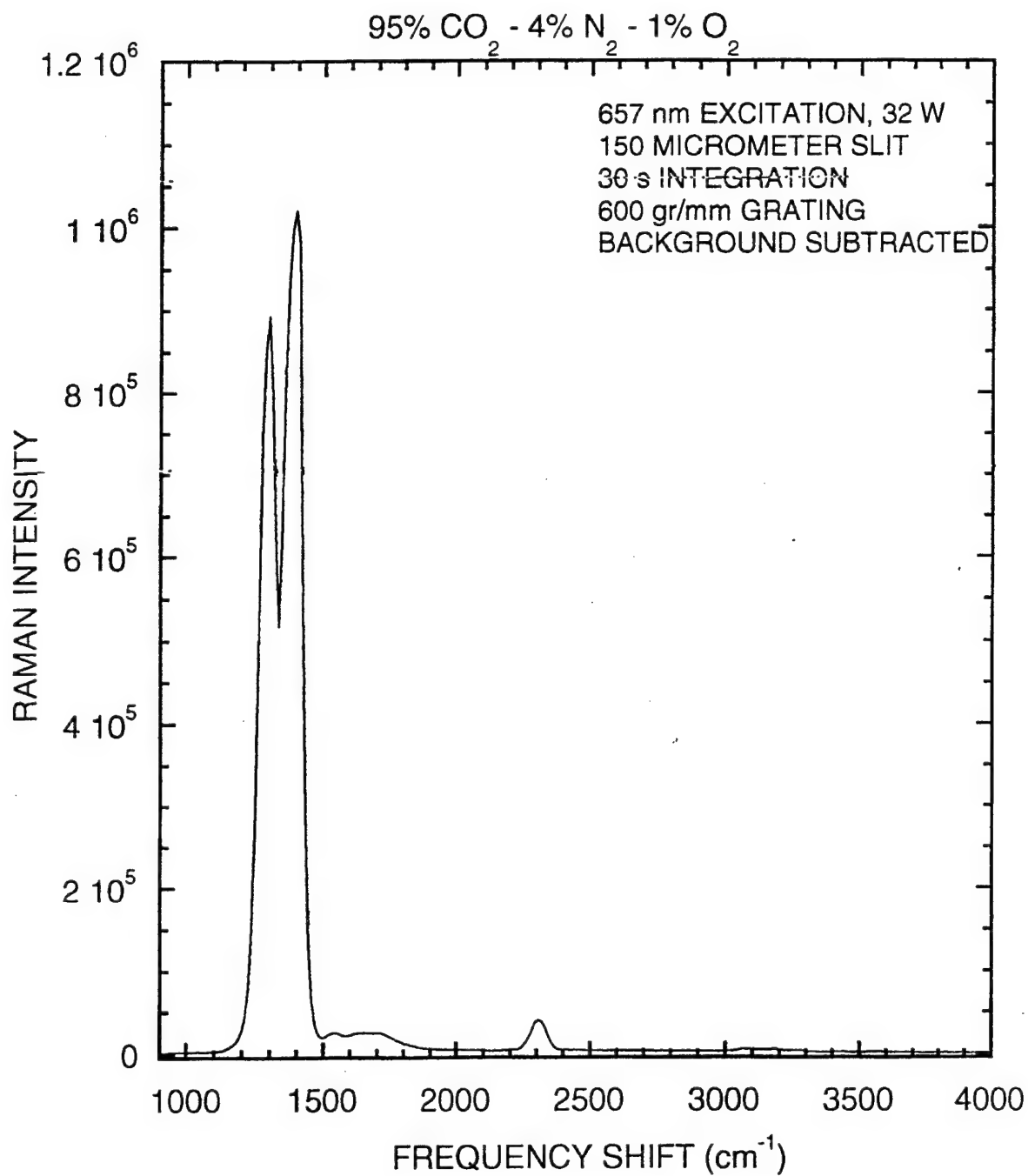


Figure 57. Peaks from the three gases. There are two Raman peaks for CO<sub>2</sub> near 1350 cm<sup>-1</sup> and one each for O<sub>2</sub> and N<sub>2</sub> at 1555 cm<sup>-1</sup> and 2331 cm<sup>-1</sup>, respectively.

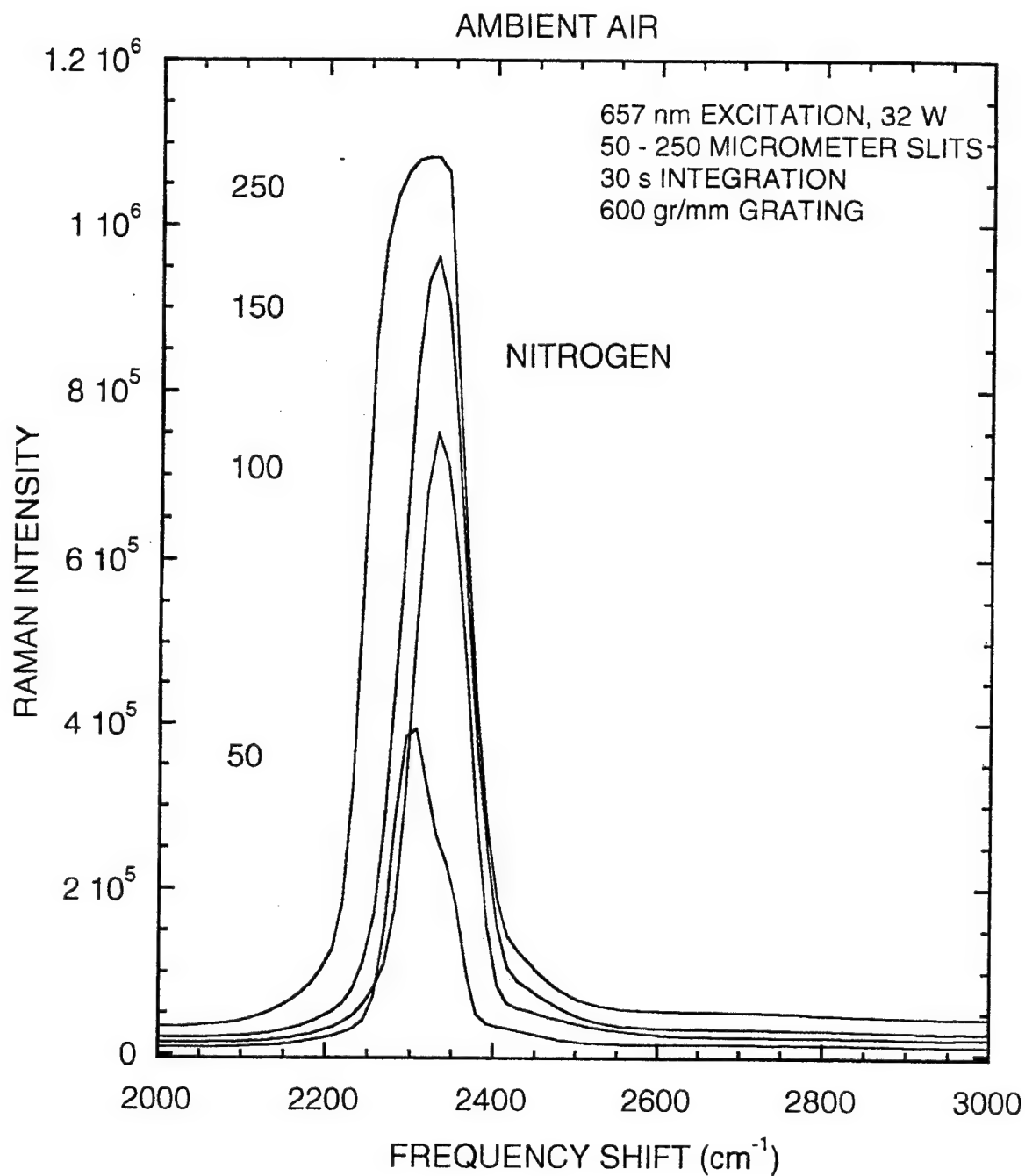


Figure 58. Nitrogen peaks obtained using different slit widths.

$\mu\text{m}$ . For a 50  $\mu\text{m}$  slit, the resolution was about 20  $\text{cm}^{-1}$  which is better than the laser source (45  $\text{cm}^{-1}$ ), and that was why we saw a side mode structure from the laser.

We also collected a Raman spectrum from butane to observe the system response in the C-H bond region near 3000  $\text{cm}^{-1}$ . Figure 59 demonstrates the results. By changing the position of the grating, we had a spectral coverage with the spectrograph from 0 to approximately 3000  $\text{cm}^{-1}$ . As seen in the figure, a relatively strong C-H peak was observed near 3000  $\text{cm}^{-1}$  with an intensity of  $\sim 1,000,000$  counts with only a 3 s integration time. We also noted that the elastic light (laser) at 0  $\text{cm}^{-1}$  was stronger than in the ambient air spectrum.

To monitor gas concentration changes with time, we recorded Raman spectra as the gas within the sample cell changed from the carbon dioxide mixture to ambient air with both the inlet and outlet open. Figure 60 shows the results where each spectrum was recorded with an integration time of 30 seconds. As expected the carbon dioxide peaks at high pixel number decrease with increasing spectrum number (time) while the oxygen and nitrogen peaks increase.

To test the stability of the power buildup system, we measured Raman spectra from ambient air for an 8-hour period (1000 spectra). From Figure 61, the nitrogen peak maximum and integrated nitrogen peak had standard deviations of 6.94 % and 4.75%, respectively. Again, this result indicates that we need to improve our design for better stability. Figure 62 depicts the first 100 of the spectra recorded overnight. We note that the random lineshape changes in the nitrogen peak we had observed previously disappeared because of the low resolution of spectrograph.

### 2.6.1 Filter Comparison

We received a high-pass dielectric filter from Omega Optical Inc. to replace the color filter we had been using in front of our spectrograph to attenuate scattered light at the laser wavelength. Our hope was that the new filter would reduce the amount of background light we have been observing in our gas-phase Raman spectra. Figure 63 compares background spectra obtained with argon gas in the sample cell using the color filter and the dielectric filter. The dielectric filter does a better job at attenuating light at the laser wavelength (zero frequency shift), becomes transmitting at a shorter wavelength, and has a higher transmission in the pass region than the color filter. However, the background peak at a frequency shift near 1300  $\text{cm}^{-1}$  is still observed in the spectra. From this data, we conclude that the laser is emitting light at a wavelength corresponding to this frequency shift and that we will not be able to eliminate it using a high-pass filter. Figure 64 shows how this background emission appears under the oxygen Raman spectrum collected from ambient air. Another approach to eliminate this background would be to place a laser bandpass filter after the laser and before the mirror cavity to block the emission. However, since narrow bandpass filters are typically only about 60% transmitting, we would sacrifice laser power if we use this approach. We can, of course, subtract the background from our collected spectra, but we add additional noise in the process.

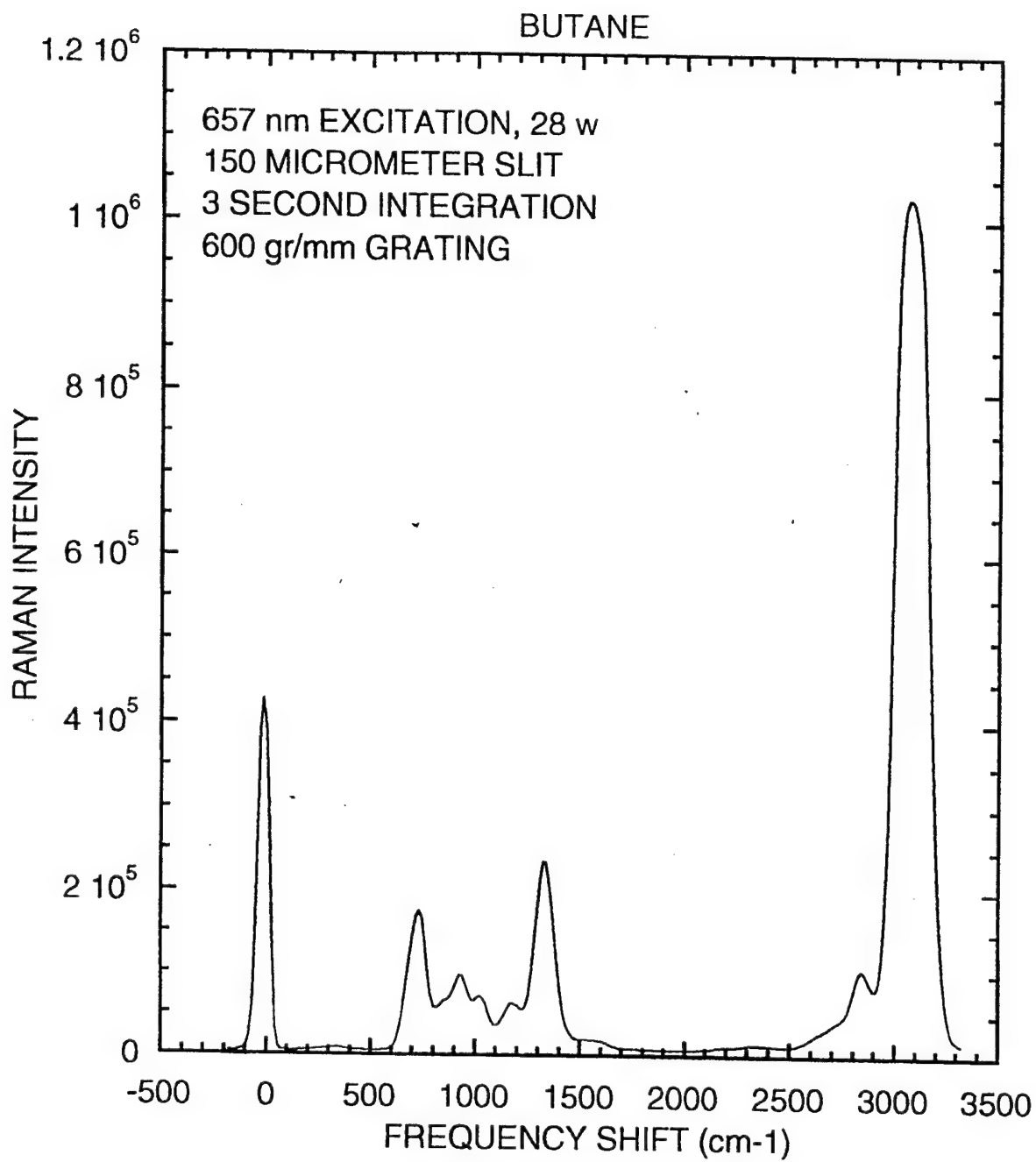


Figure 59. Raman spectra of butane.

# CARBON DIOXIDE TO AIR

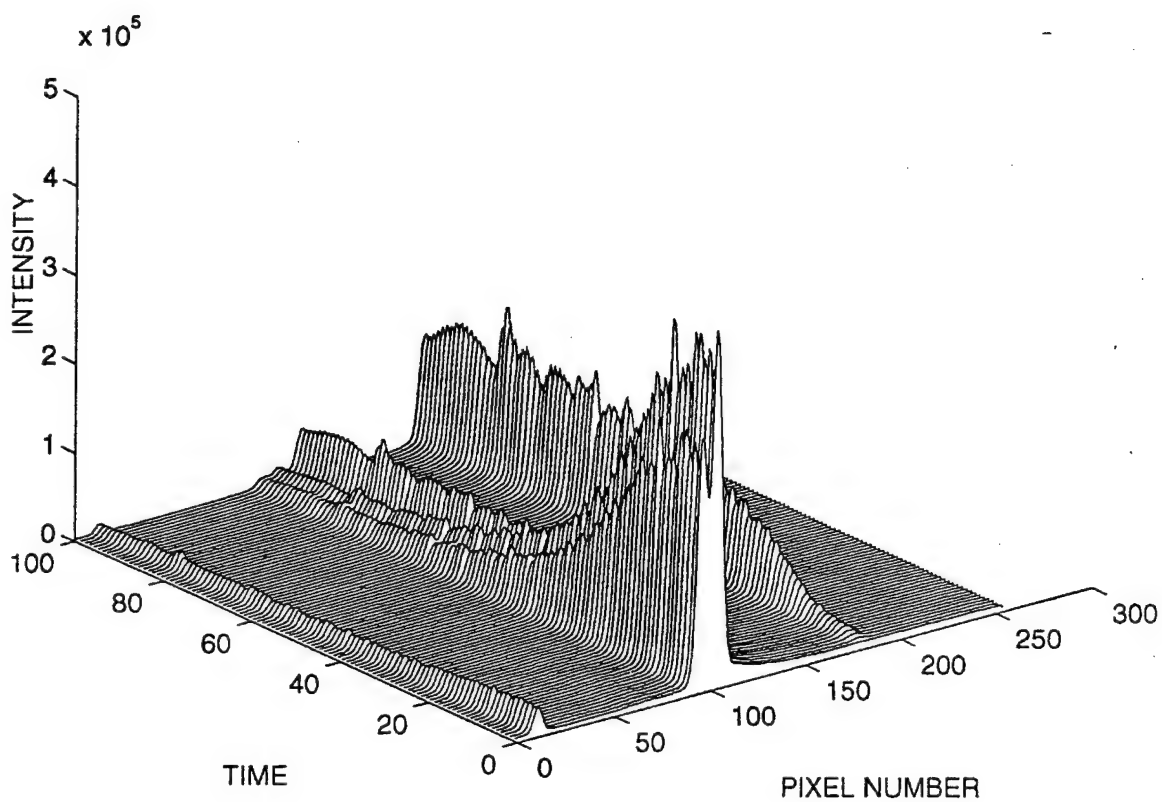


Figure 60. Raman spectra of gas concentrations over time as  $\text{CO}_2$  is replaced by ambient air.

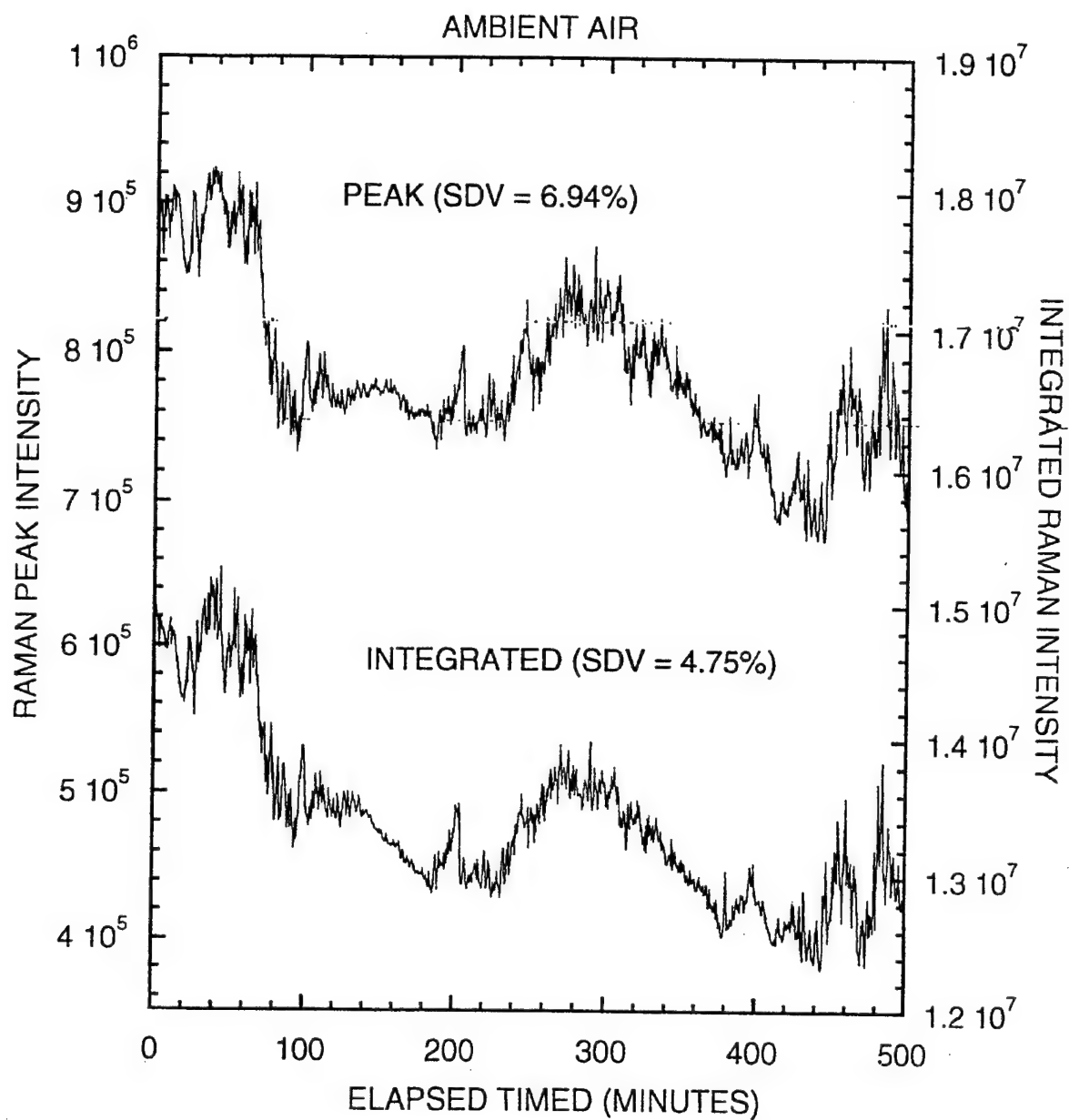


Figure 61. Raman spectra from ambient air for an 8-hour period (1000 spectra). The nitrogen peak maximum and integrated nitrogen peak had standard deviations of 6.94 % and 4.75%, respectively.



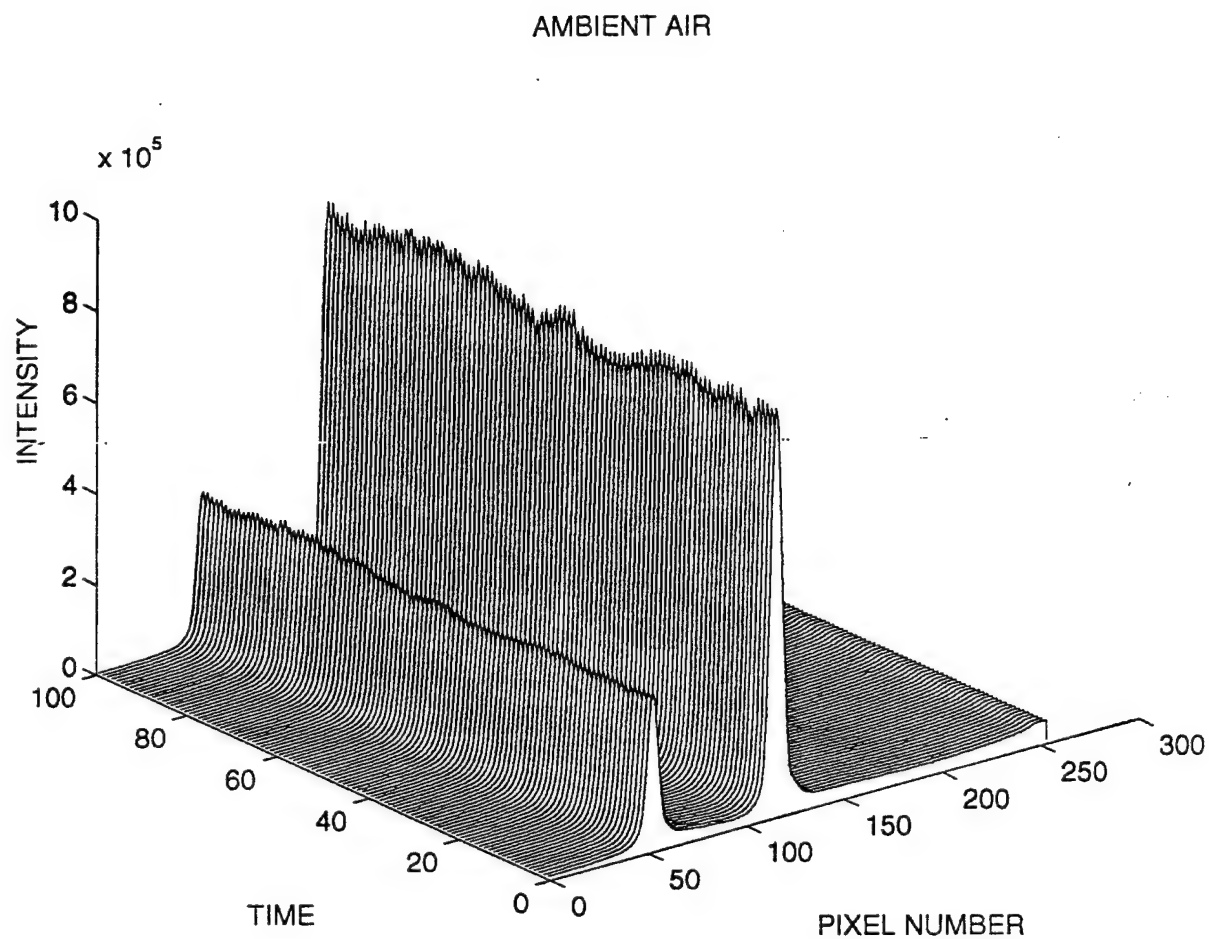


Figure 62. One hundred spectra recorded overnight to get an indication of gas phase Raman prototype stability.

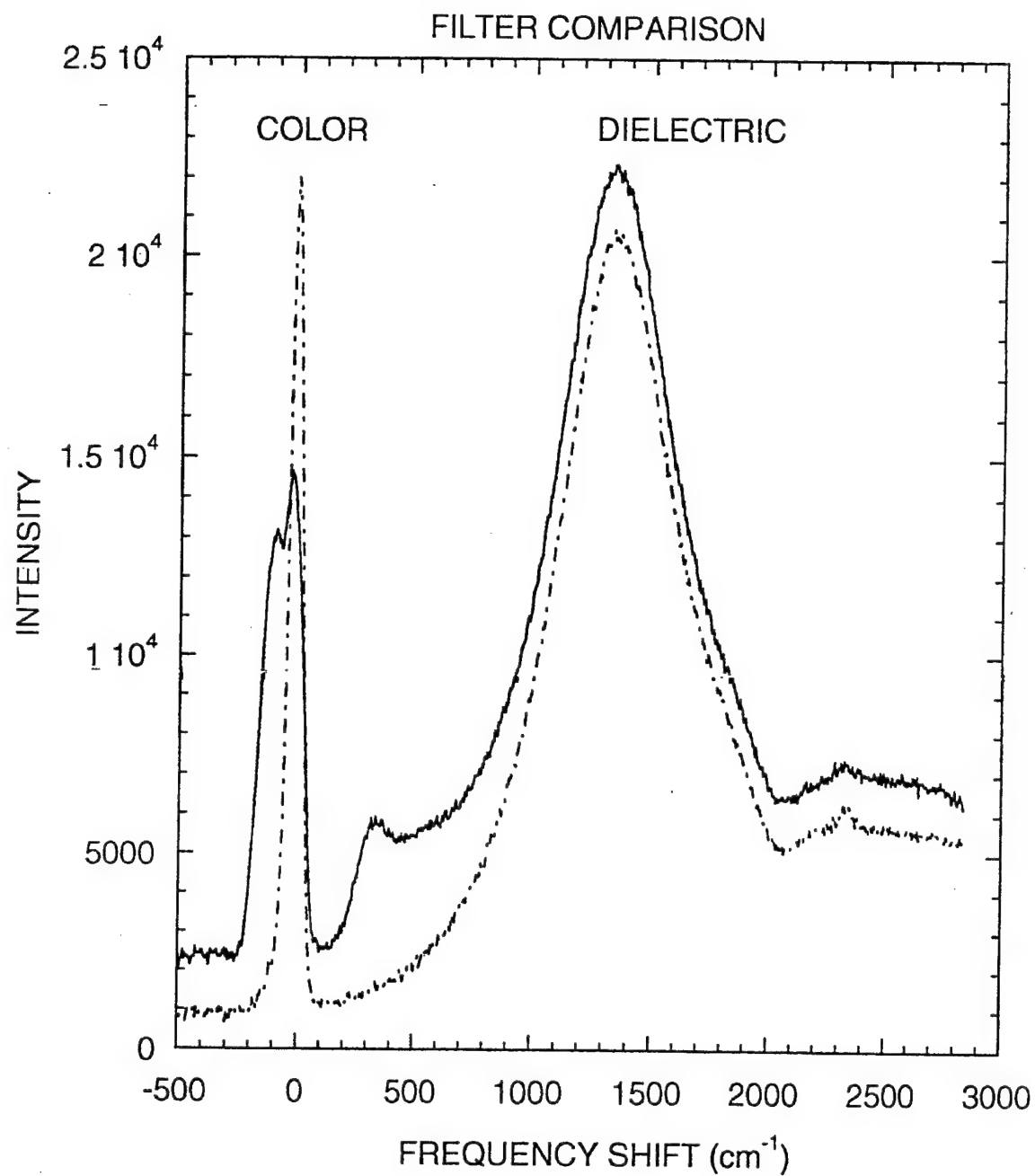


Figure 63. Background spectra obtained with argon gas in the sample cell using the color filter and the dielectric filter.

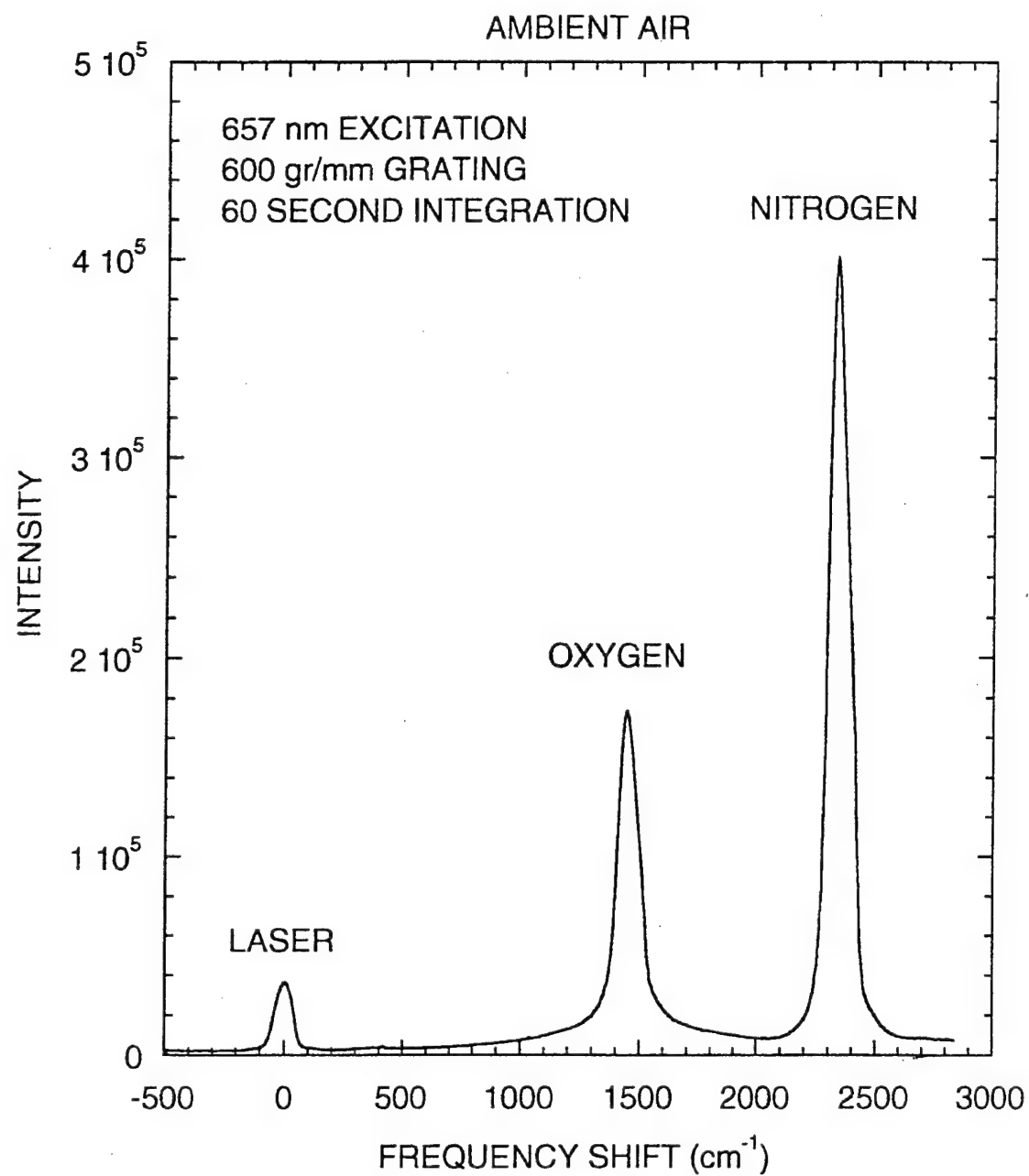


Figure 64.. Depicts how the background emission appears under the oxygen peak in Raman spectrum collected from ambient air.

emission background we observe in our collected spectra.

### 2.6.2 System Stability

We have been measuring the stability of our gas-phase Raman system by collecting spectra from ambient air repetitively over a 12-hour period. Figure 65 displays typical results with the laser operating at full current for the measured variations in the Raman peak intensity and the integrated Raman intensity. The observed standard deviations of 16.3% and 3.63% in the peak and integrated values are considerably worse than the values near 0.1% that we routinely achieve with our liquid-phase system. However, in the gas phase system we have a photodiode placed after the second mirror in the power build-up cavity which measures the light which leaks through this high-reflectivity mirror and provides a continuous measure of the laser cavity power. Figure 66 shows how the photodiode output matches the variation in integrated Raman intensity. The photodiode output doesn't track the variation in Raman peak intensity (SDV = 16.3%) nearly as well. The origin of the large peak variation is shown in Fig. 67 which plots the variation of the nitrogen Raman peak on an expanded scale over the 12-hour period. Our laser output frequency is clearly varying in a periodic fashion with a period of a few hours. We suspect that this periodic variation may be caused by the temperature controller we use for the laser cavity, but will need additional studies to verify this cause.

We attempted to improve the laser stability by operating at a lower current, but as shown in Fig. 68, the nitrogen Raman peak obtained with a laser current of 450 mA continues to exhibit a periodic frequency variation in data collected over a 12-hour period. By improving the averaging procedure for monitoring the photodiode output, we were able to achieve a good match between the integrated nitrogen peak area and the photodiode output as shown in Fig. 69. The variations in the nitrogen peak area and the photodiode output are 8.07 % and 8.06 %, respectively. By normalizing the nitrogen peak area by the measured photodiode output, we were able to reduce the normalized nitrogen peak area variation to 0.74 % from its initial value of 8.07 %. This normalized variation over a 12-hour period would provide acceptable accuracy for a variety of applications. Fig. 70 shows how the measured nitrogen peak areas were linearly related to the photodiode output values. We will continue to use the photodiode output for data normalization, but we will also attempt to improve the overall frequency stability of the system. We will first narrow the laser output using diffraction grating feedback to determine whether or not the frequency stability is improved.

### 2.6.3 Narrow Line Width Laser Operation

We narrowed the line width of our gas phase laser system to approximately 30 GHz by inserting a volume holographic grating between the laser diode and the power build-up cavity. Although the line width narrowing results in a reduction in output power, it allows us to better resolve Raman peaks from gases with similar Raman shifts. We also hoped to reduce the amount of spontaneous emission from the laser which has been appearing as unwanted background in our Raman spectra. Figure 71 shows a Raman spectrum obtained with nitrogen contained within the

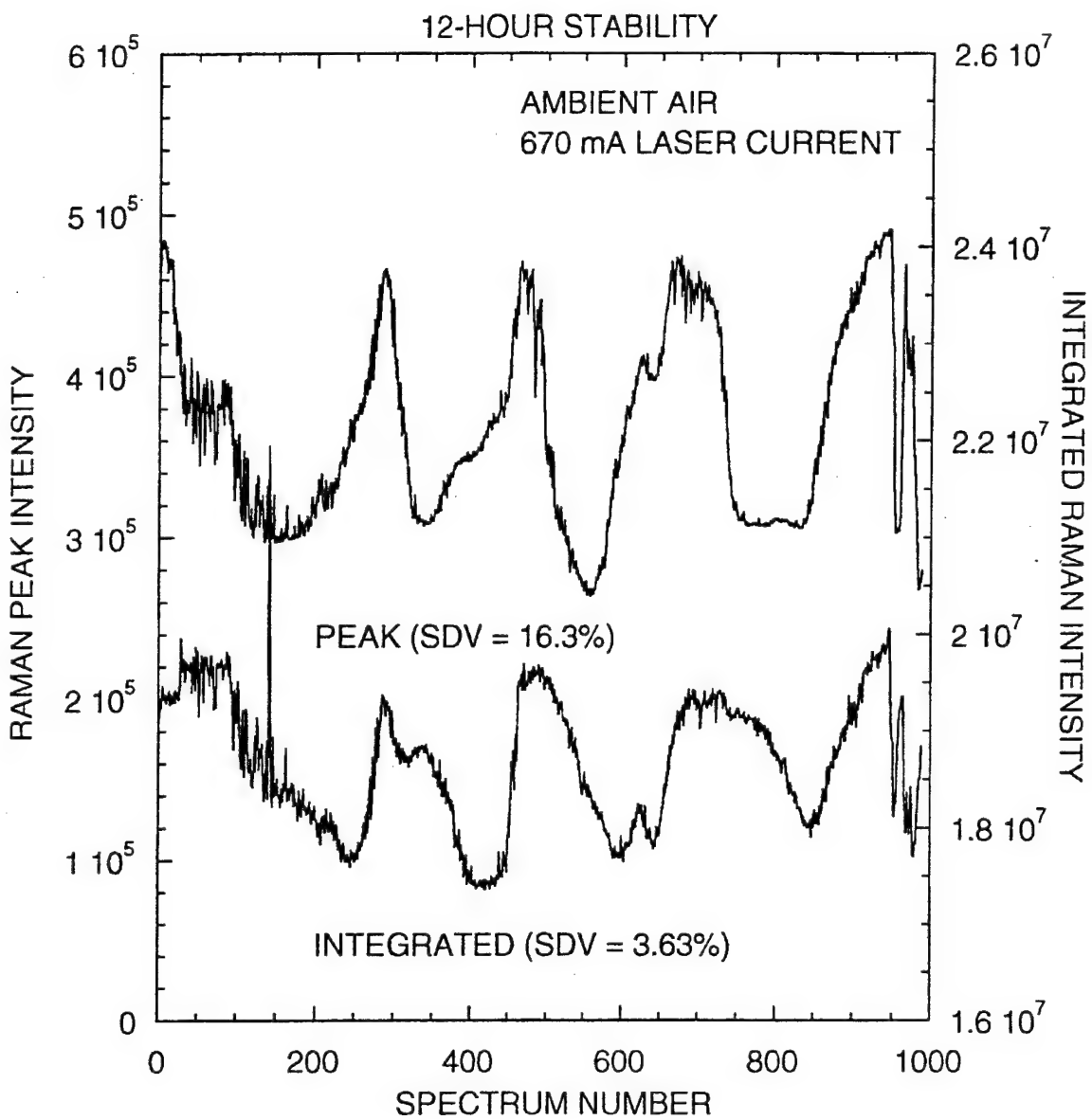


Figure 65. Display of typical results with the laser operating a full current for the measured variations in the Raman peak intensity and the integrated Raman intensity.

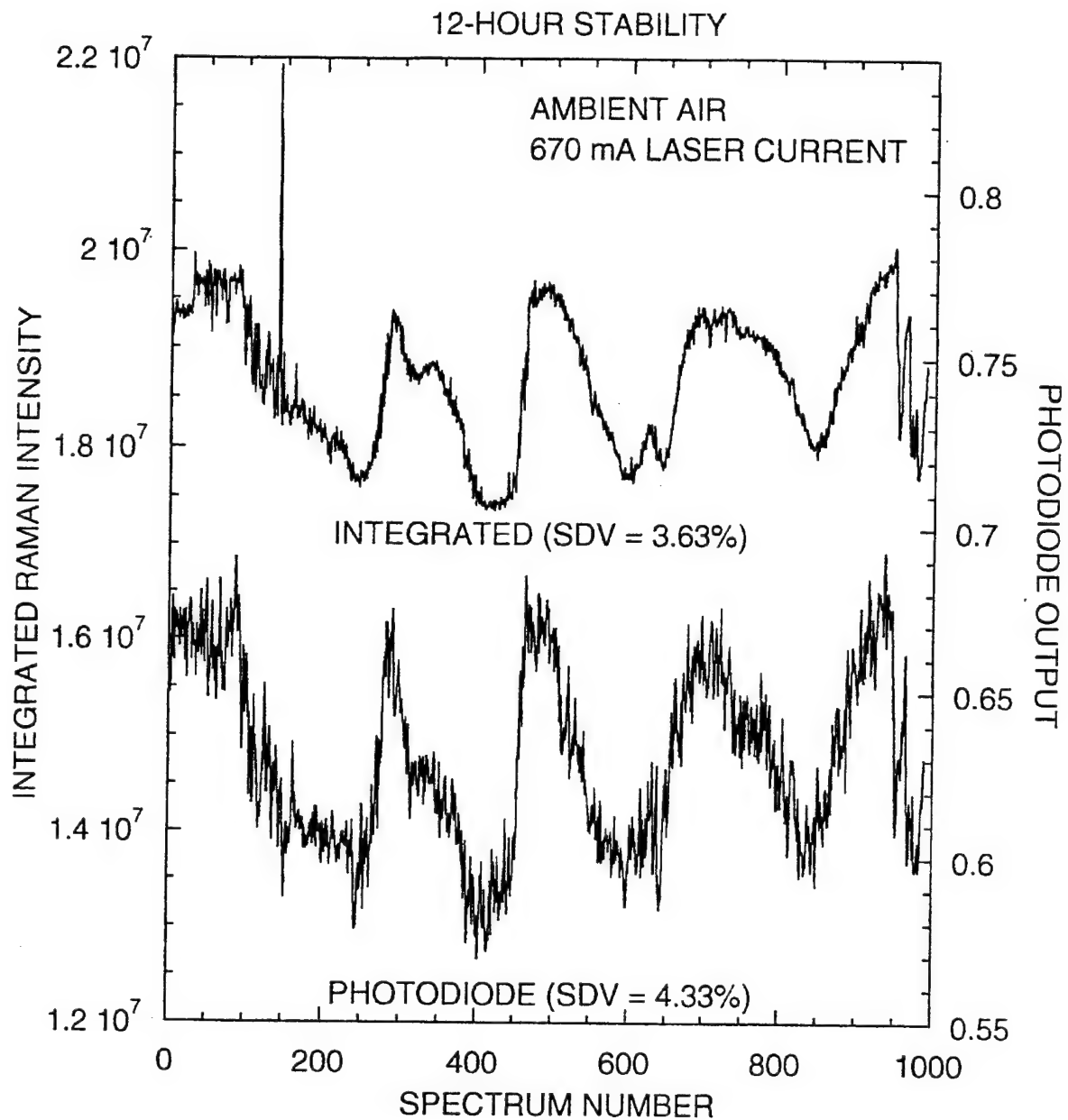


Figure 66. Demonstrates that the photodiode output matches the variation in integrated Raman intensity. The photodiode output doesn't track the variation in Raman peak intensity (SDV = 16.3%) nearly as well.

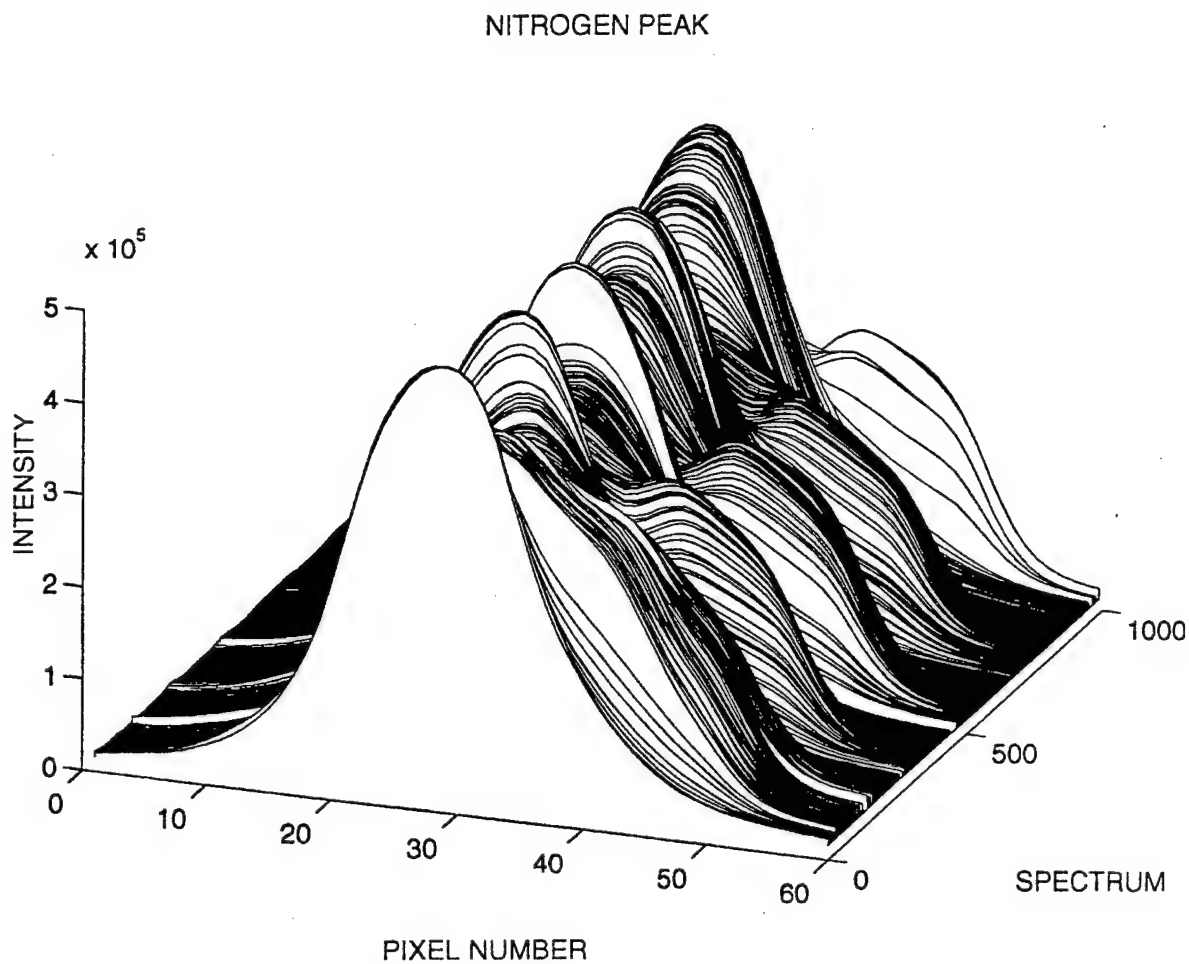


Figure 67. Plot of the variation of the nitrogen Raman peak on an expanded scale over the 12-hour period.

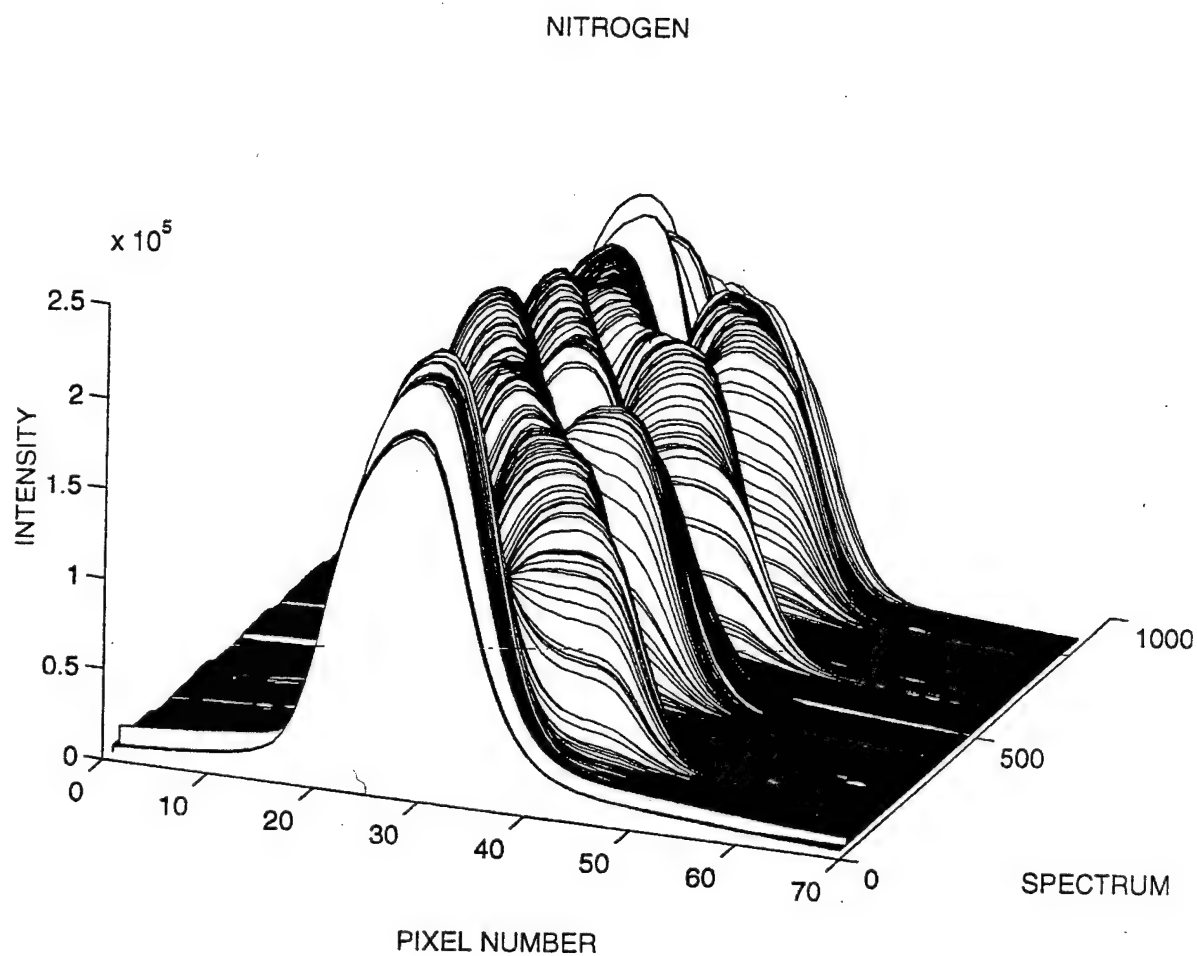


Figure 68. The nitrogen Raman peak obtained with a laser current of 450 mA continues to exhibit a periodic frequency variation in data collected over a 12-hour period.



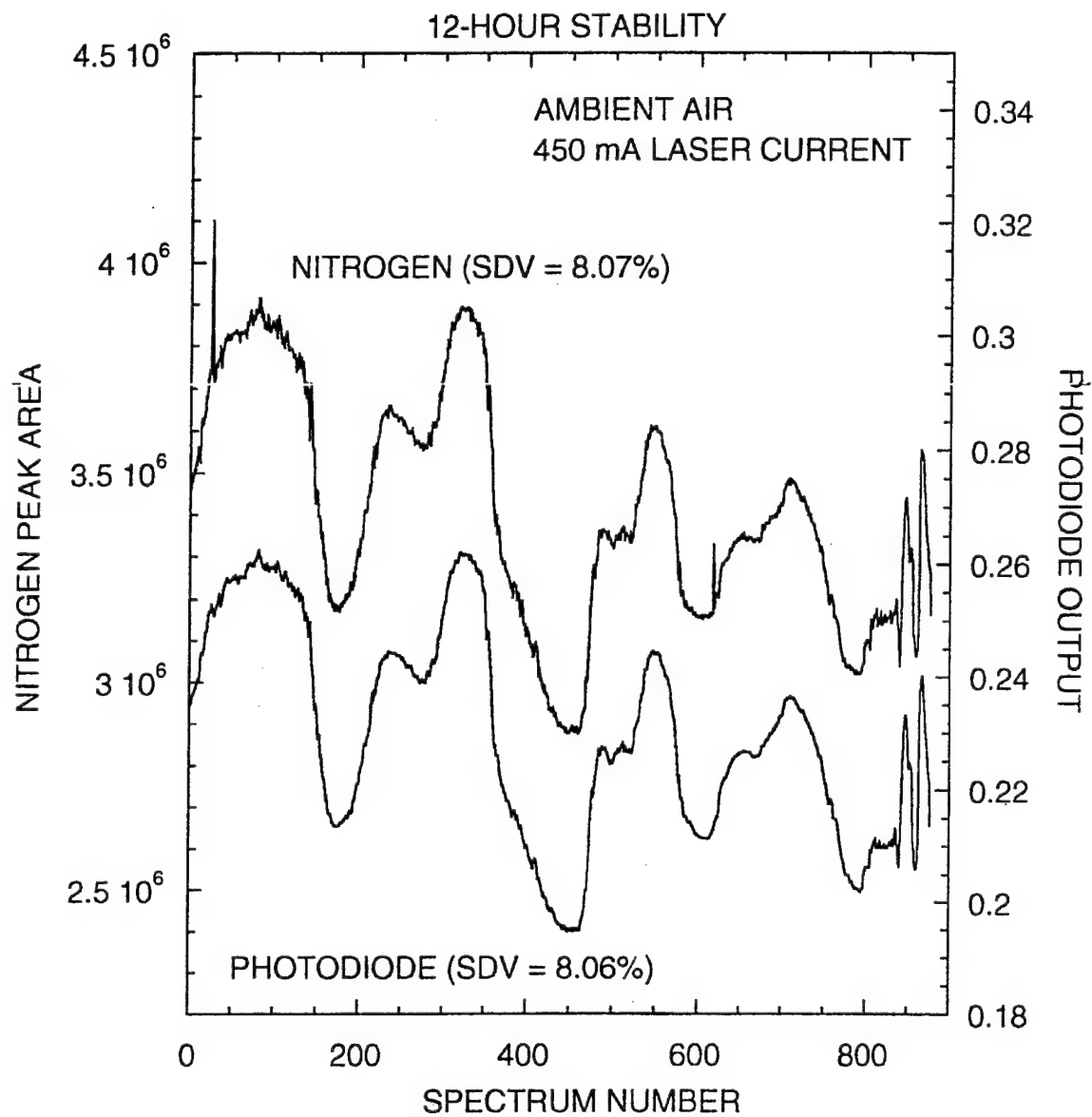


Figure 69. Twelve hour comparison between the integrated nitrogen peak area and the photodiode output. The variations in the nitrogen peak area and the photodiode output are 8.07 % and 8.06 %, respectively.

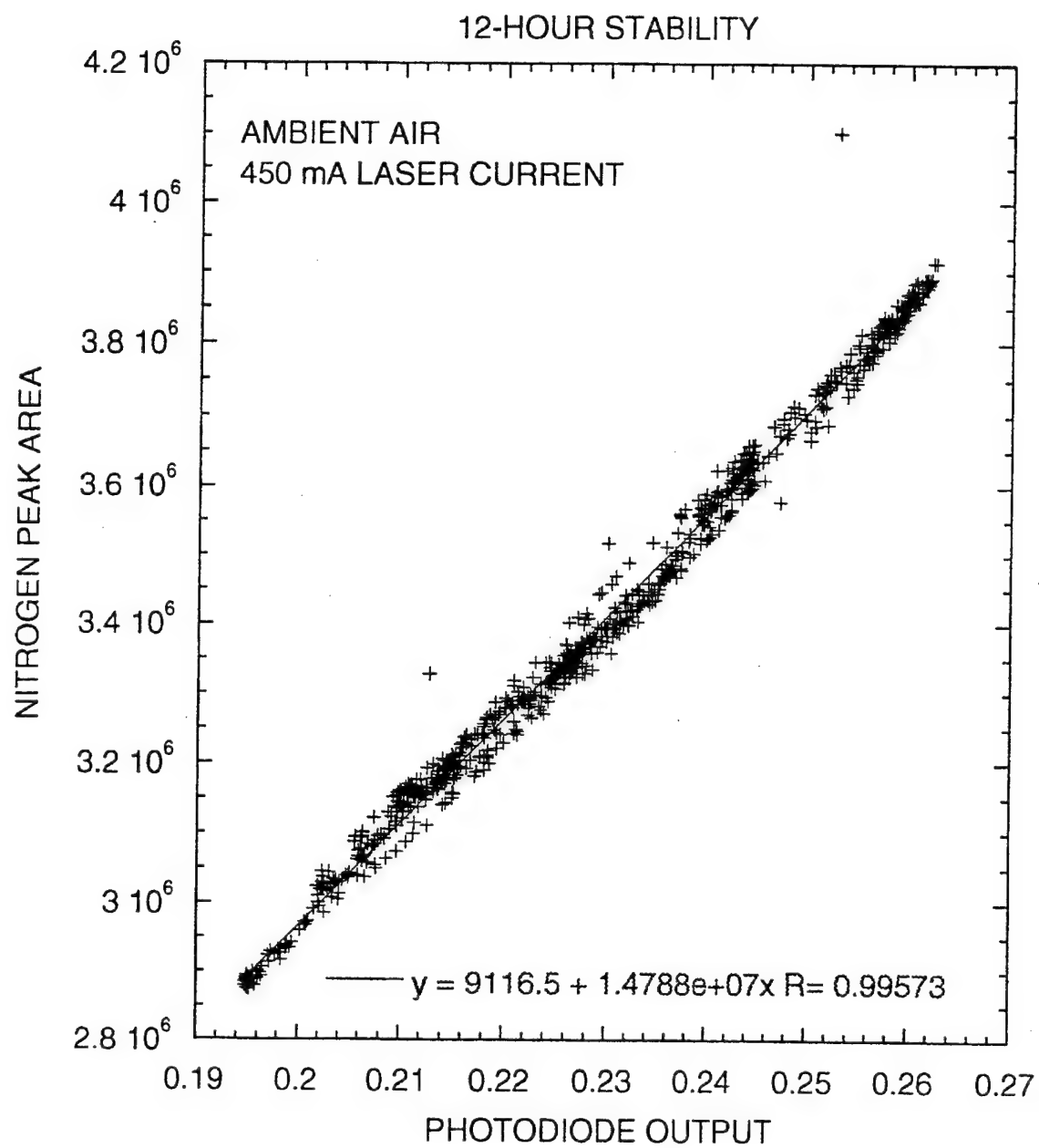


Figure 70. The measured nitrogen peak areas linearly related to the photodiode output values.

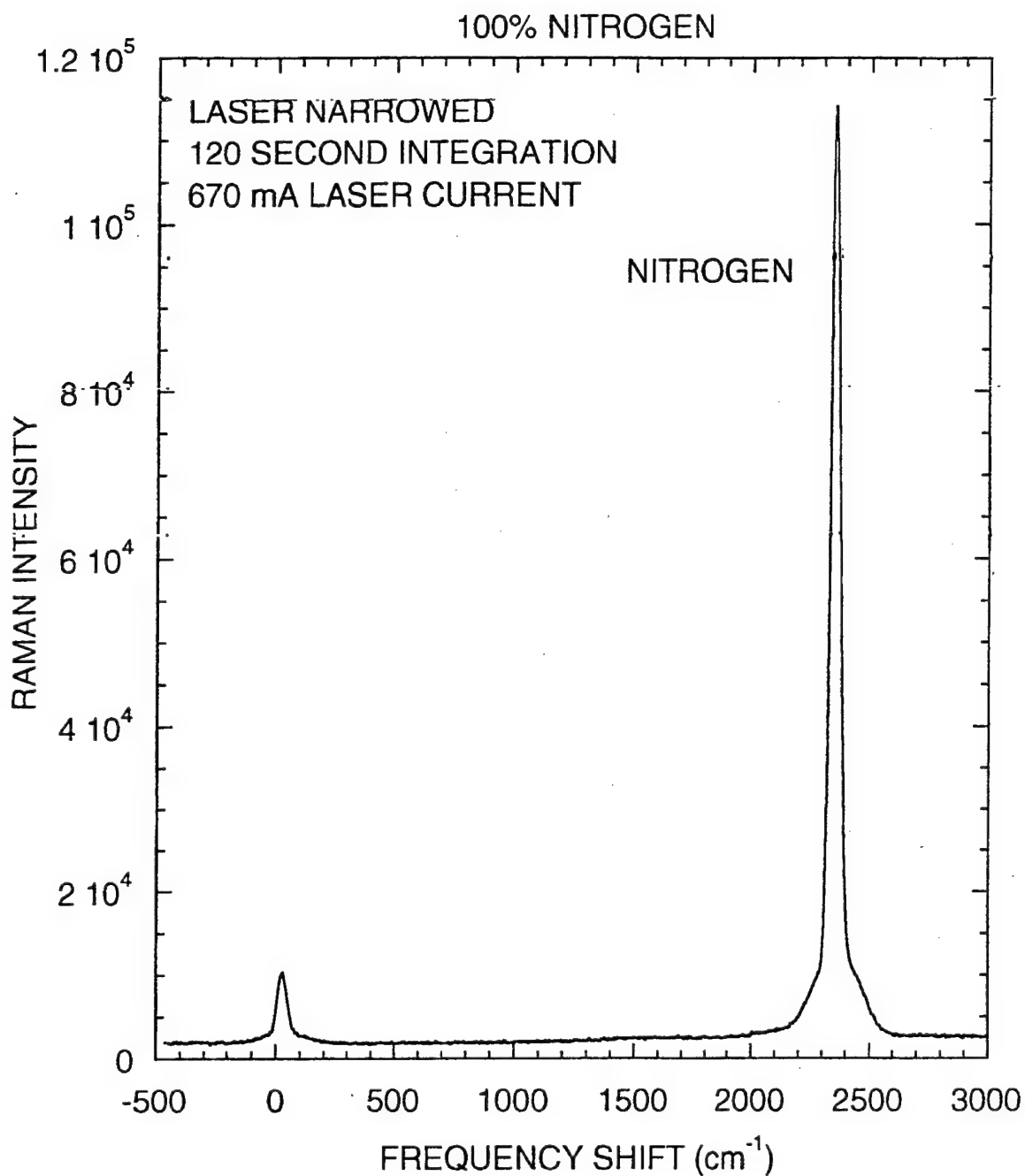


Figure 71. Raman spectrum obtained with nitrogen contained within the gas cell.

gas cell. As expected the line width of the nitrogen Raman peak is much reduced from our previous results obtained without laser line width narrowing, and the background emission near a frequency shift of  $1000\text{ cm}^{-1}$  is also reduced. Figure 72 illustrates the background on an expanded scale when argon (which doesn't have a detectable Raman signal) rather than nitrogen is contained within the gas cell. The peak at zero frequency shift is elastic scattering at the laser wavelength. Again, the background is reduced considerably compared to what we observed without laser line width narrowing.

The capability to separate closely spaced Raman peaks using the narrowed laser is illustrated in Fig. 73 which shows Raman data from a gas mixture containing 95%  $\text{CO}_2$ , 4%  $\text{N}_2$ , and 1%  $\text{O}_2$ . Even though  $\text{O}_2$  is only present at the 1% level, the oxygen peak is clearly resolved in the tail of the Raman peak from  $\text{CO}_2$ .

#### 2.6.4 12-Hour Stability Measurements

To test the stability of the line width-narrowed laser, we collected Raman data from ambient air and measured the variation in the nitrogen Raman peak intensity as well as the variation in the output of a monitor photodiode. The laser stability is clearly degraded by the line width narrowing process. With line width narrowing the Raman peak area varies with a standard deviation of 23.05% (see Fig. 74) compared to an integrated standard deviation of 3.63% without line width narrowing that we reported last month. As shown in Fig. 74, the monitor photodiode follows the Raman peak area quite well, but the variations are so large that using the photodiode signal to normalize the Raman data would probably not be feasible. Figure 75, which plots the frequency profile of the measured nitrogen peaks recorded during the 12-hour period, illustrates how the laser is varying from nearly off to full on.

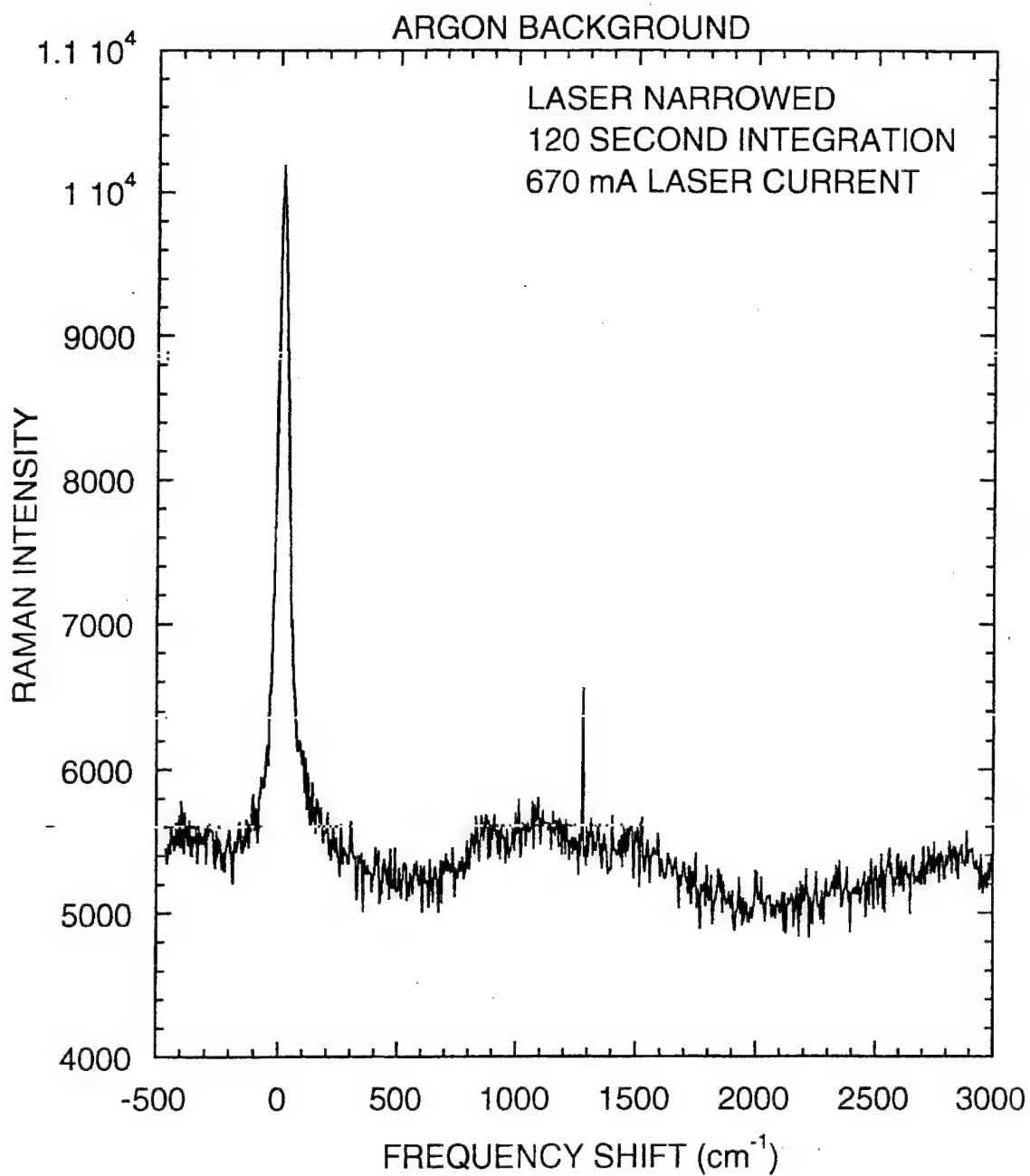


Figure 72. Background on an expanded scale when argon (which doesn't have a detectable Raman signal) rather than nitrogen is contained within the gas cell.

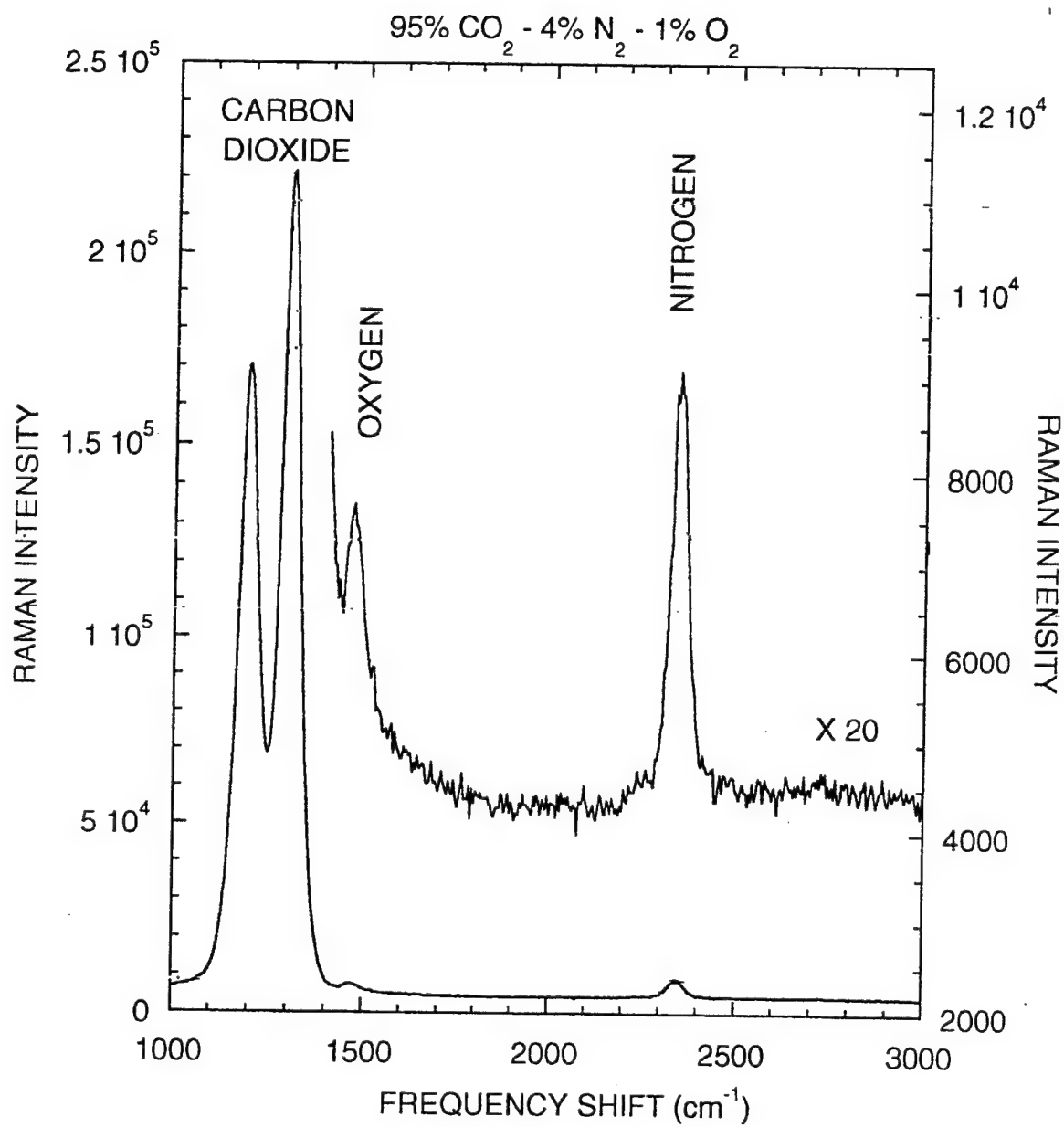


Figure 73. Raman data from a gas mixture containing 95% CO<sub>2</sub>, 4% N<sub>2</sub>, and 1% O<sub>2</sub>. Even though O<sub>2</sub> is only present at the 1% level, the oxygen peak is clearly resolved in the tail of the Raman peak from CO<sub>2</sub>.

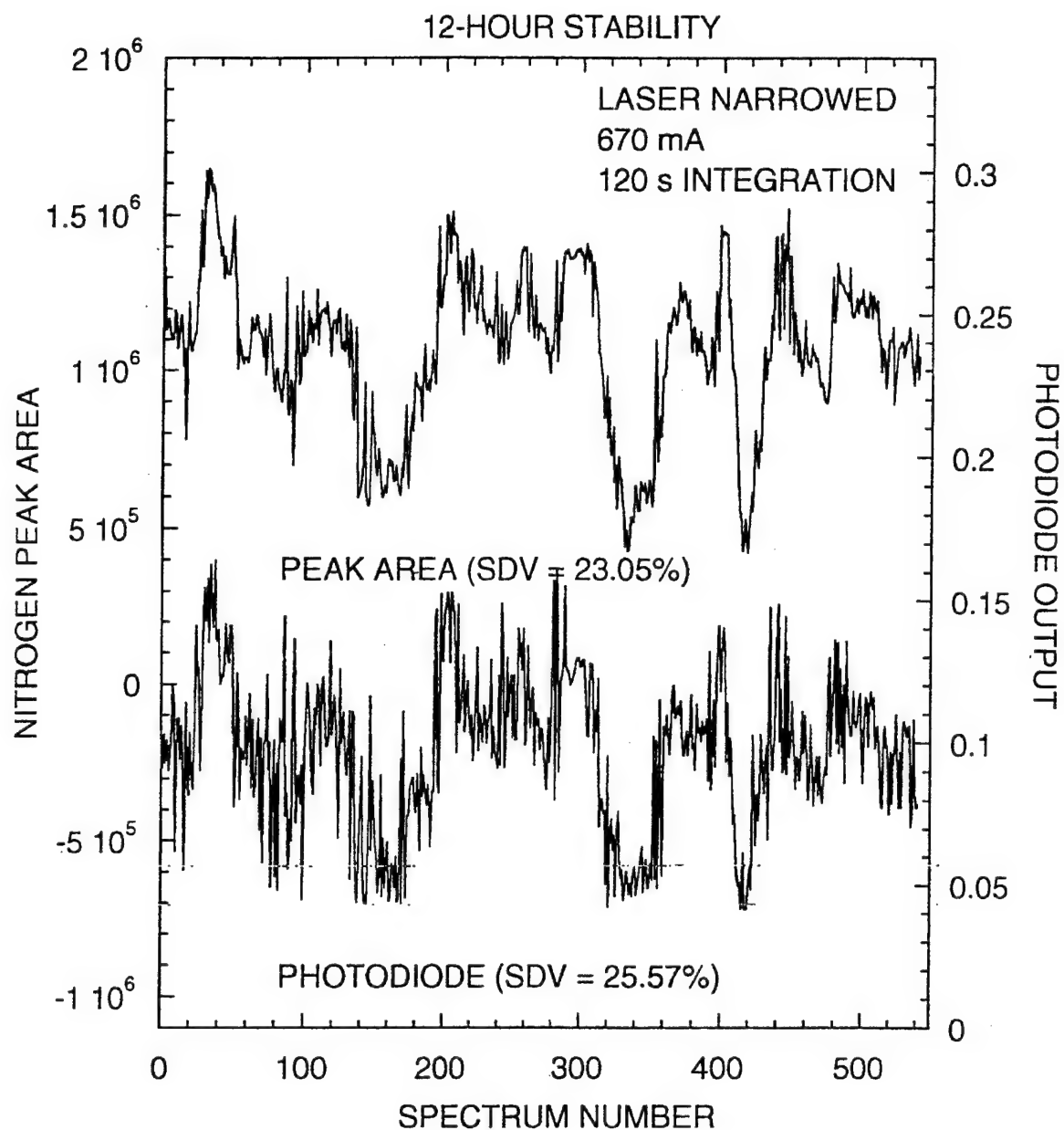


Figure 74. Comparison of the monitor photodiode output and the Raman peak area. The variations are so large that using the photodiode signal to normalize the Raman data would probably not be feasible.

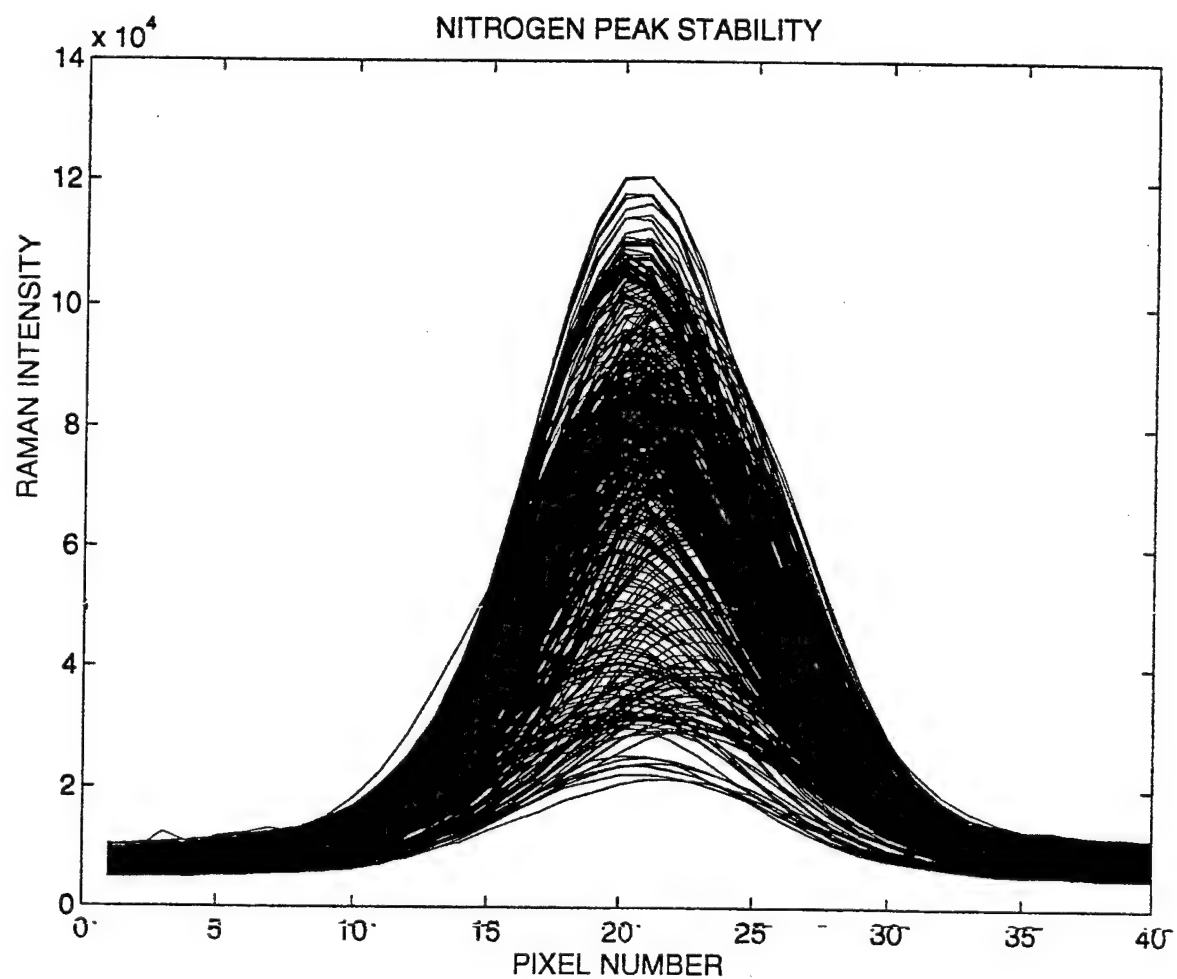


Figure 75. The frequency profile of the measured nitrogen peaks recorded during the 12-hour period.



### 3.0 BUSINESS DEVELOPMENT AND MARKETING

#### 3.1 Marketing

##### 3.1.1 Commercial Applications - Market Opportunity

Part of our research consisted of developing an evaluation of the market potential for this technology and the related applications. This information assisted us in developing a more practical and accurate business plan to assist outside investors in making investment decisions. Because of the importance of better process control in helping to reduce costs of all types of petrochemical processes, the market opportunity has increased over the last 3 to 4 years and is projected to continue to increase on an average rate of 6 to 7% over the next several years (Table 1). Process analyzer type equipment selected for this market overview analysis includes those analyzers most commonly used for industrial and pollution applications and that could be replaced with our Raman technology. Markets selected including process gas chromatographs, process mass spectrometers, nondispersive infrared (NDIR) and nondispersive ultraviolet (NDUV) analyzers, and oxygen analyzers are closely related to the market potential for Raman scattering technology. The term "process analyzer" means analyzers which are designed to operate continuously and on-line in industrial environments. The process analyzer definition, therefore, excludes laboratory analyzer types designed for bench-top operation; portable analyzers are also excluded.

##### 3.1.2 Geographic Distribution of Process Instrument Market

Application practices differ when comparing U.S. and Western European markets. End users in the United States (and those industries influenced by U.S. practice) generally prefer to use process chromatographs (and more recently process mass spectrometers) for multi-component analysis. For this reason, North American markets accounted for 50 to 55% of the worldwide unit requirements for process chromatographs and process mass spectrometers.

##### 3.1.3 Market Segmentation by End-User Groups

For process gas chromatographs and process mass spectrometers, chemical and petroleum-related end-users accounted for eighty-five percent (85%) of the 1998 market value. Except for some important applications for mass spectrometers among minerals and metal end-users, the remaining market value is dispersed among a variety of other end-users (Table 2).

##### 3.1.4 Potential OEM Instrument Company Customers

Table 3 lists potential customers (instrument suppliers) for our Raman instrument bench. These customers are all major suppliers of industrial instrumentation to the process market place. They would purchase the Raman bench on an OEM basis and incorporate the analyzer into their larger systems prior to installation at the process facility. They also represent potential investors

Table 1.

U.S. Markets for Process Chromatographs  
and Mass Spectrometers

Annual Market Forecast (1990 to 1999)\*

Year	No. of Units	Net ASP	Current Value (Millions)
1994	1,900	\$32,100	\$61.0
1995	2,100	32,700	68.7
1996	2,300	33,100	76.1
1997	2,500	32,200	76.1
1998	2,600	31,800	82.7
1999(Est.)	2,900	30,300	87.9

\*Process Control Marketplace Information Service  
ASP (Average Selling Price)

that could participate with our development. These are the candidate companies that we are pursuing for Phase III commitment and support of commercialization and marketing. Market data presented here covers analyzer hardware only. In all cases, sample handling systems, system engineering and data management equipment will add additional value for any given process analyzer installation. The total revenue potential (or multiple) compared with the analyzer hardware value will vary from a low of two times for many applications in chemicals and petroleum refining to as high as five to six times for some of the combustion and emissions monitoring (CEM) applications where turn-key systems are purchased on a guaranteed installation basis.

Worldwide requirements for the selected process analyzers totaled 24,500 units by 1999. Process mass spectrometers will exhibit the highest growth but account for a very small share of the unit requirements. Process chromatographs and process mass spectrometers will experience better than average growth because of expanding requirements for composition monitoring related to economic benefits and improved automation in chemicals and petroleum refining. NDIR/NDUV analyzers will also have better than average growth although the driving force related to their growth pattern will be tied more closely to air pollution applications driven by government regulations in the United States and Western Europe. Worldwide markets for selected process analyzers are summarized in Tables 4 and 5.

Table 2.

U.S. Markets for Selected Process Analyzers -  
Market Segmentation by End User Group  
(Percent of Market Value)

	PGC*	NDIR/UV
Chemicals	58%	23%
Petroleum refining	5	8
Oil/gas pipeline	22	2
Pulp & paper	--	8
Food, beverages, tobacco	--	7
Minerals & metals	2	12
Electric utilities	--	15
All others	13	25
	100%	100%

---

\* PGC - Process Gas Chromatographs

### 3.1.5 Prototype's Cost-of-Goods

Now that we have tested and defined the major components of the remote Raman prototype instrument, we can more accurately estimate the instrument's cost-of-goods (COG). This is important for manufacturing and marketing applications because the cost-of-goods, to a great extent, determines the size of the potential market available for the instrument. Kaiser makes a laboratory Raman instrument incorporating their \$13,000 spectrograph; the instrument costs over \$100,000. Other companies, such as Chromex also make a laboratory instrument that is very expensive. We have no chance of creating a successful business venture by building expensive Raman instruments for only specialized applications. We must reduce the COG so we can manufacture and market the technology into many simple applications with very large markets; i.e., hundreds of units per year, not tens of units.

Table 3.

## Potential Customers - Major Instrument Suppliers

Process	Mass Spectrometers	FTIR / NIR / FTNIR
Chromatographs		
ABB Process Analytics Automation/H&B	ABB Process Analytics (Milton Roy)	Anarad
Daniel Industries	Extrele/Millipore	Axxiom
Fluid Data/AMSCOR	Perkin Elmer	Bomen/ H & B
Foxboro	VG Instruments/Fisons	Bran + Luebbe
Instromet/Encal		Fluid Data
MTI Analytical		Katrina
Rosemount Analytical (La Habra Facility)		Lear Siegler
Siemens (Europe)		LT Industries
Yokogawa Electric Works (Outside of USA)		Midac
		Nicolet
		NIR Systems
		Perkin Elmer
		Rosemount Analytical (Orrville Facility)

Table 4.

Worldwide markets for selected process analyzers

UNITS	1998
Process chromatographs	5,800
Process mass spectrometers	1,700
NDIR/NDUV	<u>17,000</u>
TOTAL UNITS	24,500

VALUE (millions)	
Process chromatographs	\$158
Process mass spectrometers	38
NDIR/NDUV	<u>136</u>
TOTAL DOLLARS	\$332

Table 5.

Worldwide Markets for Selected Process Analyzers -  
1999\* Market Distribution by Geographic Region

	Percent of Units	Value (Millions)
Process chromatographs		
North America	56%	87.5
Western Europe	24	38.5
ROW (Rest of World)	20	32.0
TOTAL	100%	158.0
Process mass spectrometers		
North America	50%	19.0
Western Europe	40	15.2
ROW	10	3.8
TOTAL	100%	38.0
NDIR/NDUV		
North America	34%	46.0
Western Europe	52	70.7
ROW	14	19.3
TOTAL	100%	136.0
GRAND TOTAL		<u>\$332.0</u>

\* Estimated Values

### 3.2 Economic Benefits

#### 3.2.1 Health and Safety Considerations

##### 3.2.1.1 Ethylene Oxide Sterilization Monitoring

Many medical supplies cannot be sterilized by steam or by a radiation sterilization process. The only other practical method is the use of ethylene oxide (EtO) gas sterilization. The medical device is packaged as normal and placed in a large metal chamber. The combination of exposure to moderate heat, water vapor, and EtO gas over a period of several hours allows the gas to diffuse through the device packaging and sterilize the medical component. The sterilized parts are then exposed to moderate vacuum to pull off any residual toxic EtO gas prior to shipment and use. The effluent EtO is scrubbed from the system with water and converted into ethylene glycol which can be recycled and handled much more readily. Because of the high humidity needed to make the EtO work properly, infrared (IR) monitoring instrumentation cannot function. If the water vapor is condensed out of the system to make a measurement, the condensing water also removes the EtO that is being measured. Current EtO control technology is very crude at best and relies on mass control by weighing the EtO tank prior to starting the sterilization process and weighing the tank when it is completed to estimate the amount of EtO put into the sterilizing chamber. Most of these EtO sterilizers are small point source facilities, and routine monitoring of the EtO gas concentration is not practical because traditional monitoring instrumentation such as a mass spectrometer is too expensive. Because neither the actual residual level of EtO, nor the actual concentration that the medical devices were exposed to can be monitored, individual sterilizing strips are placed in with the components to be sterilized. These test strips are removed after processing and sent to a medical laboratory for analysis to determine if the medical devices were indeed exposed to sufficient EtO concentrations to cause sterilization. This testing requires that sterilized components must wait in quarantine for up to 5 additional days before they can be released for use. The sterilization industry wants to develop parametric release of EtO-sterilized components, but this requires extensive monitoring of the sterilization process: (1) the actual exposure levels that the components were exposed to and (2) the residual levels in order to minimize post sterilization holding times to meet recently approved ISO/AAMI 11135 (industry) requirements. Parametric release of EtO-sterilized components will greatly reduce sterilization costs. In addition, optimum monitoring instrumentation will assist in controlling unwanted EtO release into the atmosphere. For control purposes, EtO detection at the 0.5 to 1% level would be more than adequate. For parametric release, more sensitive detection would be required, probably on the order of 50 to 300 ppm.

##### 3.2.2 Economic Benefit to the Steel Industry

Most steel is fabricated when it is soft, untempered, and non-hardened state. This allows for more economical machining, forging, and other processing. To obtain the high strength and hardness required for operation, steel components are placed in a carburizing oven

and heated while in the presence of carbon containing gases, such as methane ( $\text{CH}_4$ ). When heated to 800 to 1,200 °C, the methane disassociates, and free C is available to diffuse into the steel. This produces an outer layer that has a high carbon content and is very hard and resilient to wear, while allowing the inner core to remain low in carbon content and remain tough rather than brittle. Because this process brings out the best properties of steel, it is very commonly used. The concentrations of gases used for heat treatment are in the low to high percentile range. For example, hydrogen would be present from 30 to 90 percent, nitrogen at 40%, methane at 1 to 2% and carbon monoxide at 5 to 20%. The primary problem is that each individual steel fabricator needs his own carburization oven. This is why there are some 20,000 steel fabricating ovens around the U.S. alone. Poor control of the carbonization process results in excess  $\text{CH}_4$ , CO and  $\text{CO}_2$  released into the atmosphere. Detection limits on the order of 0.5 to 1% would be adequate for most gas phase monitoring applications. Raman techniques should be ideal for this application. Infrared (IR) cannot measure  $\text{O}_2$ , nor is it particularly effective measuring  $\text{CO}_2$  when moisture is present. Paramagnetic technology can measure  $\text{O}_2$ , but is slow. A mass spectrometer has difficulty determining the difference in mass of CO and  $\text{N}_2$  and is very expensive and maintenance intensive.

### 3.2.3 Potential Post Applications

#### 3.2.3.1 Military

The successful development of laser-diode-based Raman instrumentation can help lower the cost of these devices in the long run by increasing their demand and the number that are manufactured. This opens up the use of this broad-based, full-spectrum technique for many different military field and on-site industrial applications. There currently are various ASTM approved tests for measuring many gasoline components and related environmental pollutants. However, these tests are routinely difficult, slow, and each requires expensive specialized and unique instrumentation. The full spectrum capabilities of Raman allow most if not all the necessary tests to be performed quickly, continuously, and with one instrument. This provides the military with the capability of monitoring fuels as they are dispensed and using the same or similar instrument for monitoring hydrocarbon contamination in ground water in and around military bases, potable water supplies, discharge from navy ships and environmental controls in submarines.

#### 3.2.3.2 Government - Federal and Local Agencies

The EPA can use this technology in a portable configuration for compliance monitoring of tank farms, refineries, and gas stations as well as other fuel vendors. The ability of Raman to identify different brands of gasoline could aid the determination of sources of gasoline spills.



### 3.3 Patent Application

We submitted a patent application January 14, 1999 covering our compact, robust, and optically fast (f/1.4) spectrograph. Our latest U.S. patent office action indicates that our patent was for the most part accepted and only with minor changes should be awarded.

### 3.4 Center for Devices and Radiological Health

To comply with the regulations specified in FDA 21 CFR, sections 1040.10 and 1040.11 for laser products, we are required to modify and or test the current laser device to incorporate the following:

(1) Performance testing

We must perform power measurement tests to determine power output of the system using a prescribed test method. Our laser is a class IV device.

(2) Remote interlock connector

A Remote interlock must be added to the laser controller (back panel). We plan to install an interlock connector between the AC to DC power link.

(3) Key control

A turn-key switch is needed to replace the current lighted on-off switch. In addition, we also need to add a LED as a laser-on indicator. A 12 V LED is acceptable.

(4) Manual reset

In the event of an unexpected power failure, the laser must be off when power is restored. We need to add a power reset switch between the AC to DC power link of the laser controller.

(5) Shutter

A manual or remote control shutter must be installed in the laser head. We plan to use a 45' rotational solenoid as a mechanical arm for the remote shutter. A spring will bring the arm to the on position when 12 VDC power is off.

### 3.5 Trade Shows

#### 3.5.1 Pittsburgh Conference - March 1999 - Orlando, Florida

We attended and displayed our Raman instrumentation for the third time at the March 1-5, 1999 Pittsburgh conference for industrial and process instrumentation. This conference had around 35,000 attendees and nearly 2500 exhibitors. It is the largest show of its kind in the US. We cannot not afford to attend many of these types of shows, so we focused our attention on the largest. It was held in Orlando, Florida and was well attended.

We had around 135 contacts this year, slightly more than the 125 contacts at the 1998 show. More importantly, the quality of the contacts were much better. We met many more original equipment manufacturers (OEM) and fewer sales reps just interested in obtaining a new product offering. Since we have not yet formally introduced a gas-phase Raman analyzer, we use this trade show to talk to potential customers about their gas-phase applications. There were ~7 companies exhibiting Raman instrumentation of various types: process instruments, laboratory, general purpose, and Raman microscope systems but none had gas-phase instrumentation.

We had inquiries with domestic petroleum companies including Exxon, ARCO, Phillips Petroleum, Ashland Oil, Sinclair Oil, in addition to foreign companies like Elf the largest petroleum company in France, and the world's largest refinery located in South Korea as well as Gas Unie (Netherlands) and BP (British Petroleum - U. K.) We met with industry representatives of Peugeot and Ford to discuss measuring fuel performance and how Raman spectra could be used to measure differences in different brands, and blends of gasoline. We feel that some of these companies could be a source of additional Phase III funding for commercialization of our technology. We had many independent representatives (both domestic and foreign) approach us with interest in distributing our technology.

### 3.5.2 Compact, Robust Spectrometer

Having a working spectrometer at the show, really helped demonstrated the simplicity of the Raman system. At the trade show we ran liquid samples that people brought by the booth as well as some prepared samples of benzene/toluene to illustrate the good resolution of our compact spectrometer. This demonstration allowed companies to see what the gas-phase instrumentation was like. Some of these companies discussed their interest in an OEM relationship. These companies included the following:

<u>OEM Contact</u>	<u>Market</u>
ASI, Instruments.	Process Control
Bruker Optics	Process Control
Applied Automation	Process Control
EIC	Process Control
Orbital Science Corp.	Process Control
Yokogawa Electric	Process Control
Petrospec	Laboratory
Ametek	Process Control
Foxboro	Process Control

Overall, we felt that the trade show was well worth the effort and expense. If we capitalize on the interest in our stabilized lasers, and make inroads with our laser and compact spectrometer we should be able to commercialize our equipment for gas-phase applications.

### 3.6 Strategic Alliance - Laser Corporation

We developed a funding commitment from Laser Corporation (Salt Lake City, UT) for an investment totaling \$180,000. These funds have been and will continue to be used for support of ongoing research and development that was started with our Phase I and II DoD SBIR contracts in addition to supporting Phase III commercialization. Laser Corporation (holding corporation of American Laser Incorporated) manufactures argon and krypton lasers. They know that these gas lasers are slowly being replaced by solid state devices. Laser Corporation is interested in working closely with us to develop economical laser-diode-based products that can ultimately incorporate their manufacturing expertise as well as other product opportunities involving solid state lasers and optical equipment. Laser Corporation has excellent design and manufacturing capabilities that compliment our instrumentation development activities. We will utilize this expertise to our advantage by their close participation in our company.

### 3.7 Possible OEM Relationship - Atmospheric Recovery Incorporated

In addition, we have had discussions with Atmospheric Recovery, Incorporated, concerning their interest in incorporating our Raman technology into their steel processing control equipment. Atmospheric Recovery manufactures process control equipment for the steel carbonization industry. They need a compact, robust analyzer that can simultaneously measure methane, oxygen, carbon monoxide and nitrogen in percentile concentrations. When we feel we have developed sufficient long-term stability in our prototype we will follow up with Atmospheric Recovery about an OEM relationship.

## 4.0 CONCLUSIONS

### 4.1 Raman Instrument Definition

#### 4.1.1 Laser Source

The laser source has turned out to be the single most important component in our Raman system. The stability of the instrument is directly related to that of the laser source. It was necessary to develop a narrow linewidth, frequency-stabilized Raman laser for this project. We ended up developing and applying for a patent on a novel, external-cavity, stabilized diode laser incorporating volume-holographic optics. This allowed our laser to be extremely stable with respect to intensity and frequency. More importantly, we can use this technology for any wavelength at which we can obtain a diode laser device. This component has been so successful that the frequency-stabilized laser has become a product opportunity on its own. Even prior to completing this Phase II, we have sold and delivered several Raman lasers to users in the U.S. and in Europe for use with liquid-phase Raman scattering. For gas-phase Raman spectroscopy we need much more laser power and this poses problems with overall system stability and longevity. For enhanced gas component resolution we want to have a narrow laser linewidth. However, testing to date has shown that narrowing the laser linewidth reduces the ASE and improves resolution, overall the narrow linewidth adds a lot of instability. We have some ideas of how to maintain the narrow linewidth necessary for improved resolution and reduced ASE while improving the long-term stability.

#### 4.1.2 Sample Cell Design

We developed several sample cell configurations. We will not finalize the sample cell design until we have settled on a final solution for linewidth narrowing of the laser source. These two aspects are closely related and effect one another. The methods we use to stabilize the laser and narrow its wavelength influence the space available for the gas cell and collection optics.

#### 4.1.3 Compact, Robust and Optically Fast Spectrograph

We developed a compact, robust and optically fast ( $f/1.4$  optics) spectrograph (Patent pending) that will work well with either gas-phase or liquid and solid-phase Raman scattering. The system can be built with traditional machining techniques and conventional diffraction grating components. The spectrograph is quite small, incorporates a rather inexpensive CCD (Kodak series 400) built by Santa Barbara Instruments Group (SBIG). The spectrograph is not particularly temperature sensitive. However, for the maximum stability we recommend that the spectrograph be temperature controlled when used in ambient conditions where the temperature swings are greater than 5 degrees C. The spectrograph is designed to use a rather small, inexpensive CCD chip. We can cover  $\sim 750 \text{ cm}^{-1}$  with our current dispersion. The resolution when using a  $50 \text{ }\mu\text{m}$  slit is  $\sim 5 \text{ cm}^{-1}$  and approximately  $2.5 \text{ cm}^{-1}$  when using a  $25 \text{ }\mu\text{m}$  slit. We

have provisions build into the spectrograph for adding additional laser line rejection filtering for reducing the base line of the Raman spectra.

#### 4.1.4 System Performance

The overall prototype system performance is quite satisfactory for many applications where gas component analysis is limited to  $> 1\%$ . The best long-term stability achieved was on the order of 0.74% which required a photodiode following circuit. This level of stability is very adequate for many gas-phase applications. With out the use of a photo-diode follower, the stability was on the order of 7 to 8%. Frequency stability of the laser source is good and is  $<15$  Ghz ( $0.5 \text{ cm}^{-1}$ ) over long periods of time. The spectrograph lends itself to being very stable because of its simple design and small footprint. With no moving components, we expect the spectrograph to be very reliable. Using an appropriate laser line rejection filter we can readily filter elastic and laser line scattering. The spectrograph has provisions to easily change the slit width to accommodate several slit sizes.

#### 4.1.5 Calibration Schemes

Calibration schemes remain to be fully developed. Again, we feel that the calibration techniques will be dependent upon the overall system stability and methods we use to stabilized the laser source. However, with the present instrument stability, a calibration is necessary perhaps every few hours, although the calibration procedure can be quite quick ( $\sim 5$  minutes) to maintain an overall system stability of 1%. Calibration consists of flushing the flow cell with pure argon to obtain a background signal, since argon has no real Raman signal. Then flushing the flow cell with a none gas concentration such as gas standards or room air. The computer characterizes the location and magnitude of the key Raman peaks and compares those with previous calibration runs. The whole process of flushing and making measurements requires about 5 minutes and is easily automated via the computer program. The peak heights are analyzed with respect to laser power to determine if the laser is operating at its correct power level, if the laser frequency is correct, and to determine if there is contamination on the flow cell window. All of these factors must be carefully monitored when the instrument is used for continuous process control applications.

#### 4.1.6 Software Control

Our software has been developed around *Windows 95*. The software allows for control of sample pump, calibration pump, in addition to duration and frequency of sampling. Instrument operation parameters, such as laser operating current, temperature, output power, and instrument temperature, are constantly monitored and evaluated to ensure that the spectrograph and laser are operating correctly under changing environments. The software collects Raman data, analyzes the spectra, and computes sample concentrations when appropriate calibrations have been made.

We are currently designing the software to be updated remotely via the Internet and/or a modem. This offers faster and better customer service and allows for remote diagnostic testing and evaluation.

#### 4.1.7 Applications - Process Control and Pipe-line Monitoring

We are currently evaluating potential of applying the Raman system toward process control applications where analysis speed is critical and where sensitivity requirements are on the order of 1.0 %. Typical applications include replacement for gas chromatographs (GC) in petroleum pipeline monitoring. The Raman spectrograph can be used to analyze the concentrations of high-pressure gases in 30 to 60 seconds as compared to 20 minutes with conventional GC technology. The Raman instrument can evaluate the combustible / noncombustible ratio in natural gases in < 1 minute and the equipment could be much less maintenance intensive compared to a GC.

## REFERENCES

1. Raman, C.V. and Krishnan, K.S., *Nature*, **121**: 501, March 1928.
2. Van Wagenen, R.A., Westenskow, D.R., Benner, R.E., Gregonis, D.E. and Coleman, D.L., "Dedicated Monitoring of Anesthesia and Respiratory Gases by Raman Scattering," *Journal of Clinical Monitoring*, **2(4)**: 215, Oct., 1986.
3. Westenskow, D.R., Smith, K.W., Coleman, D.L., Gregonis, D.E. and Van Wangenen, R.A., "Clinical Evaluation of a Raman Scattering Multiple Gas Analyzer for the Operating Room," *Anesthesiology*, **70**: No.2, Feb., 1989.
4. Smith, L.M., Osakie, G. and Peters, T., "Raman Spectroscopy for On-line Multiple Component gas Analysis," Albion Instruments, *ISA - Proceedings*, New Orleans, LA. Oct. 14-18, 1990, Presentation and proceedings.
5. Schrotter, H.W. and Klockner, H.W., "Raman Scattering Cross Sections in Gases and liquids," in *Raman Spectroscopy of Gases and Liquids*, Weber, A. ed. (Springer-Verlag), New York, 1979.
6. Garrison, A.A., Muly, E.C. Roberts, M. J., Trimble, D.S. and Moore, C.F., "Raman Spectroscopy for On-line Distillation Process Control," *ISA Proceedings*, Vol. 44, part 1, pp. 257-363, Oct. 1989.
7. Niemczyk, T.M., Delgado-Lopez, M. and Newman, C.D., "Multichannel Raman Spectroscopy Tackles Industrial Problems," *Laser Focus World*, March, 1993, pp 85-98.
8. Pemberton, J.E., Sobocinski, R.L., Bryant, M.A., and Carter, D.A., "Raman Spectroscopy Using Charge-Coupled Device Detection," *Spectroscopy*, **5**: 2 (1990).
9. Murray, C.A. and Dierker, S.B., "Use of an unintensified Charge-Coupled-Device Detector for low-light-level Raman Spectroscopy," *Opt. Soc. Amer*, Vol 3, 1986, p. 2151.
10. Wang, Y. and McCreery, R.L., "Evaluation of Diode Laser/Charge Coupled Device Spectrometer for Near-Infrared Raman Spectroscopy," *Anal. Chem.* **61**: pp.2647-2651 (1989).
11. Tedesco, J.M., Owen, H., Pallister, D.M., and Morris, M.D., "Principles and Spectroscopic Applications of Volume Holographic Optics," *Anal. Chem.* **65**: pp.441A-449A (1993).
12. Adar, F.R. and Purcell, F. "Remote Raman Analysis for Process Monitoring Applications," Spex Industries, Edison, NJ., 1993 Product Application Notes.

13. Owen, H., Battey, D.F., Pelletier, M.J., and Slater, J. B., "New Spectroscopic Instrument Based on Volume Holographic Optical Elements," *SPIE Proceedings*, Vol. 2406, 1995.
14. Sadtler Research Laboratories, Inc. 3316 Spring Garden Street, Philadelphia, Pa., Vol. 1,2, 1974.



## DISTRIBUTION LIST

AUL/LSE Bldg 1405 - 600 Chennault Circle Maxwell AFB, AL 36112-6424	1 cy
DTIC/OCP 8725 John J. Kingman Rd, Suite 0944 Ft Belvoir, VA 22060-6218	2 cys
AFSAA/SAI 1580 Air Force Pentagon Washington, DC 20330-1580	1 cy
AFRL/VSIL Kirtland AFB, NM 87117-5776	2 cys
AFRL/VSIH Kirtland AFB, NM 87117-5776	1 cy
Process Instruments, Inc. 825 North 300 West, Suite 225 Salt Lake City, UT 84103-1414	3 cys
AFRL/DE Kirtland AFB, NM 87117-5776	1 cy
Official Record Copy AFRL/DELS/Filipietz	3 cys

